Changes in Arctic vegetation, precipitation and its effects on carbon emissions from thawing permafrost in the 21st century

Hylke D. Hoogland

July 5, 2020

Contents

Abstract

Context: The rapidly changing climate in the Arctic induces changes in Arctic ecosystems. The thawing of the permafrost may release large quantities of greenhouse gasses that accelerate warming even more. The Pleistocene Park aims to preserve the permafrost by restoring the ecosystem of the Pleistocene: the mammoth steppe. This will change the evaporation of the region, which will in turn change precipitation downwind. As the release of CH_4 from permafrost depends on the water table depth, this will also change these emissions.
Aims: In this thesis, I determine the degree of change in precipitation for the Arctic in various future scenarios. In some of these scenarios the tundra is completely replaced by mammoth steppe. An attempt to translate the precipitation changes to CH_4 emission changes is also made.
Methods: I use statistical models based on the current distribution of vegetation and evaporation therefrom to make predictions of evaporation in future scenarios. The evaporated water will be tracked using U-track to determine where it precipitates. Upscaling the equation for CH_4 emission from Olefeldt et al. (2013) will provide insight in the release of CH_4 from thawing permafrost.
Results: The statistical models for evaporation deviate from reanalysis data from GLEAM on average with 20.8%. The precipitation change attributable to vegetation change is found to be much smaller than this average deviation in all scenarios (<5%), and therefore the resulting precipitation estimates are not significant.
Conclusions: Precipitation that evaporated most recently from tundra regions does not fall in regions where the CH_4 emission is estimated to be especially sensitive to added moisture. Although no significant estimate of CH_4 emission change can be made, the increase in CH_4 emission due to the large scale implementation of the Pleistocene Park method is therefore unlikely to exceed the reduction in emissions achieved otherwise.

1 Introduction

The future change of the Arctic climate is of great interest. The polar regions are warming faster than other parts of the world (IPCC, 2014). This causes, among other problems, thawing of permafrost (SWIPA, 2017). The permafrost soils contain large amounts of organic carbon, which has been preserved by the frozen soil. This carbon reservoir is estimated to contain 900 to 1000 Gt of carbon, which is about 5 times the amount of carbon added to the atmosphere since pre-industrial times (Zimov et al., 2006). Upon thawing, this organic carbon can decompose, releasing primarily the greenhouse gasses carbon dioxide (CO_2) and methane (CH_4). The thawing of permafrost is thus an important component in climate change. The release of greenhouse gasses from permafrost is controlled by many processes, but soil moisture has significant influence on this process. Wet conditions favour the release of CH_4, while dry conditions favour the release of CO_2. In this master thesis, I will therefore study soil moisture changes in future climate scenarios for the permafrost.

The great improvement in numerical reanalysis (Copernicus Climate Change Service, 2017), climate modelling, extension of observational datasets and syntheses thereof (Olefeldt et al. (2013), Olefeldt et al. (2016), Song et al. (2018)) in recent years allow for a data-based study of the processes governing the soil moisture in permafrost regions. The thawing of permafrost causes an increase in soil moisture and thereby an increase in greenhouse gas emissions. The evaporation and consequent precipitation will also change. The goal of my master thesis is to study the role of Arctic vegetation in these changes.

At the Pleistocene Park in Chersky, a grassland ecosystem is created with the aim to conserve the permafrost by drying the soil through increased transpiration and cooling the soil through the trampling of insulating snow by animals. I will thus investigate what the difference would be in precipitation patterns across the Arctic between a future scenario where the treeline is displaced northward, and a future scenario where large parts of the tundra are replaced by a grassland ecosystem as in the Pleistocene Park.

The northward expansion of the treeline will change the evapotranspiration of a region and thereby the amount of precipitation downwind. If this precipitation falls on permafrost, it will contribute to the soil moisture and thus to the increase of CH_4 emissions. The processes which will be a part of my master thesis are the carbon cycle, water cycle and climate-vegetation feedback, described below.

1.1 Effect of thawing on permafrost carbon emissions

The processes governing the release and uptake of these gasses are complex, though in general wetter and warmer soil conditions favour the release of methane (Lai (2009), Tang et al. (2016), McGuire et al. (2018), Shingubara et al. (2019)). Local measurements of CO_2 and CH_4 fluxes have been conducted across the Arctic, in European Russia (e.g. Diáková et al. (2016)), Siberia (e.g. Merbold et al. (2009), Walz et al. (2018), Tuovinen et al. (2019)), China (e.g. Song et al. (2020)), Alaska (e.g. Bond-Lamberty et al. (2016), Natali et al. (2015)), and Canada (e.g. Estop-Aragonés et al. (2018)). See also Van der Molen et al. (2007) for a comparison of older local carbon flux measurements (Table 6). Although these studies provide information and understanding on a local level only (in both space and time), the measurements are of importance to calibrate Earth System Models (ESMs) and verify post-processed satellite data. Olefeldt et al. (2013) used 155 such measurements to derive empirical equations for methane flux depending on meteorological and environmental parameters. Though many studies have focused on methane emissions during the growing season, methane emissions from permafrost have also been detected in the non-growing season (Michaelson and Ping (2003), Wang et al. (2011), Grogan (2012)) and may dominate annual emissions locally (Zona et al., 2016).

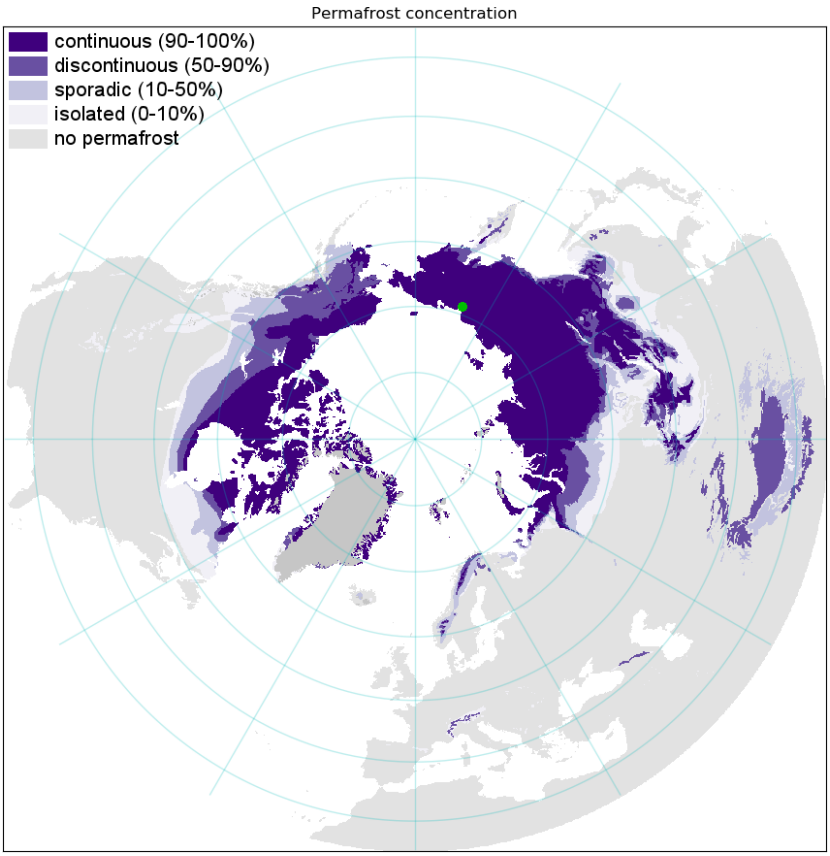

Figure 1: Map showing the extent and concentration of permafrost. The data was compiled by Brown et al. (2002) from various sources and dates representing average conditions in the late 20th century. The green dot indicates the location of the Pleistocene Park. The outline of isolated permafrost will be shown in all subsequent maps in various colors.

1.2 Effect of thawing permafrost on water balance

Changes in soil moisture are to a large degree caused by changes in precipitation. Therefore the source of the precipitated water needs to be known. Vazquez et al. (2016) used a Lagrangian tracking scheme (see also Seibert and Frank (2004)) to determine the sources of moisture in the Arctic drainage basin. Their study is based on the assumption that negative values of precipitation-evapotranspiration difference (P-E) indicate evapotranspiration from a region while positive values indicate precipitation. However, this method does not take into account that evaporation and precipitation can occur simultaneously. They concluded that the sub-tropical Atlantic and Pacific oceans provided most moisture to the Arctic, with contributions from land limited to the summer.

Most of the carbon decomposition takes place in the melting season and large parts of the permafrost region experience little precipitation in winter due to the presence of cold anti-cyclones (particularly over Eurasia). Spring melt of winter snowfall will temporarily increase soil moisture. However, due to the still shallow impermeable permafrost, the excess water is expected to be lost to runoff quite quickly (see also Serreze et al. (2002)). Although Vazquez et al. (2016) determined the oceans to be the largest source of Arctic precipitation, the impact of land vegetation changes on evaporation and consequently soil moisture content can still be substantial.

A terrestrial region can obtain moisture from advection from another region, or from evapotranspiration within the region. The fraction of precipitation originating from the latter is termed 'moisture recycling'. Brubaker et al. (1993) found that there is strong seasonal variability in the intensity of moisture recycling. The intensity of moisture recycling also depends on the size of the studied region, since evapotranspired moisture is more likely to precipitate if it travels over the region for a longer time (Trenberth, 1999). The moisture recycling intensity gives information of the dependence of a region on its own or nearby moisture content (Staal et al., 2018).

Analysis specific to the Arctic region was performed by Serreze et al. (2002), focusing on the Arctic ocean drainage basin. They found that runoff relative to precipitation is larger for river basins with substantial permafrost cover. Thawing permafrost may also have contributed to increased annual discharge of the Yenisey river. Rawlins et al. (2010) found in their analysis that various trends show an intensification of the Arctic freshwater cycle, though with low confidence (see also Dufour et al. (2016)). Despite increases in water availability, soil drying is expected in significant parts of the permafrost region due to increased drainage from thermokarst landscape erosion (Lawrence et al. (2015), Olefeldt et al. (2016)).

1.3 The permafrost vegetation-climate feedback

Finally the distribution of vegetation can have an impact on the soil moisture content. Vegetation influences soil wetness and temperature by root extraction, transpiration, surface roughness changes, trapping of snow, albedo changes, litter production and all combinations thereof. Vegetation response to climate change depends on many variables, though temperature and moisture availability are consistently identified as significant (Köppen (1884), Körner (1998), Grace et al. (2002)). In the Arctic, climate change induced temperature increase is expected to cause northward expansion of taiga forest at the expense of tundra ecosystems (Holtmeier and Broll (2007), Song et al. (2018)). An increase in biomass with time is termed 'greening', while a loss of biomass with time is termed 'browning'. Large scale greening has been observed due to increased plant growth in milder conditions (Ju and Masek, 2016), though excessive warming also causes browning in some regions (D'Arrigo et al., 2004).

A major consequence of the expansion of forest is a decrease in the high-latitude albedo, resulting in increasing absorption of solar radiation and there-

fore higher temperatures (MacDonald et al., 2008). Increased shrubbiness also causes more snow to be trapped and thereby insulates the ground from the most severe winter weather, effectively heating the permafrost. Taller shrubs (and trees) also transpire more water than shorter ones (Bonfils et al. (2012), Jafarov et al. (2018), Loranty et al. (2018)). Depending on where this extra transpiration precipitates, it will have an influence on soil moisture content and carbon emissions. Liang et al. (2014) studied the distribution of trees along the taiga-tundra ecotone (the transition zone between these ecosystems) near Chokurdakh, to find that the soil moisture content has a significant influence in determining this distribution. Possible increases in soil moisture may prevent tree growth if the soil becomes too wet.

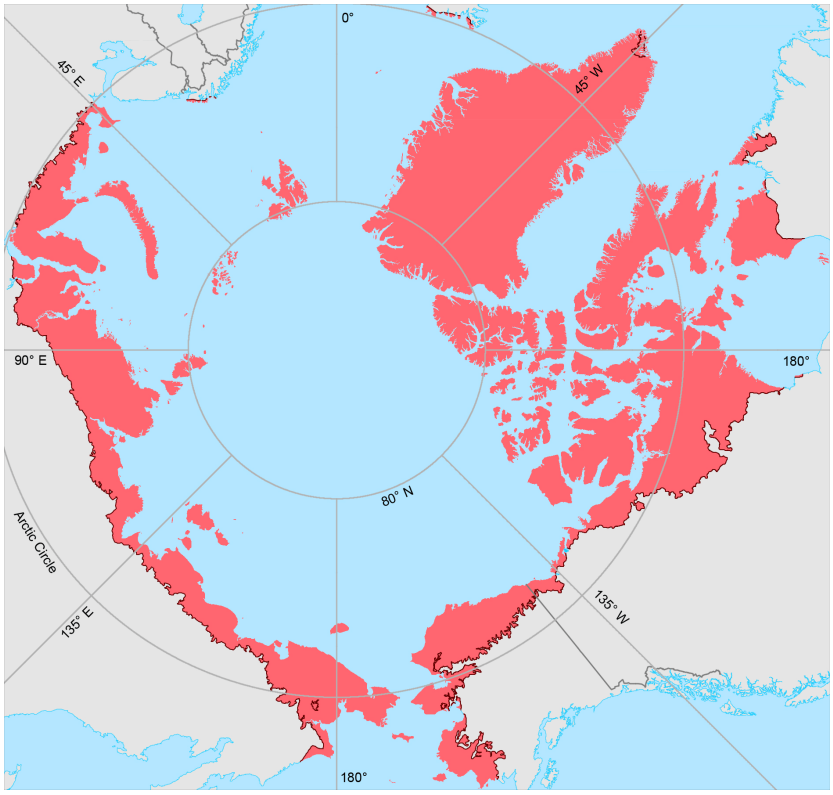

Figure 2: Map showing the area north of the treeline in red (U.S. Fish and Wildlife Service)

2 Aims

The introduction above presents a broad range of permafrost processes. Though these processes are quite different, they all interact with each other. My master

thesis focuses on the interaction between these processes.

This master thesis will aim to determine the change in soil moisture due to changes in vegetation for the future climate, relative to current conditions. These changes are important for the release of methane from Arctic wetlands. The focus will thus lie on permafrost areas (see figure 1), particularly regions now covered with a tundra ecosystem (see figure 2). A statistical model for vegetation growth in permafrost regions will be made. This will be done by investigating where tundra and taiga grow currently and under what climatic conditions. I aim to determine the geographic distribution of the origin of the water in the soil in thawing permafrost regions, similar to Vazquez et al. (2016). An attempt will be made to attribute a part of the change in soil moisture to a shift in the treeline. Furthermore, the same procedure will be conducted for a scenario where significant portions of the tundra and northern taiga area are replaced by highly productive grassland (also known as mammoth steppe), as exemplified by the Pleistocene Park in Chersky (Zimov, 2005). From the soil moisture, an estimate of the carbon fluxes can be made.

2.1 Pleistocene Park

During the last ice age, large parts of the northern hemisphere was covered by polar steppe, dominated by grasses. The animals which the abundance of grass sustained trampled the snow in winter, reducing the insulating effect it has on the ground. This helps to cool the permafrost in winter and reduce the active layer which thaws in summer. Grass also has a higher evapotranspiration rate than modern tundra vegetation. The soil thus remained dryer, reducing the release of methane. The Pleistocene Park aims to restore these conditions in the Arctic, starting in Chersky. The aim of this master thesis is thus to investigate the large scale hydrological effect of this ecosystem change.

2.2 Research questions and structure

The principle research questions are presented as follows:

Concerning the hydrology:

- Where does the precipitation that falls on permafrost originate?
- How does the water balance (precipitation, evaporation and runoff) of the permafrost change for various future scenarios?
- How does evaporation differ between tundra and taiga regions?
- Which areas will wetten or dry as a result of a shift in the treeline?
- Which areas will wetten or dry as a result of restoring the mammoth steppe in the tundra?

Concerning the carbon cycle:

- How to estimate CH_4 emissions from permafrost?

- How high is the CH_4 emission for different scenarios?

The structure of my thesis is as follows. In section 3 I will describe the datasets used and the methods to analyze them. These datasets represent permafrost concentration (3.1), frozen soil probability (3.2), land-cover (3.3) and evaporation (3.4) datasets. Methods used to track moisture in the atmosphere (3.5), estimate the environmental variables governing vegetation (3.6) and estimate methane fluxes (3.7). Models and scenarios are also described in this section (3.8). In section 4 I list the results obtained with these methods and data. Section 4.1 assesses the accuracy of the statistical models I derived. Section 4.2 then describes the changes that occur in future scenarios relative to the present day situation. Moisture source and sink regions are described separately in section 4.3. Finally, an attempt to describe the expected changes in methane emissions is performed in section 4.4. Discussion and conclusion can be found in section 5 and section 6, respectively.

3 Methods & data

3.1 Permafrost concentration

The permafrost concentration is largely based on the data by Brown et al. (2002). This data was compiled from various sources and dates representing average conditions in the late 20^{th} century. However, for this analysis lakes are removed. The lake mask is taken from ERA5 (Copernicus Climate Change Service, 2017). This is especially noticeable in western Canada. The resulting permafrost concentration is shown in figure 3.

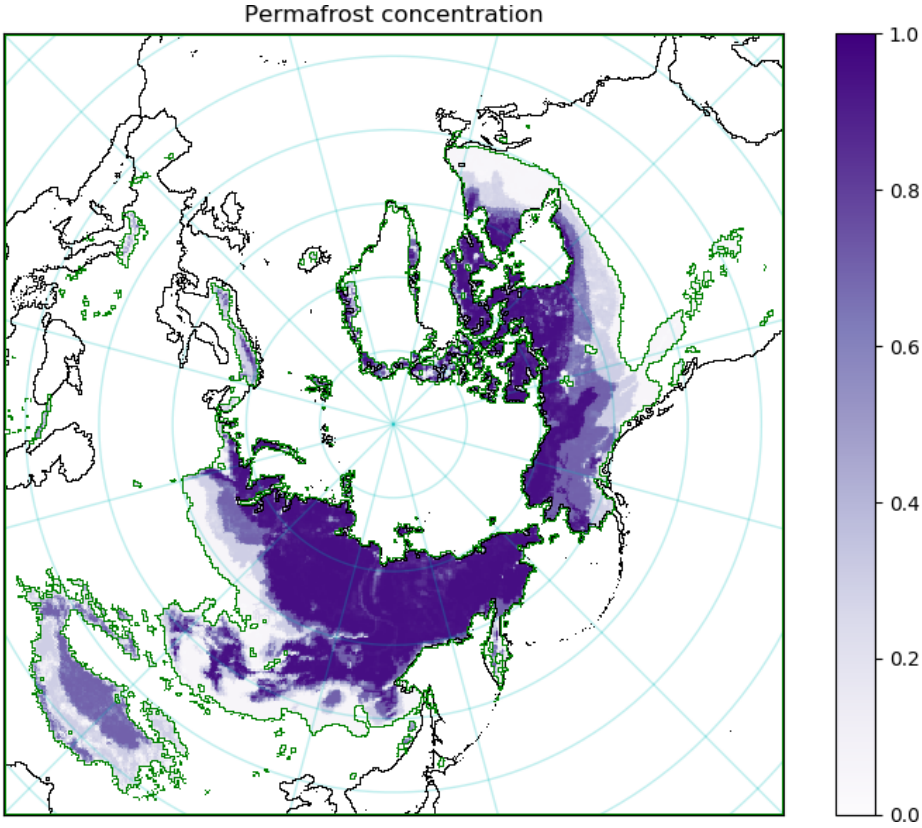

Figure 3: Permafrost concentration from Brown et al. (2002). The green line shows the extent of isolated permafrost. The extent of isolated permafrost will be shown in all subsequent maps, in various colors.

3.2 Frozen soil probability

When determining sources of precipitation, it is important to distinguish between precipitation that falls on frozen soil and precipitation that falls on unfrozen soil. The probability that soil is frozen in a particular month, assuming Gaussian distributed temperature probabilities, is defined as

$$Q(T_s) = \frac{1}{2}\left(1 - erf\left(\frac{T_s - 273.15K}{\sigma_{T_s}}\right)\right) \tag{1}$$

where T_s is the skin temperature in Kelvin, σ_{T_s} is the 1σ Gaussian distributed uncertainty in this quantity and erf is the error function, defined as

$$erf(x) = \frac{2}{\sqrt{\pi}} \int_0^x e^{-t^2} dt \tag{2}$$

Here, t is a dummy index. The function smooths the probability around the 0°C isotherm. The skin temperature is taken from ERA5 reanalysis data for the period 1990-2019. The 1σ Gaussian distributed uncertainty is determined by assuming that the various models which participate in the ERA5 reanalysis accurately represent the natural variability. The standard deviation of these models for any particular month would thus equal the standard deviation of the temperature distribution. This yields an estimate for the probability of frozen soil in every month. By averaging all months for the 1990-2019 period an estimate for the frozen soil probability can be made for every month at the present time.

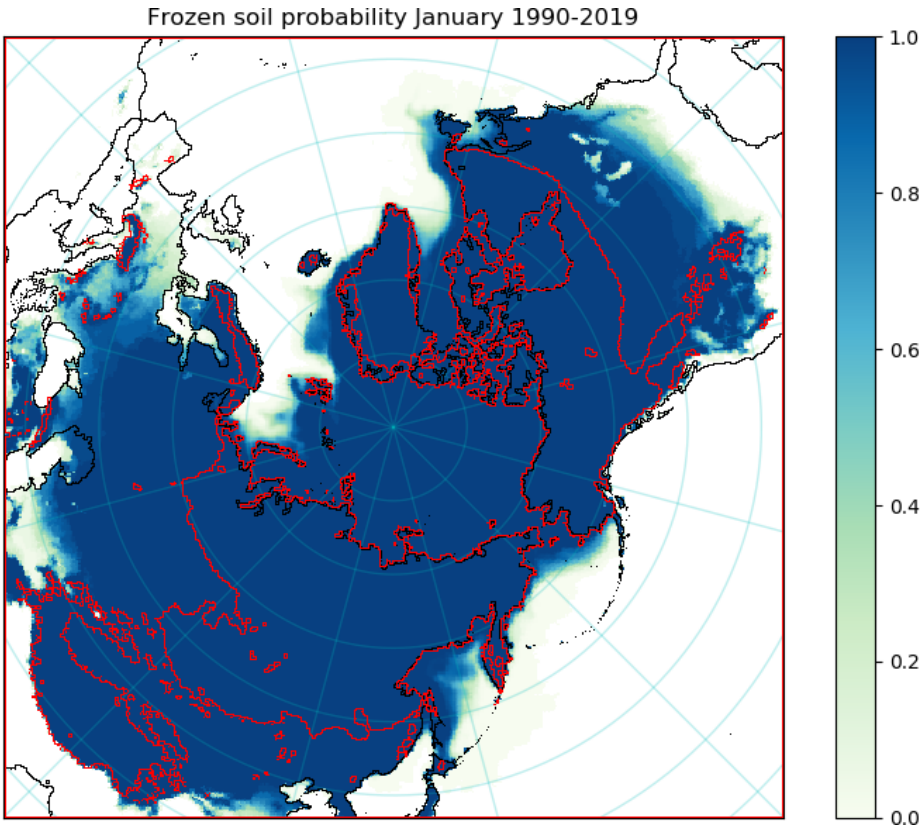

Figure 4: The probability that soil is frozen in the month of January for the period 1990-2019.

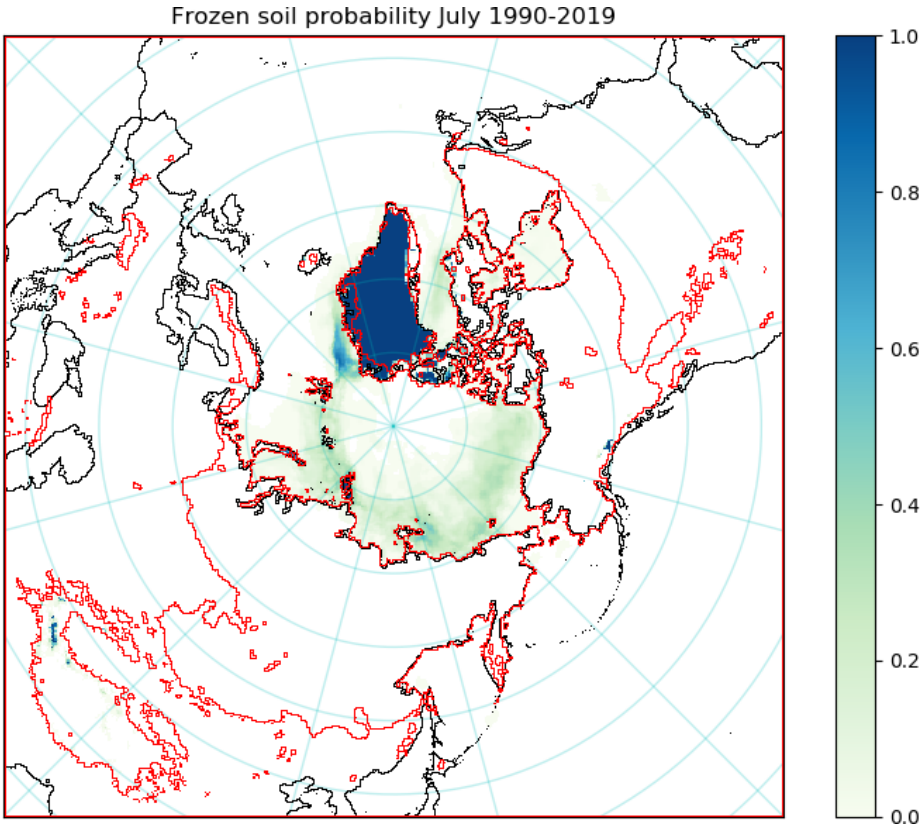

Figure 5: The probability that soil is frozen in the month of July for the period 1990-2019.

3.3 Land-cover

A distinction will be made between precipitation originating from regions covered with tundra, and those covered with taiga. I define the density of tundra cover as

$$tundra = pf \cdot \left(1 - \frac{2t}{s} - b\right) \tag{3}$$

clipped between 0 and 1, where pf is the concentration of permafrost from Brown et al. (2002) (see figure 3), t is the density of tall vegetation cover, s is the density of short vegetation cover and b is the relative amount of bare (non-vegetated) ground, from Song et al. (2018). The equation was designed to resemble figure 2. In short, it means that tundra occurs on permafrost where the cover of short vegetation is twice as dense as the cover of tall vegetation. Taiga is subsequently defined as

$$\begin{aligned} taiga &= pf \cdot (1 - b) - tundra \\ &= pf \cdot \frac{2t}{s} \end{aligned} \tag{4}$$

Hence in this case, it is assumed there is no tundra nor taiga on soils not underlain by permafrost. Note that taiga may refer to boreal forests not underlain by permafrost as well in other literature. The total area covered by tundra defined this way is 8.68 million km^2, for taiga it is 6.77 million km^2.

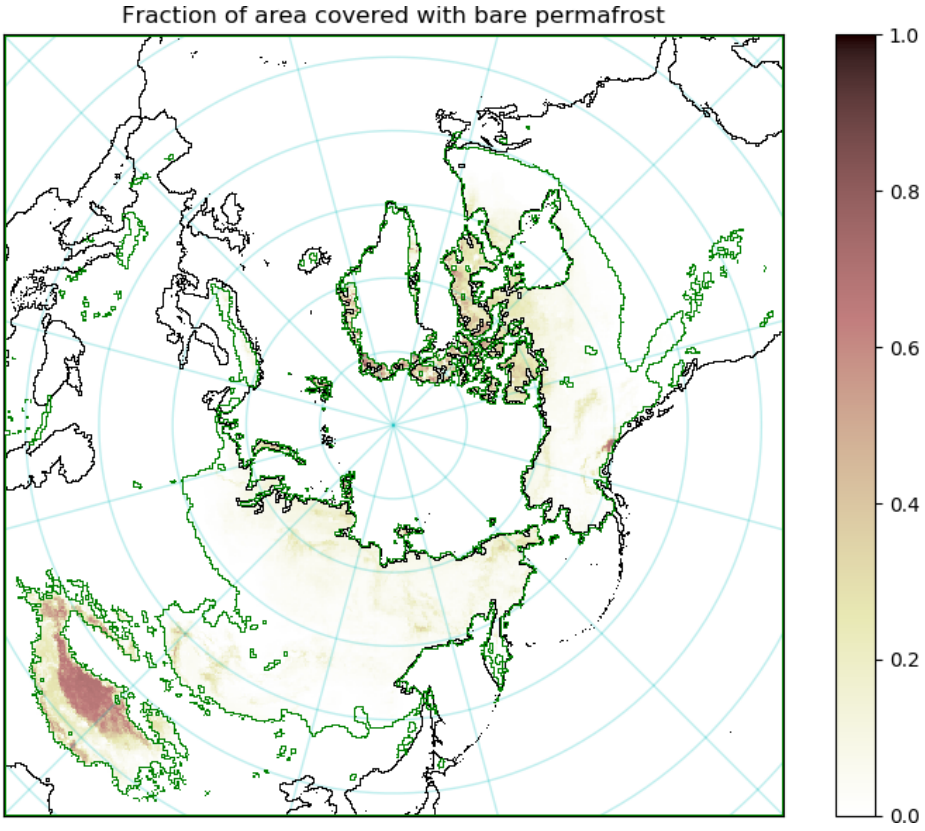

Figure 6: Bare permafrost density for the period 1982-2017.

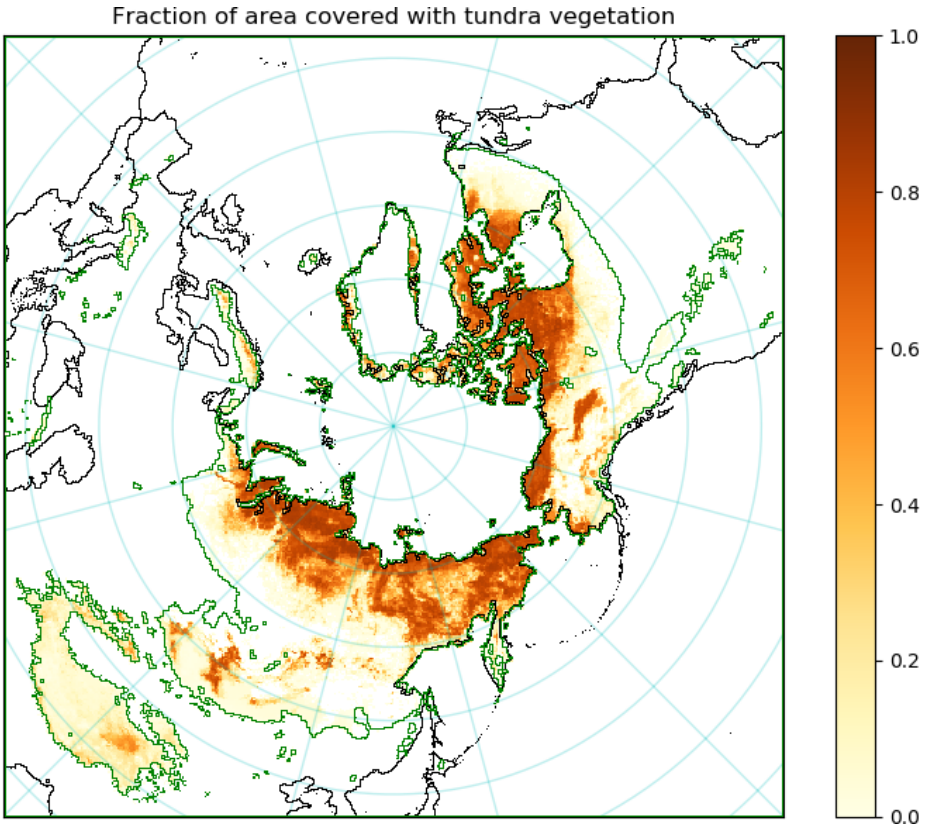

Figure 7: Tundra cover density for the period 1982-2017.

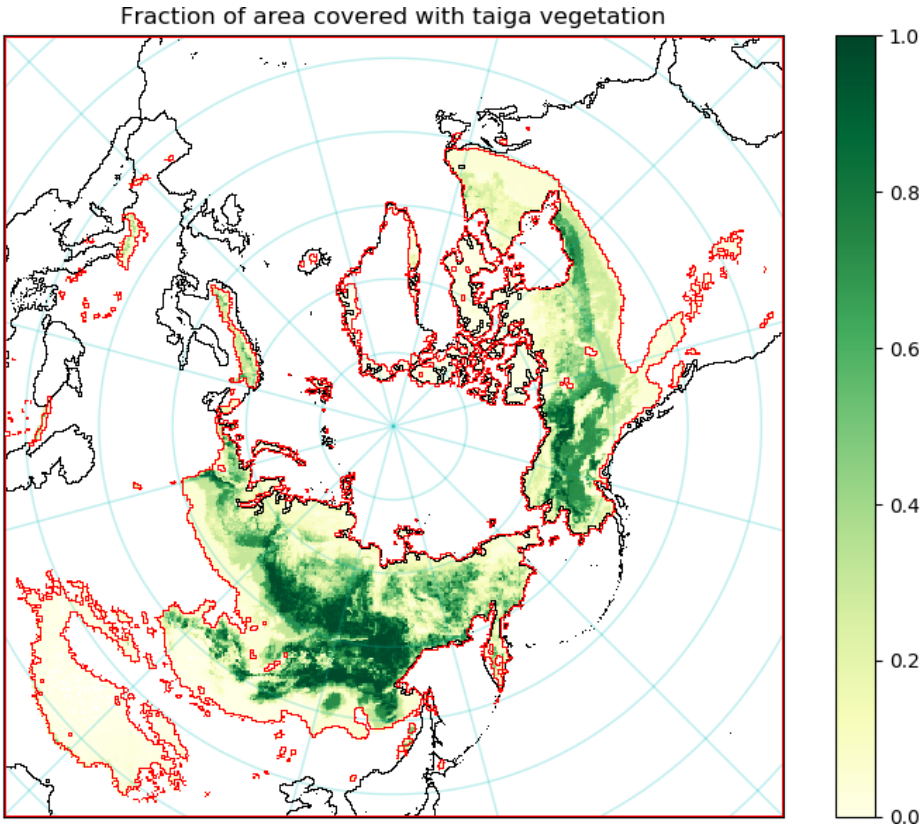

Figure 8: Taiga cover density for the period 1982-2017.

3.4 Evaporation

The evaporation data set used is a combination of evaporation from ERA5 for the ocean, and GLEAM (Miralles et al. (2011), Martens et al. (2017)) for land. At the coast, the average of both data sets is taken. Since the time span of GLEAM is from 2003 to 2018, this time span is taken to be representative of current mean conditions.

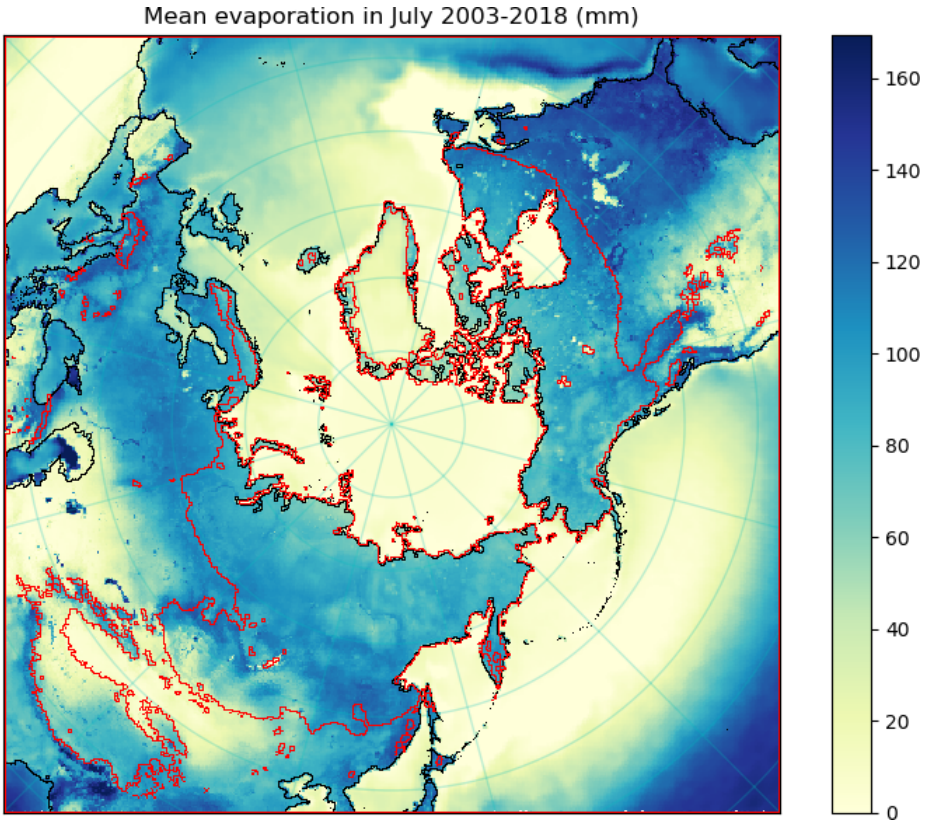

Figure 9: Mean evaporation in July for the period 2003-2018.

3.5 U-track

The moisture tracking scheme U-track returns the precipitation probability for evaporation from each grid cell. The resolution is 0.5x0.5 degree. A map of precipitation sources for a particular month, for precipitation falling on thawed permafrost soil, can thus be made as follows:

$$map_{sources_{i_{thawed}}} = \sum_j \left(\sum (mst_{i,j} \cdot pf \cdot (1 - Q_i)) \right) \tag{5}$$

where $mst_{i,j}$ is the moisture tracking output from U-track for month i for location j and Q_i is the frozen soil probability for the same month. These maps may then be multiplied by evaporation maps to convert the result to $mm\ s^{-1}$. The sink locations for evaporation coming from permafrost soils can also be determined. If this precipitation falls on thawed soils, then

$$map_{sinks_{i_{thawed}}} = \sum_j (evp_{i,j} \cdot mst_{i,j} \cdot pf_j \cdot (1 - Q_i)) \tag{6}$$

where $evp_{i,j}$ is the evaporation in month i from location j, taken from the evaporation dataset described in section 3.4. To obtain the same results for precipitation falling on frozen soils, $(1 - Q_i)$ should be replaced by Q_i.

3.6 Derivation of vegetation relations

3.6.1 Vegetation occurrence

Using the definitions from section 3.3 and climatological data from ERA5, a statistical model for the occurrence of each vegetation type is derived. The climatological parameters which most accurately describe the distribution of taiga and tundra as defined in section 3.3 are found to be the skin reservoir content and the 2 meter air temperature, both averaged over the growing season. Unfortunately the skin reservoir content is not available as a variable in the CMIP6 and ISIMIP archives at the time of my thesis. The second best parameter from ERA5 to be used in combination with the growing season temperature was found to be the soil moisture in layer 2, as defined by ERA5 (swvl2, from 7 to 28 cm below the surface). Since the soil moisture is defined differently in CMIP6 models, a linear combination of various parameters is used to estimate the soil moisture in layer 2. These are 'Moisture in Upper Portion of Soil Column' (mrsos), 'Total Soil Moisture Content' (mrso) and 'Soil Liquid Water Content' (mrlso). By comparing CMIP6 models for the historical climate with ERA5 data for the same period, the following relation was found:

$$swvl2 = 4.269 \cdot 10^{-4} \cdot mrsos + 3.154 \cdot 10^{-4} \cdot mrso - 1.611 \cdot 10^{-5} \cdot mrlso \quad (7)$$

The average deviation of this relation with the swvl2 from ERA5 is 24.4%.

The growing season is defined to be the time for which the 2 meter air temperature is above freezing. The relations are derived for average conditions over the period 1982-2016, because this is the period over which Song et al. (2018) collected data. The difference between the original and reconstructed vegetation data seemed to be related to the growing season sensible heat flux and the growing season mean net short-wave radiation flux. Therefore, a correction based on these variables was also applied.

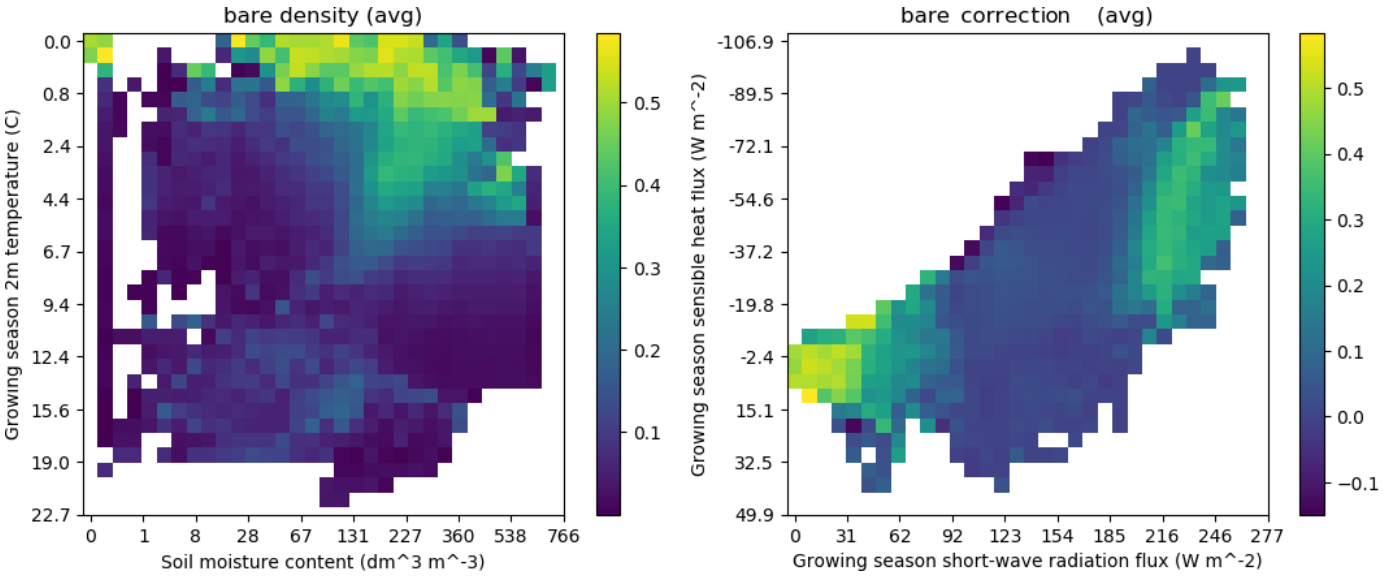

Figure 10: Relations used to estimate the occurence of bare ground

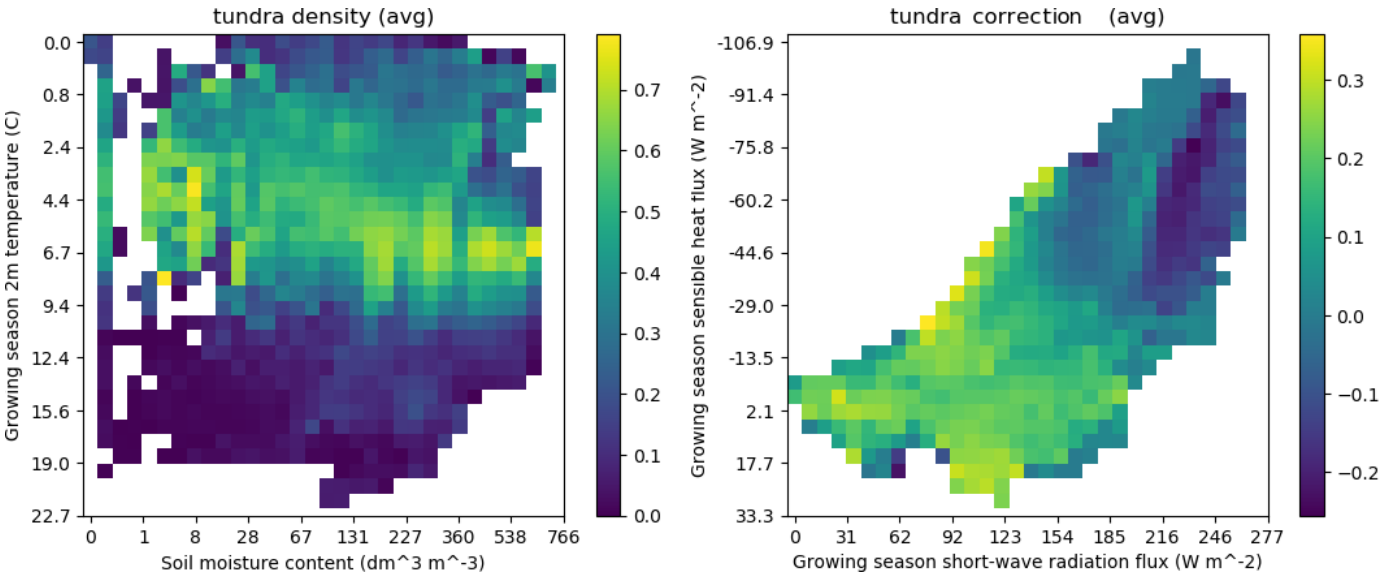

Figure 11: Relations used to estimate the occurence of tundra

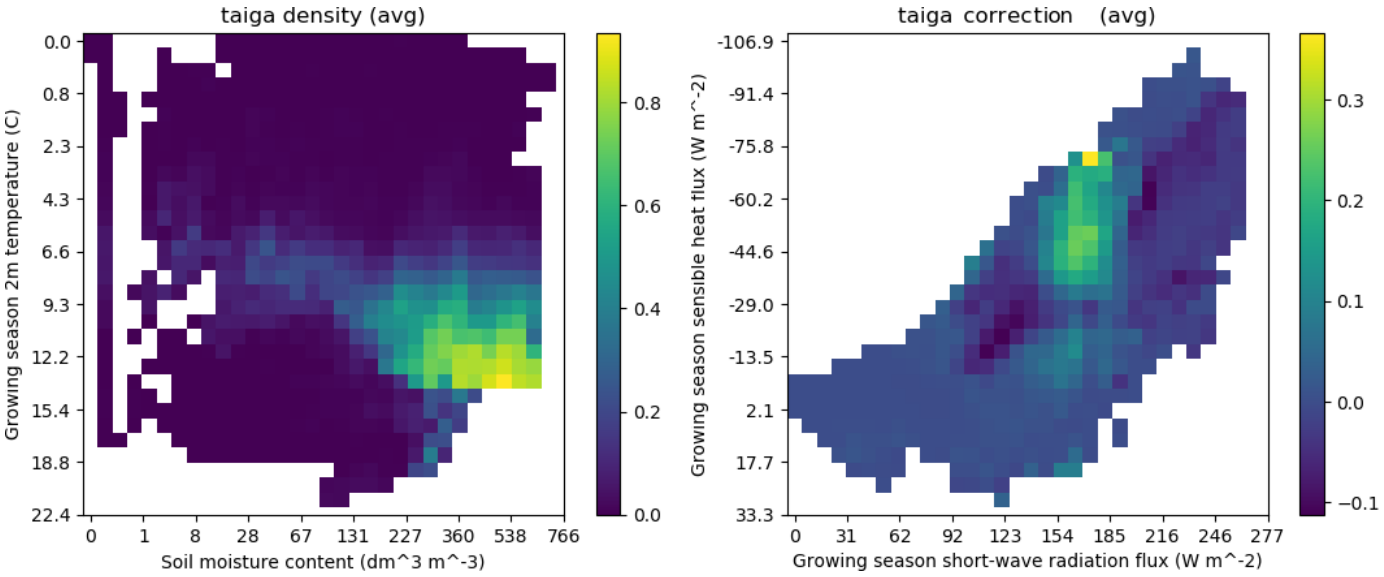

Figure 12: Relations used to estimate the occurence of taiga

In order to ensure as good a coverage as possible for the future scenarios, the regions with no data were filled through linear interpolation. For conditions outside the interpolated range, the vegetation cover is set to bare.

3.6.2 Vegetation evaporation

Using a similar method as above, the amount of evaporation from vegetation types may also be determined. The parameters which best describe the evaporation rate are vapour-pressure deficit and the soil moisture in layer 2, as defined by the ERA5 (swvl2). The vapour-pressure deficit is derived from the 2 meter air temperature and 2 meter dew point temperature. The dew point temperature is the temperature an air parcel would have if it would be saturated with water. In other words, the dew point temperature is the temperature below which water in an air parcel would condensate. To compute the saturation vapour-pressure, the equations from Buck (1996) are used,

$$\begin{cases} P_s(T) = 0.61121e^{\left(18.678-\frac{T}{234.5}\right)\frac{T}{257.14+T}} & T > 0°C \\ P_s(T) = 0.61115e^{\left(23.036-\frac{T}{333.7}\right)\frac{T}{279.82+T}} & T \leq 0°C \end{cases} \tag{8}$$

which are modifications of the equations from Buck (1981). These equations show very small deviations from the observed values for saturation vapour pressure listed in the table from Haar et al. (1984). Vapour-pressure deficit (in kPa) is thus defined as

$$P_{def}(T_a, T_d) = P_s(T_a) - P_s(T_d) \tag{9}$$

where T_a is the 2 meter air temperature and T_d is the 2 meter dew point temperature.

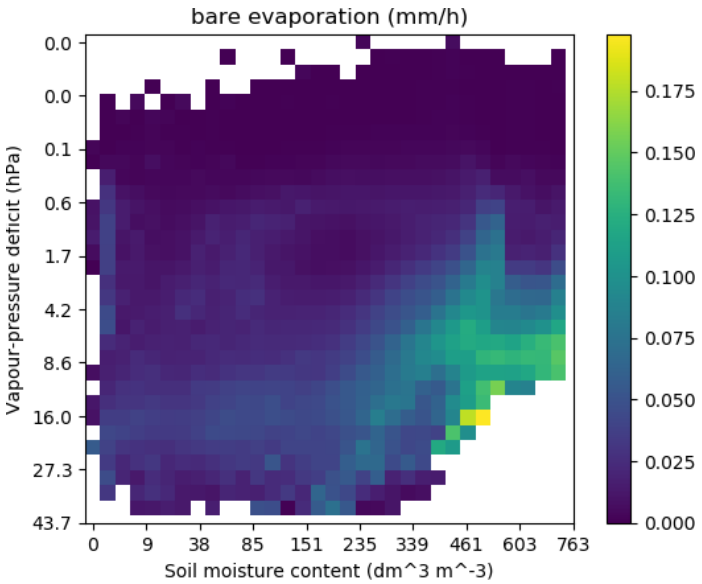

Figure 13: Relation used to estimate the evaporation from bare ground

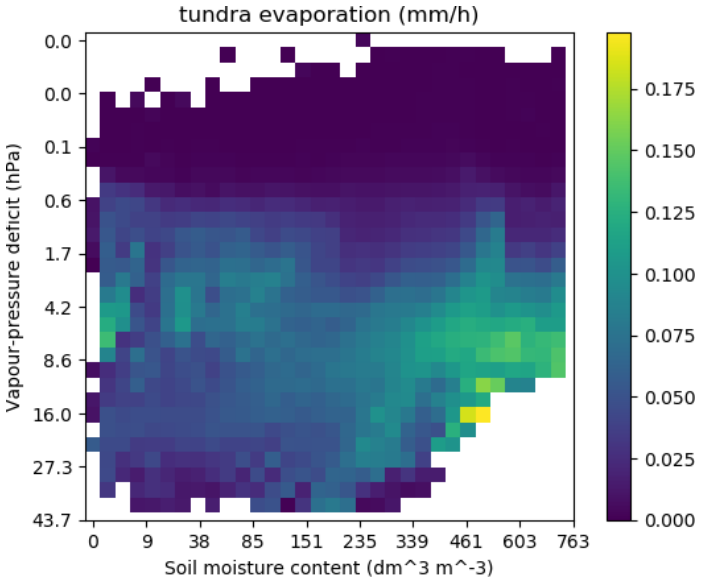

Figure 14: Relation used to estimate the evaporation from tundra

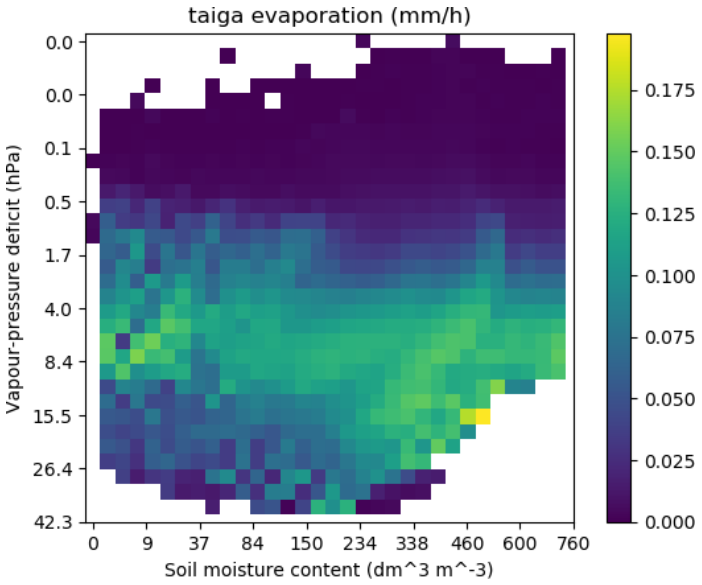

Figure 15: Relation used to estimate the evaporation from taiga

The evaporation data sets used to estimate evapotranspiration from vegetation is from GLEAM. Because the GLEAM data set runs from 2003 to 2018 and the data set from Song et al. (2018) runs from 1982 to 2016, the relations are based on monthly averaged conditions from 2003 to 2016.

From figures 13 to 15 we see that evaporation tends to increase slightly for similar conditions from bare, to tundra and taiga. Although we may therefore expect an evaporation increase in the future due to the northward movement of the treeline, conditions will also change which may in some areas lead to evaporation decrease. As with the vegetation distribution, gaps are filled by linear interpolation.

3.7 Controls on methane emissions

Methane emissions will be estimated from the relation found by Olefeldt et al. (2013):

$$\log_{10}(F_{CH_4+5}) = a + b \cdot {Z_{wt}}^2 + c \cdot {Z_{wt}}^3 + d \cdot T_s + e \cdot Z_{wt} \cdot T_s + f \cdot S_{dom} + g \cdot S_{pres} + h \cdot S_{dom} \cdot T_s \quad (10)$$

where Z_{wt} is the water table depth in cm and T_s is the surface temperature in °C. F_{CH_4+5} is the methane flux in mg CH_4 m^{-2} d^{-1} +5. S_{dom} is 1 if sedges are the dominant type of plant cover, else 0. S_{pres} is 1 if sedges are present but not dominant. The constants are $a = 0.859, b = -4.94 \cdot 10^{-4}, c = -8.96 \cdot 10^{-6}, d = 7.04 \cdot 10^{-2}, e = 1.77 \cdot 10^{-3}, f = 0.926, g = 0.164$ and $h = -5.17 \cdot 10^{-2}$.

Equation 10 is only valid during the growing season. Therefore, the derived methane flux is multiplied with the thawed soil probability defined in section 3.2:

$$F_{CH_4} = F_{CH_4} \cdot (1 - Q) \tag{11}$$

The equation is however very uncertain, and given the lack of large scale methane flux observations, the accuracy of upscaling this equation to pan-Arctic scales is highly uncertain. When converting the values to a linear scale (i.e. getting rid of the logarithm), the standard deviation of the equation with the observations is on average 24.1%.

3.7.1 Sedge cover

Sedges are a family of grass-like plants (Cyperaceae). Areas where the vegetation is dominated by sedges have been shown to emit more CH_4 than areas with similar conditions where this is not the case (see Olefeldt et al. (2013) and references therein). Sedge cover is estimated from the Circum Arctic Vegetation Map (CAVM, CAVM-Team (2003)). This map shows the vegetation physiology for the tundra determined from satellite observations of surface conditions. Sedges occur mostly in moist lowland regions. Based on the descriptions given with the map, I estimate the sedge cover for each physiology as defined by the CAVM, shown in table 1.

Physiology	estimated sedge cover
Barrens	
B1	0.0
B2	0.0
B3	0.0
B4	0.0
Graminoid tundras	
G1	0.1
G2	0.6
G3	0.8
G4	0.9
Prostrate-shrub tundras	
P1	0.5
P2	0.0
Erect-shrub tundras	
S1	0.0
S2	0.0
Wetlands	
W1	1.0
W2	0.9
W3	0.9

Table 1: Sedge cover estimated for each physiology as defined by the CAVM

In order to use the values in table 1 with equation 10, I redefine S_{dom} and S_{pres} as

$$\begin{cases} S_{dom} = 2(S - 0.5) \\ S_{pres} = 1 - 2|S - 0.5| \end{cases} \tag{12}$$

clipped between 0 and 1, where S is the estimated sedge cover. The uncertainty in S_{dom} and S_{pres} is estimated to be 0.2.

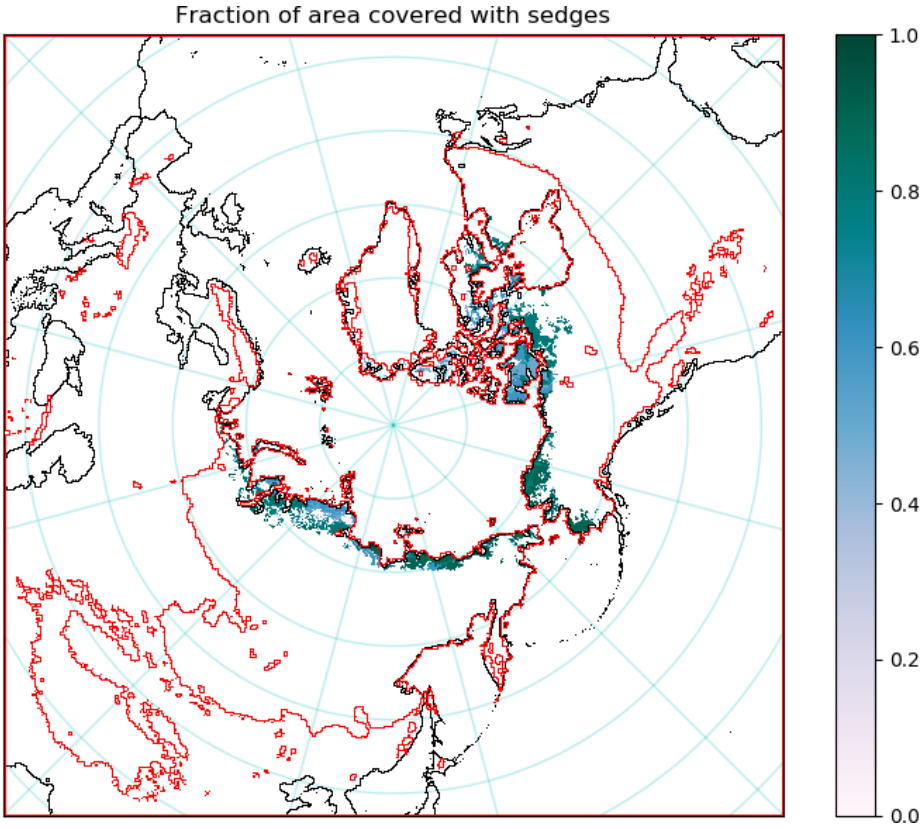

Figure 16: Sedge cover density estimated from CAVM data.

3.7.2 Water table depth

The water table depth has a large influence on the CH_4 flux as predicted by equation 10 from Olefeldt et al. (2013). To obtain pan-Arctic data for water table depth, modelled water table depth data provided by Reinecke et al. (2019) is used. This dataset represents steady-state conditions in the current climate. The dataset does not show any relation with the observations listed in Olefeldt

et al. (2013). This may be because the observations might not represent steady-state conditions, nor the average conditions of the size of the pixels from the model from Reinecke et al. (2019). In an attempt to make the model results from Reinecke et al. (2019) compatible with equation 10, the model results are scaled such that the mean and the standard deviation equal those of the observations from Olefeldt et al. (2013) at the same locations. For Greenland, which is not included in the dataset from Reinecke et al. (2019), the water table depth was assumed to be 0. The influence of Greenland on this particular study is thought to be minimal, due to the large ice cap where negligible organic decomposition occurs. A seasonal cycle is estimated by adding the difference of the total monthly precipitation, snow melt, run-off and evaporation to the average over the months June up to and including September (the period in which the observations were taken).

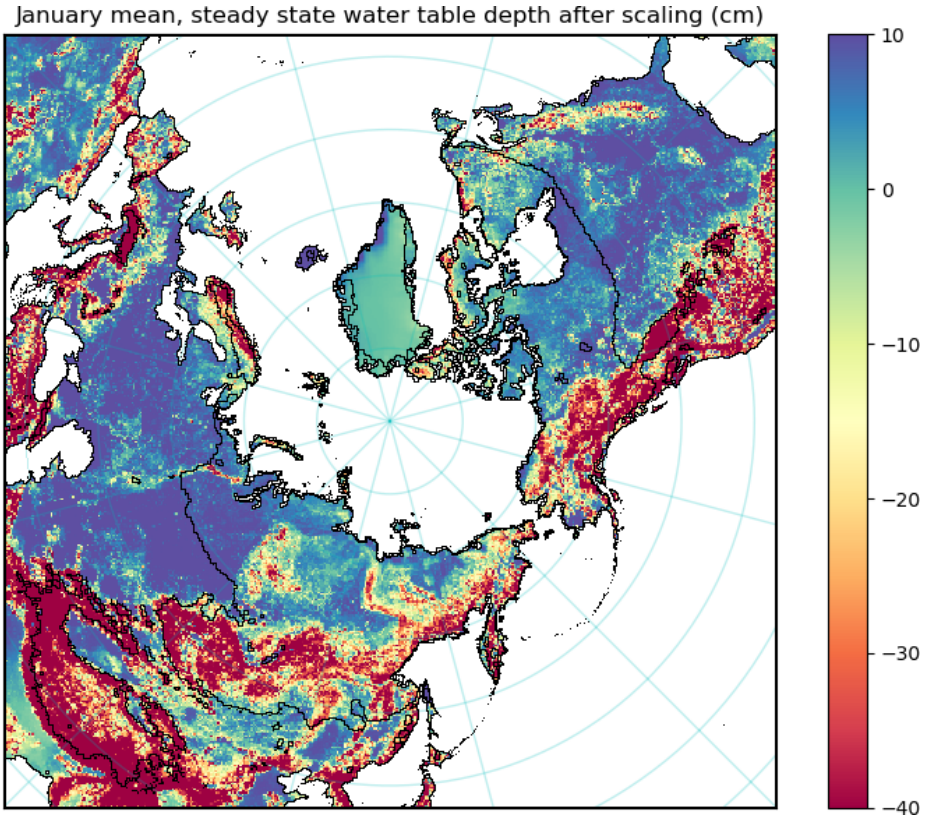

Figure 17: Water table depth in cm for January after the scaling procedure.

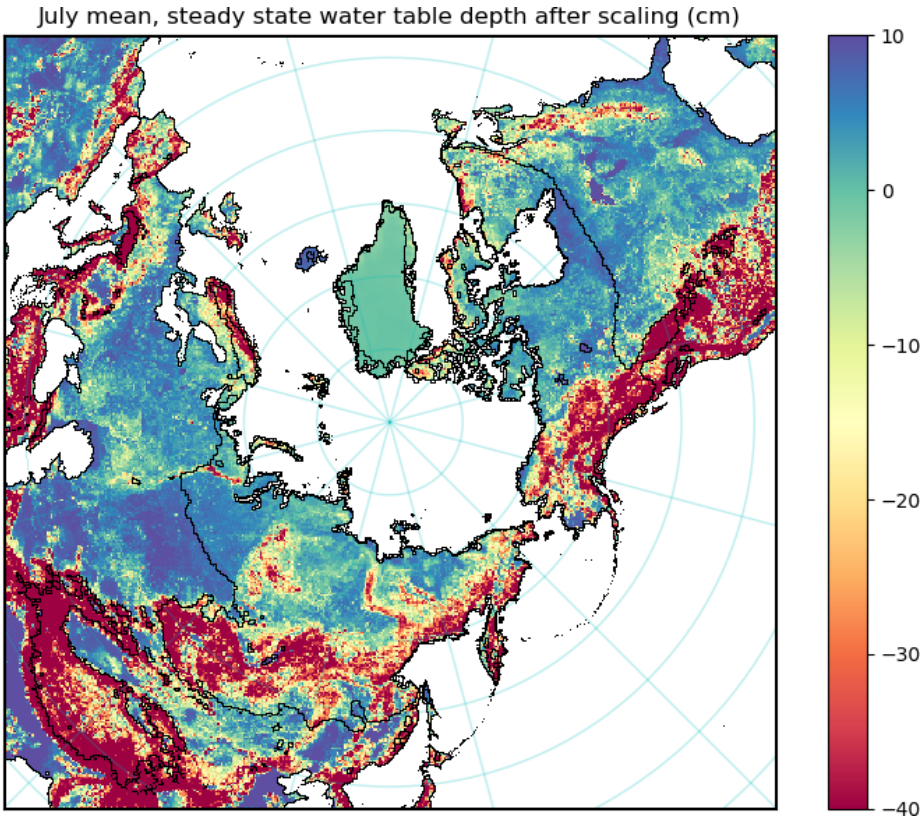

Figure 18: Water table depth in cm for July after the scaling procedure

We see that after scaling, large parts of western Siberia and eastern North America are flooded in January. These regions do not have a large influence on the predicted methane flux from the permafrost, as will be shown in the next section.

3.7.3 Sensitivity of methane emissions to changes in water table depth

In order to estimate how future changes in precipitation patterns may change methane emissions from permafrost, the sensitivity of methane emissions to changes in water table depth needs to be known. This is acquired by derivation of equation 10 with respect to Z_{wt} after eliminating the logarithm:

$$F_{CH_4} = 10^{\log_{10}(F_{CH_4}+5)} - 5 \tag{13}$$

$$\begin{aligned}\frac{\partial F_{CH_4}}{\partial Z_{wt}} &= \frac{\partial}{\partial Z_{wt}}\left(10^{\log_{10}(F_{CH_4+5})} - 5\right) \\ &= ln(10)\cdot 10^{\log_{10}(F_{CH_4+5})}\cdot\frac{\partial}{\partial Z_{wt}}\log_{10}(F_{CH_4+5}) \\ &= ln(10)\cdot 10^{a+b\cdot {Z_{wt}}^2+c\cdot {Z_{wt}}^3+d\cdot T_s+e\cdot Z_{wt}\cdot T_s+f\cdot S_{dom}+g\cdot S_{pres}+h\cdot S_{dom}\cdot T_s} \\ &\quad\cdot(2b\cdot Z_{wt}+3c\cdot {Z_{wt}}^2+e\cdot T_s)\end{aligned} \tag{14}$$

Combining all discussed datasets and equations allows to estimate the methane flux and sensitivity to changes in the water table depth. Using equation 10, figure 19 shows the expected methane emission flux.

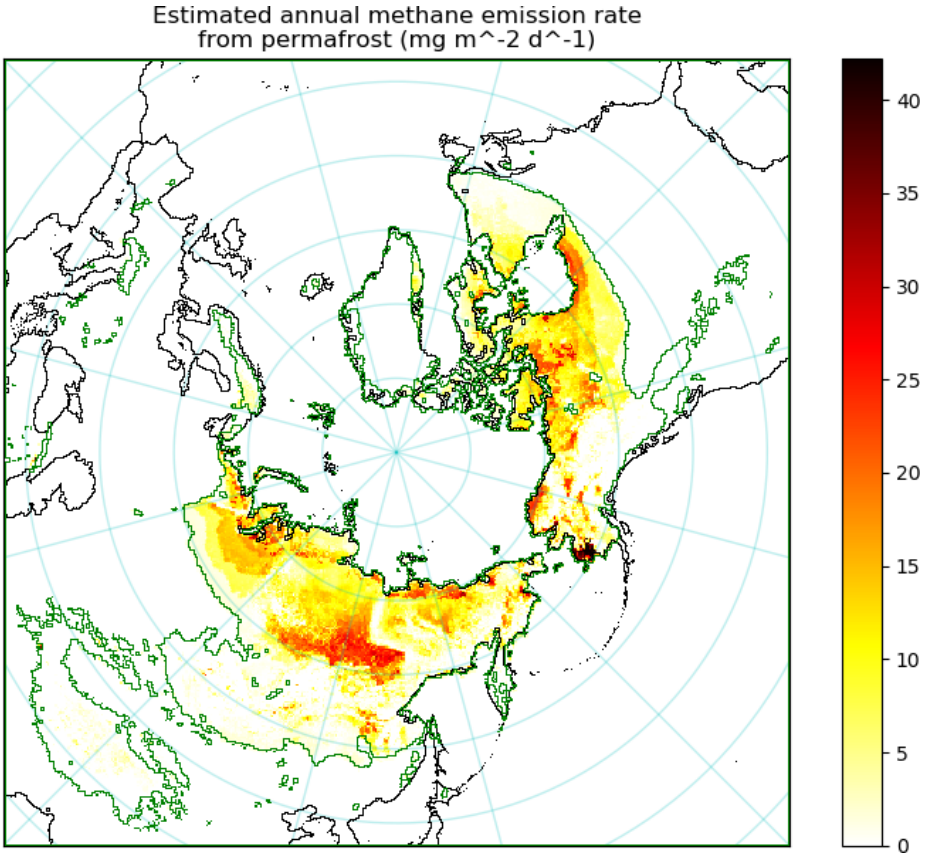

Figure 19: Estimated annual methane emission rate from permafrost.

The highest methane flux is thus expected in Southwest Alaska in the Yukon-Kuskokwim delta. This is a wet region with relatively high temperatures (for the permafrost) throughout the year, but cool summers such that there exists

mostly tundra cover. This tundra is rich in sedges. These factors contribute to the high expected methane flux in this region. As an example, the mean annual temperature for the city of Bethel is -1°C and the mean July temperature is 13°C (NOAA, 2020).

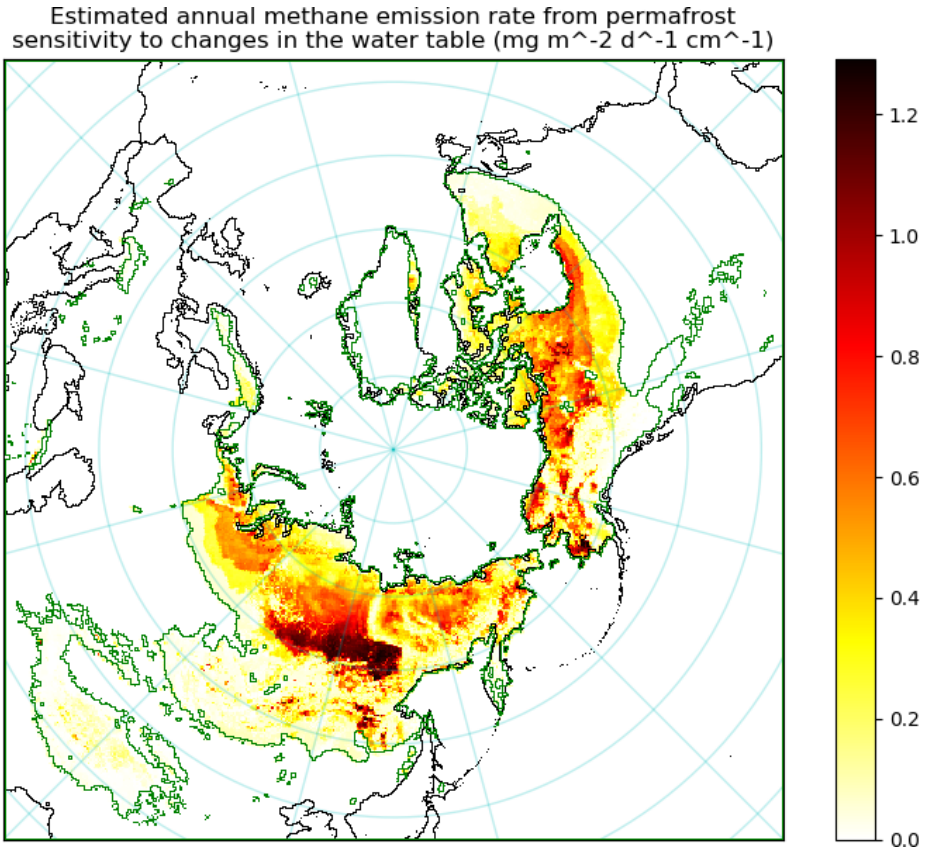

Figure 20: Estimated annual methane emission rate from permafrost sensitivity to changes in the water table depth

When using equation 14, we obtain figure 20 which shows the amount the methane flux would increase in mg m^{-2} d^{-1} if the water table would increase by 1 cm. We see that, besides the Yukon-Kuskokwim delta mentioned earlier, there is a large region between the Aldan and Vilyuy rivers in central Siberia which is highly sensitive to increasing wetness. This is a very continental region, with extremely cold winters but also warm summers. The high summer temperatures are beneficial for methane release. Currently the region is relatively dry and covered with taiga forest. But increased wetness could cause a large increase of methane release in summer. For example, the average July temperature in

Yakutsk is 19.5°C (Pogoda, 2020).

Note that there is currently no public dataset which shows the same variable and therefore the accuracy of the predictions from figures 19 and 20 can not be determined.

3.8 Future scenarios

3.8.1 Models and scenarios

The changes that occur in the hydrological cycle in the Arctic depend on the scenario. I choose to study the most divergent scenarios, pre-industrial control and RCP8.5 for the time period 2070-2100, as defined by the IPCC (2014). These scenarios are compared to reanalysis data from ERA5 (Copernicus Climate Change Service, 2017) and historical runs from CMIP6 and ISIMIP to quantify the changes. For all scenarios, I assume that all models are equally valid and that the most accurate representation of future climates is the mean of as many models as possible. As not all models report the same variables, not all models are available for all variables. ISIMIP models are used for evaporation and runoff over land. Evaporation over the ocean is taken from CMIP6 models. A full list of models used for each variable in each scenario can be found in the appendix.

3.8.2 Remnants of the mammoth steppe

Although the mammoth steppe ecosystem has largely disappeared after the onset of the Holocene (Dale Guthrie, R. (2001), Zimov et al. (2012)), there are still areas in Central-Asia where the ecosystem is similar to the mammoth steppe. Pavelková Řičánková et al. (2014) have identified the Altai-Sayan mountains as such a region. I assume that the short vegetation in this region behaves like the mammoth steppe vegetation. To define a region from which evaporation data will be extracted, I make use of the WWF Terrestrial Ecoregions of the World dataset (Olson et al., 2001). I define the mammoth steppe region as consisting of the contiguous part of the following terrestrial ecoregions defined by Olson et al. (2001):

- Altai alpine meadow and tundra
- Sayan intermontane steppe
- Sayan alpine meadows and tundra
- Selenge-Orkhon forest steppe
- Great Lakes basin desert steppe
- Khangai mountains alpine meadow
- Khangai mountains conifer forest

- the Mongolian part of the Altai montane forest and forest steppe

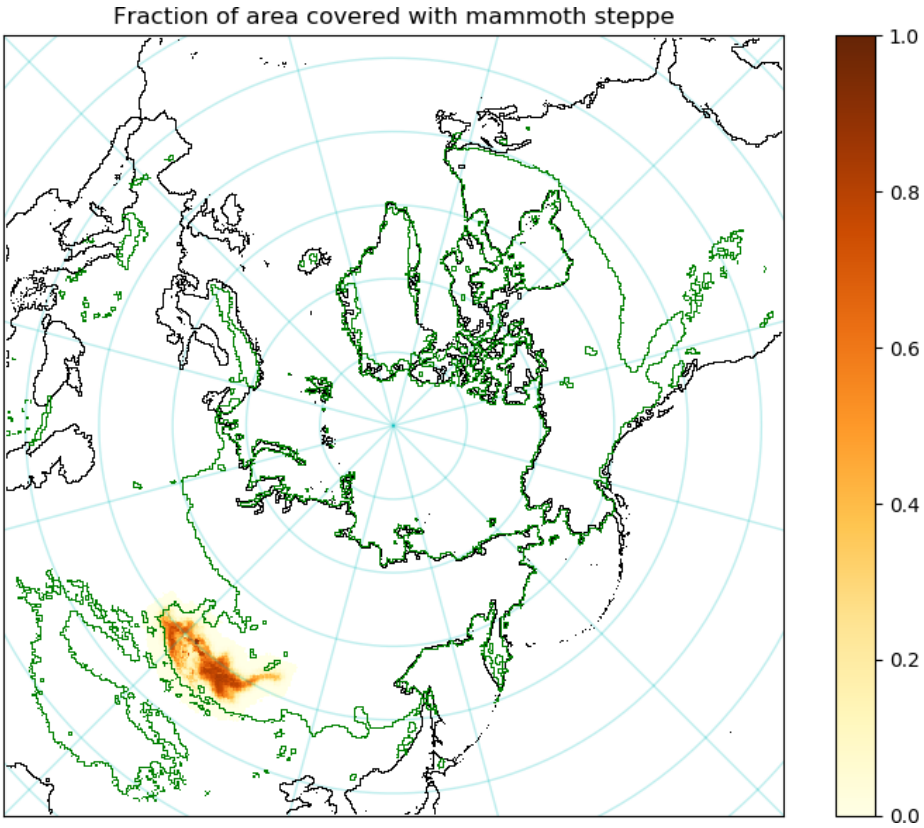

Figure 21: Mammoth steppe density for the period 1982-2017.

The resulting mammoth steppe density is shown in figure 21. Figure 22 shows the relation for evaporation that is found for short vegetation in these areas, relative to what was determined for tundra. In general, the evaporation is lower than for tundra. Therefore, we might expect drying in regions which receive precipitation from the tundra in a scenario where the tundra would be replaced by mammoth steppe. This is opposite to what is expected from the Pleistocene Park (Zimov, 2005).

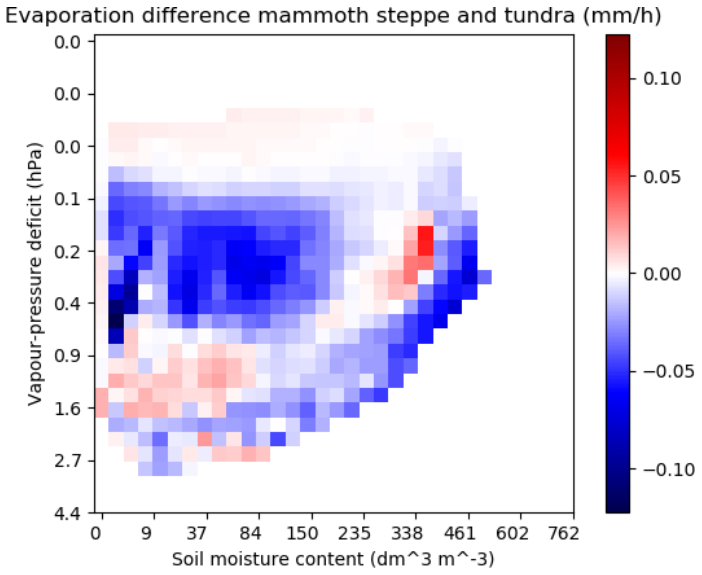

Figure 22: Relation used to estimate the evaporation from mammoth steppe, relative to the evaporation from the tundra from figure 14

The expectation for the Pleistocene Park is that soil moisture content will decrease when tundra is replaced by a steppe ecosystem (Zimov, 2005). It is however not clear how large the decrease will be. Therefore, in predicting evaporation from the mammoth steppe, the soil moisture content is not changed. The results can be interpreted as representing an upper limit to the evaporation, as evaporation generally increases with soil moisture content.

Although Zimov (2005) notes that increased transpiration from grasses cause drying of the soil when replacing tundra with steppe, this is not apparent from the relation shown in figure 22. Evaporation from mammoth steppe appears to only exceed evaporation from tundra in very specific conditions. Possible explanations include that either the region used here does not accurately depict the expected vegetation type for the Pleistocene Park, or that there are other environmental factors outside those studied here that decrease the evaporation. Although transpiration might increase, other forms of evaporation may decrease to yield an overall decrease in total evaporation. Finally, the uncertainty in the relation found here may be larger than the evaporation it predicts.

The results regarding a restoration of the mammoth steppe in the tundra will therefore be limited to assessing which regions will be most affected by such a change. It is as of yet unclear whether this change will be positive or negative. For these results, see section 4.3.3.

4 Results

4.1 Accuracy of statistical models

4.1.1 Vegetation distribution

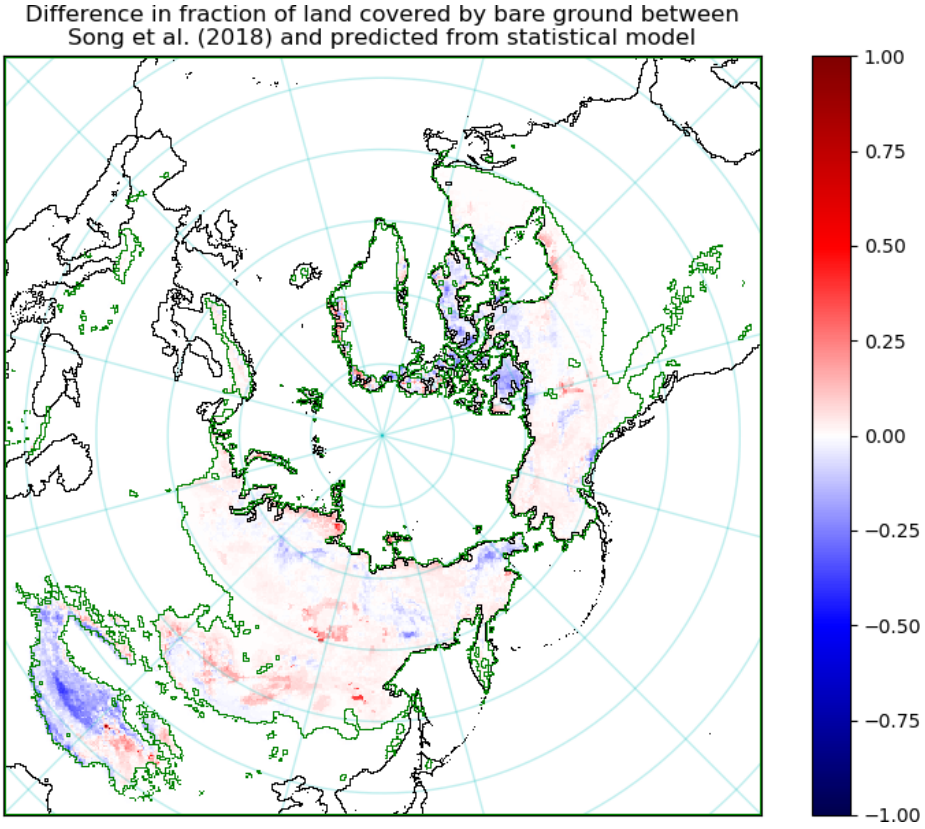

Figure 23: Difference between predicted bare ground and data from Song et al. (2018) for 1982-2017.

The accuracy of the statistical models described in sections 3.6.1 and 3.6.2 is assessed by comparing the predictions from the statistical model for the present with the original data used to derive the statistical model. The expected distribution of vegetation types, based on the growing season skin reservoir content and 2m air temperature, is compared with data from Song et al. (2018). Averaged over the permafrost area, the difference is 3.6% for bare ground, 7.8% for tundra and 7.6% for taiga before a correction based on growing season sensible heat flux and short-wave radiation is applied. After this correction, these reduce to 3.2%, 7.3% and 6.6% respectively. However, the difference between original

and predicted datasets is highly variable in geographic distribution, and can be up to 60%.

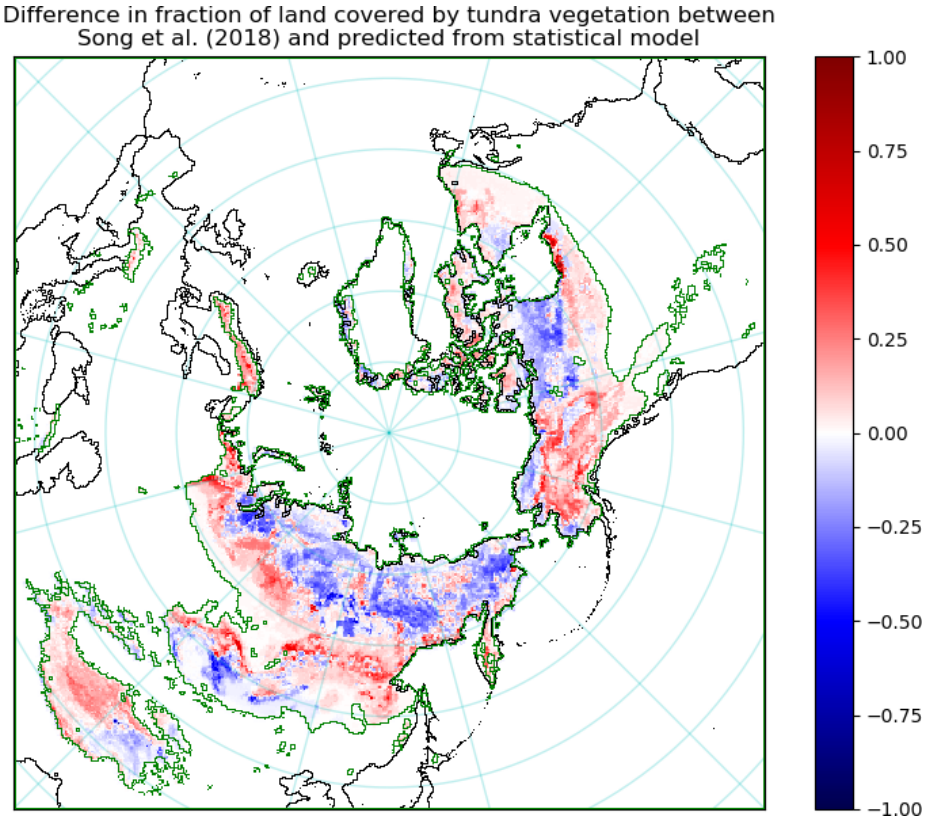

Figure 24: Difference between predicted tundra cover and data from Song et al. (2018) for 1982-2017.

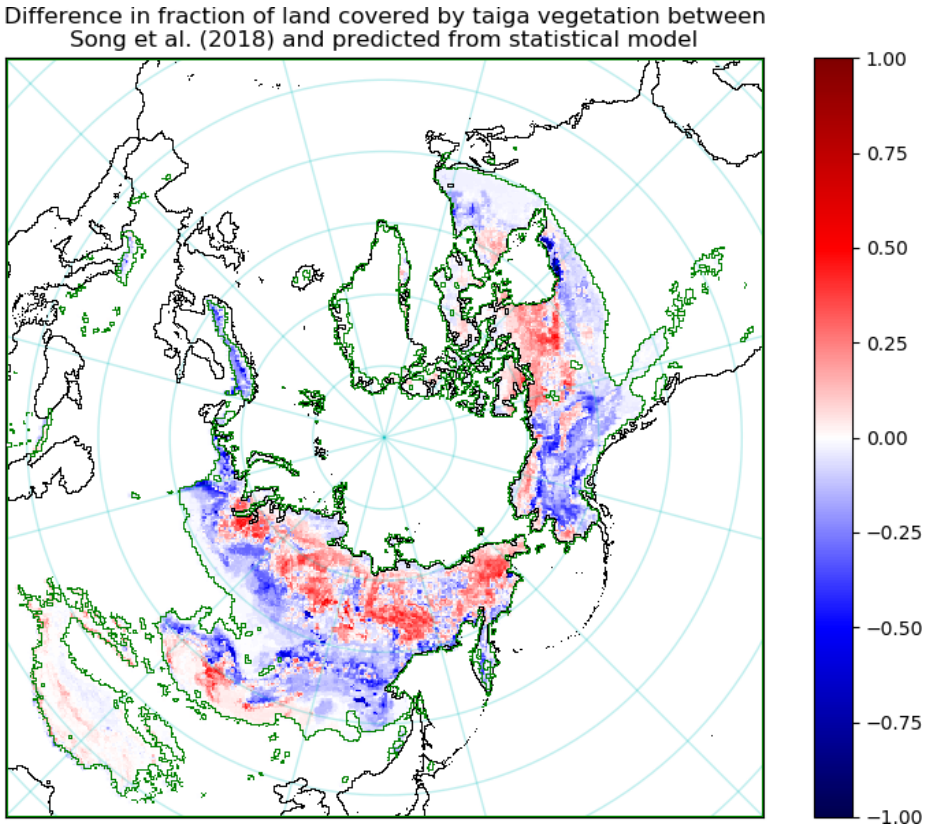

Figure 25: Difference between predicted taiga cover and data from Song et al. (2018) for 1982-2017.

Plotting the reconstructed vegetation distribution against the observations and making a best fit line shows that this line is very close to the line of equality. Hence the residuals do not depend on the vegetation cover density itself. The occurrence of taiga is predicted to be slightly lower than observed (figure 28). I choose not to correct for this discrepancy as it is uncertain whether the same deviation can be expected in future climates. The standard deviation from this line is 2.6% for bare ground, 3.4% for tundra and 3.1% for taiga.

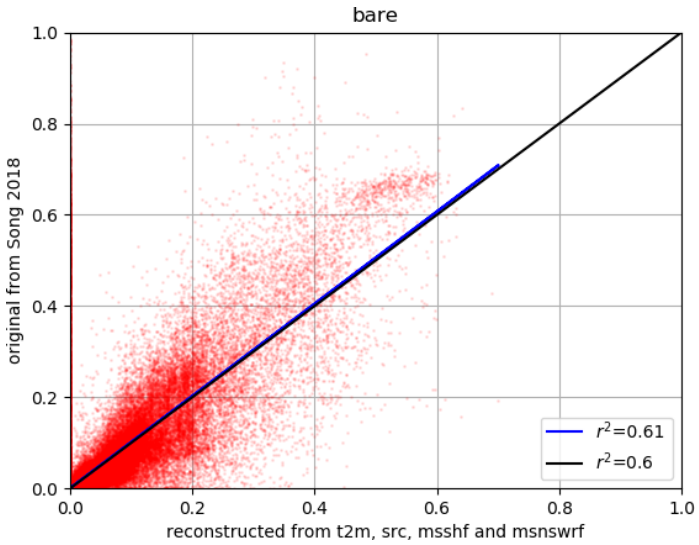

Figure 26: Fit (blue) to the reconstructed bare ground fraction with the data from Song et al. (2018) compared with the line of equality (black).

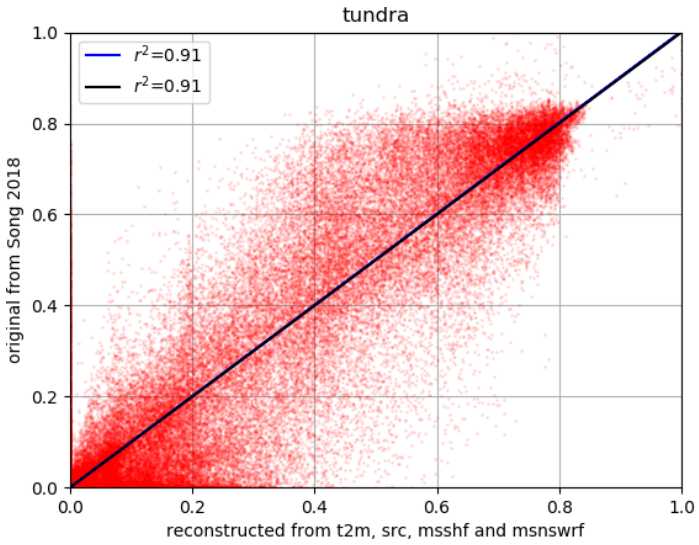

Figure 27: Fit (blue) to the reconstructed tundra fraction with the data from Song et al. (2018) compared with the line of equality (black)

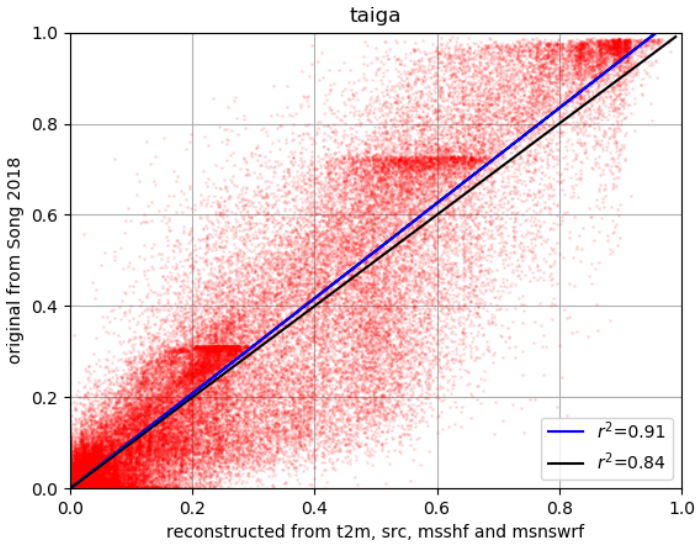

Figure 28: Fit (blue) to the reconstructed taiga fraction with the data from Song et al. (2018) compared with the line of equality (black)

4.1.2 Vegetation evaporation

The performance of the statistical model for evaporation is assessed by predicting the vegetation distribution first, after which the evaporation is predicted for each vegetation type. The deviation between the model and observations thus also includes the deviation in the vegetation distribution model. The average relative difference over the year between predicted evaporation and data from GLEAM is 20.8%. At 31.7%, the evaporation coming from bare ground shows a significantly higher deviation. Evaporation originating from tundra vegetation shows a 23.5% deviation with GLEAM data while for taiga this is 15.1%. As with the vegetation distribution model, the deviation varies greatly across the permafrost area. Areas where the model performs worse than average are tundra areas around the Hudson Bay, the Arctic coast of East-Siberia, Mongolia and Tibet. The Canadian Arctic archipelago, West-Siberian tundra regions and taiga regions in general perform better than average.

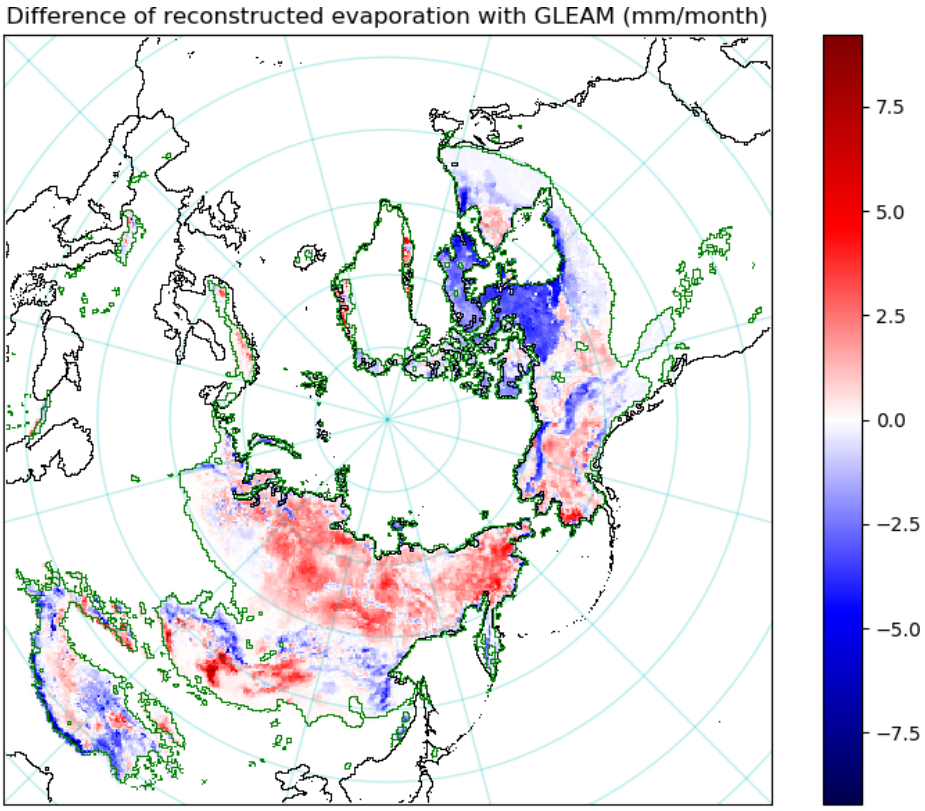

Figure 29: Difference between predicted evaporation and data from GLEAM for 2003-2017. Blue indicates regions where the predicted evaporation is lower than observed.

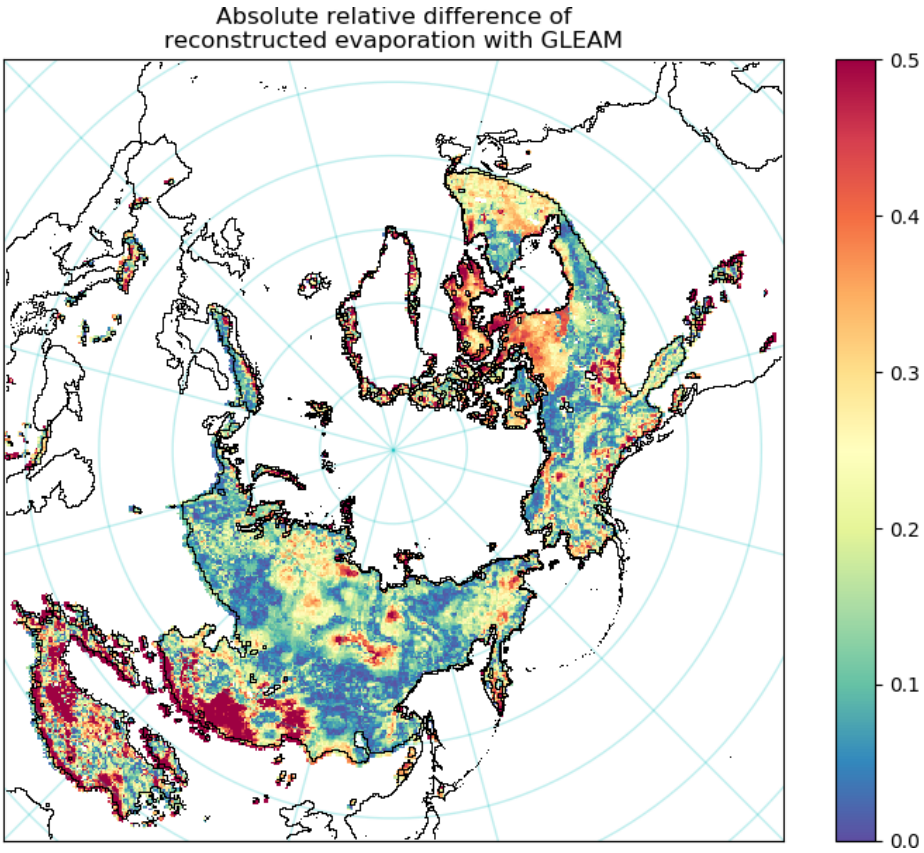

Figure 30: Absolute relative difference between predicted evaporation and data from GLEAM for 2003-2017.

Annual reconstructed evaporation corresponds well with annual evaporation observed by GLEAM (figure 31). For high evaporation rates, the reconstructed evaporation is too low more often than for low evaporation rates.

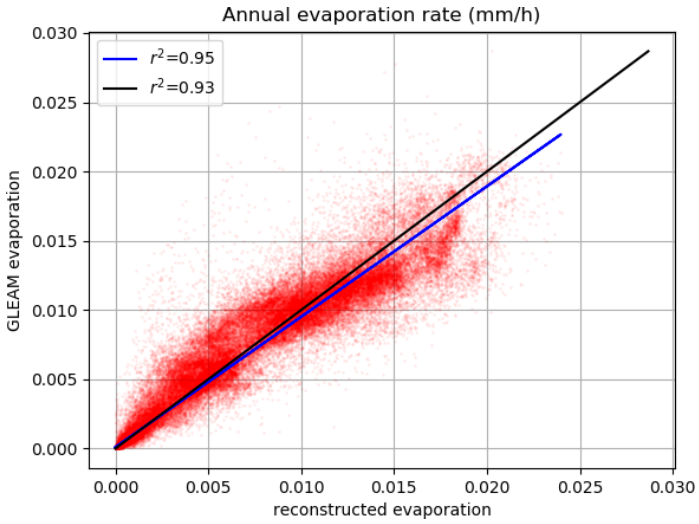

Figure 31: Fit (blue) to the reconstructed evaporation with the data from GLEAM compared with the line of equality (black)

4.2 Future scenarios

The future scenarios studied are the pre-industrial control scenario (piControl) and the most extreme global warming scenario RCP8.5, as defined by IPCC (2014). These are the most divergent scenarios used by the IPCC (2014) and are therefore expected to show the most prominent changes.

4.2.1 Vegetation cover and evaporation

Vegetation cover for the future scenarios was not estimated directly using the variables discussed in section 3.6.1. Instead, the predicted vegetation cover for the future scenarios was compared with the prediction for the current climate (see also section 4.1.1). The difference between the prediction for the current climate and both future climates was added to the vegetation definitions derived from Song et al. (2018) (see figures 6 to 8). The final vegetation distribution predictions for both scenarios are made by scaling these data such that bare, tundra and taiga vegetation sum to 1 everywhere on the permafrost. For my thesis, I am interested in the changes that occur due to vegetation change in these scenarios relative to the current situation. Therefore, I will report only predicted change for all variables in future scenarios, rather than their absolute values. Tundra and taiga cover are most interesting for the following analysis. Therefore bare ground cover is not shown.

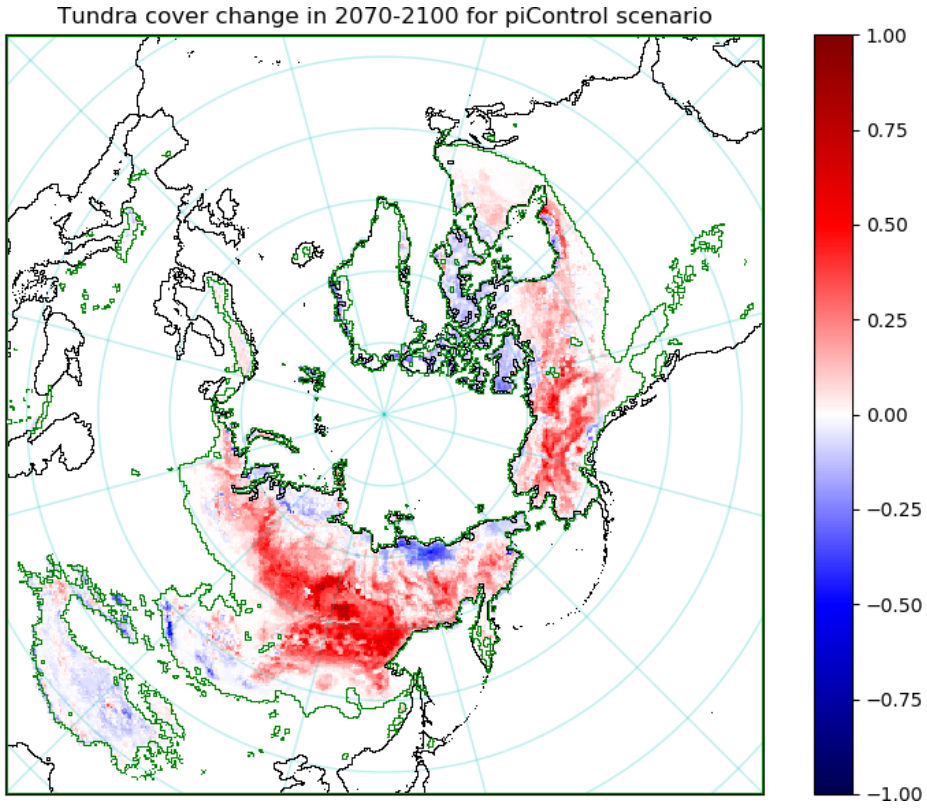

Figure 32: Change of tundra vegetation cover, relative to the data from Song et al. (2018) for the piControl scenario.

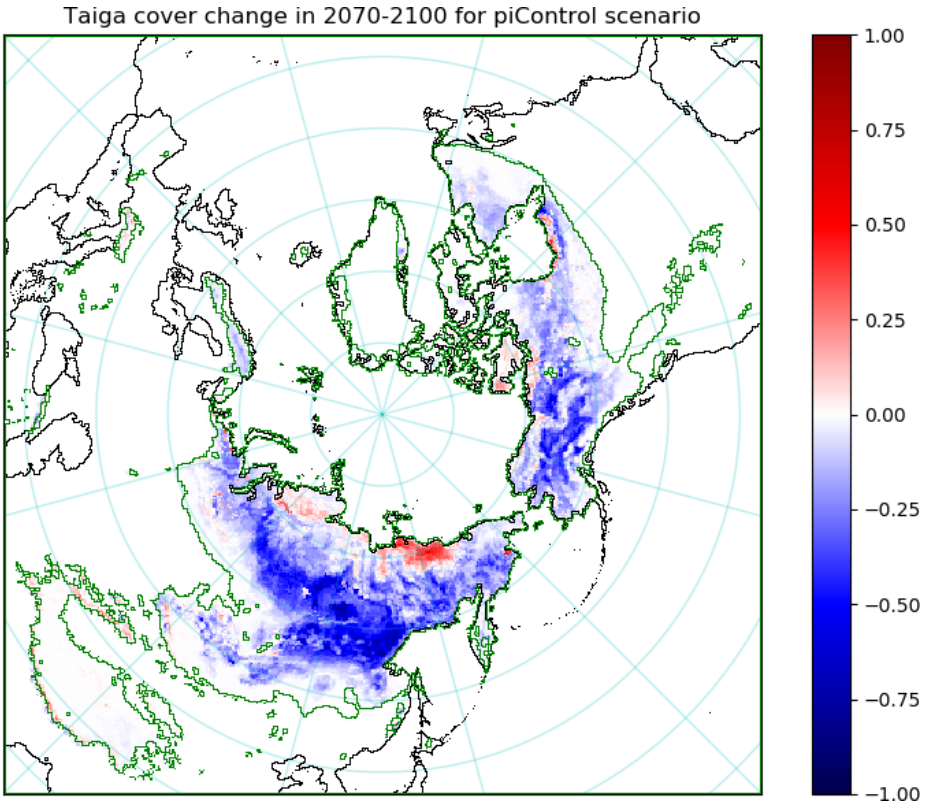

Figure 33: Change of taiga vegetation cover, relative to the data from Song et al. (2018) for the piControl scenario.

In the pre-industrial control scenario, average temperatures are lower than today (figure 32). This causes all vegetation bands to migrate southwards. The increase of taiga seen in figure 33 in northern Siberia is not realistic. This is due to uncertainty in the cold region of the statistical model for taiga.

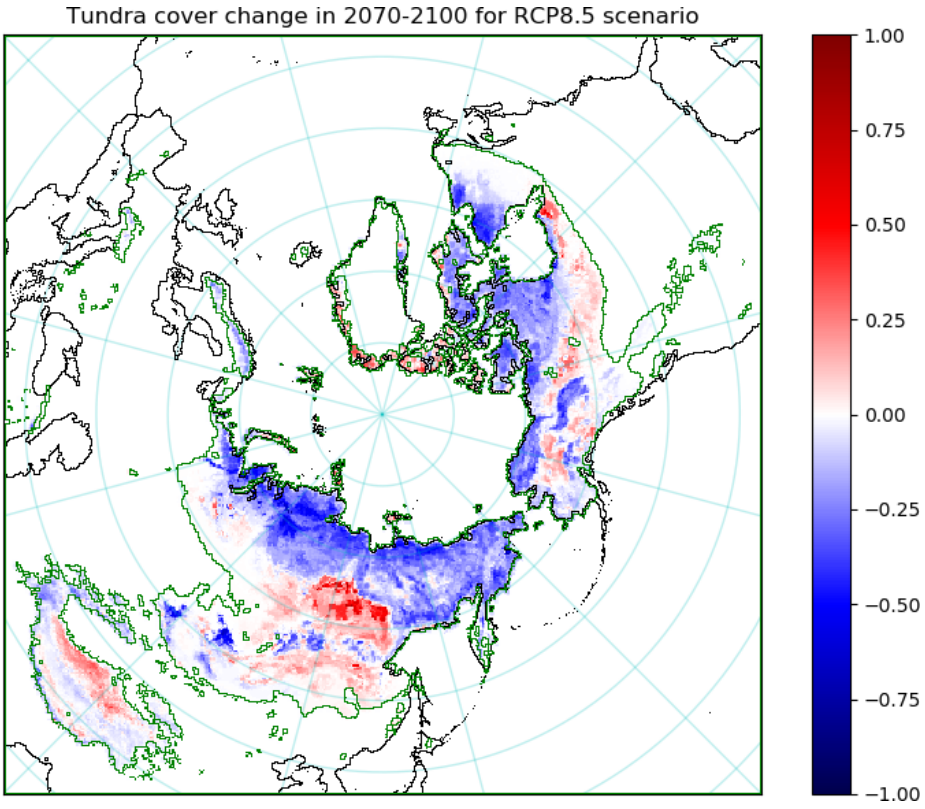

Figure 34: Change of tundra vegetation cover, relative to the data from Song et al. (2018) for the RCP8.5 scenario.

In the RCP8.5 scenario, we see that vegetation bands migrate northwards, due to increased temperatures (figure 34). An exception occurs in the southern Lena river basin in central Siberia. Higher values for the soil moisture content are predicted here which favour tundra cover despite the high temperatures. Whether it is realistic that taiga cover decreases over this area is not clear. It seems unlikely though that it would be replaced with tundra cover.

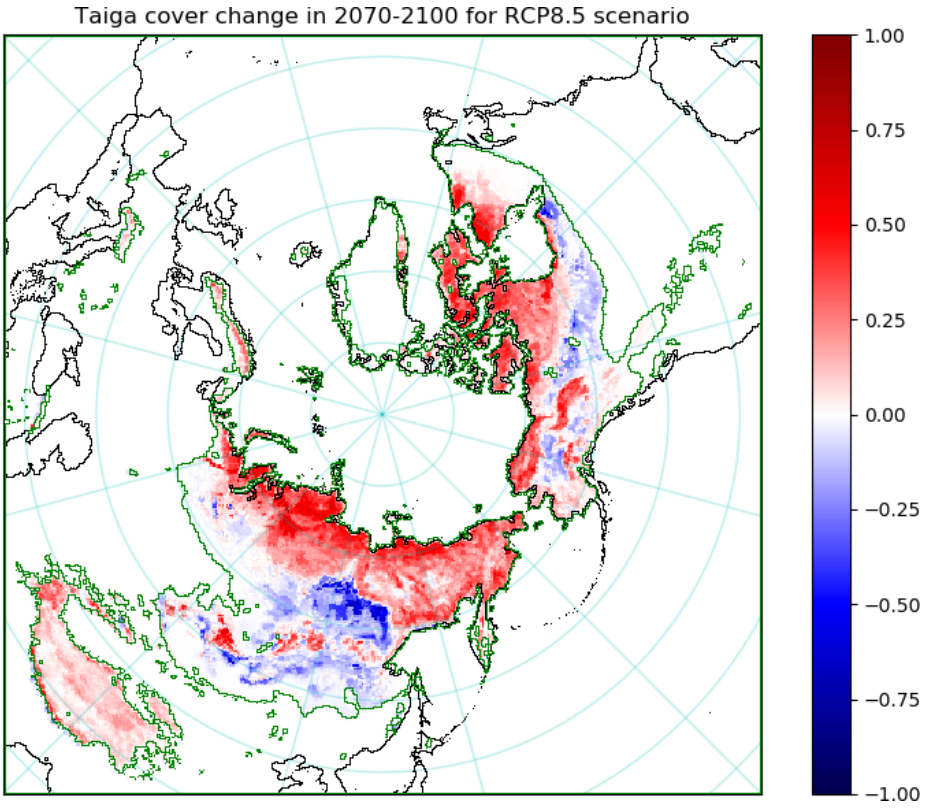

Figure 35: Change of taiga vegetation cover, relative to the data from Song et al. (2018) for the RCP8.5 scenario

4.2.2 Predicted evaporation change due to vegetation change

Assuming that bare ground, tundra and taiga vegetation will evaporate the same amount of water under the same conditions in the future, we can use the statistical models derived in section 3.6.2 to estimate changes in evaporation in the future due to the changes we have seen occurring in the vegetation cover in the previous section. The results are split in thawing ('summer') and freezing ('winter') seasons, to show the differences in evaporation during the growing season and the non-growing season. This is done by applying the method described in section 3.5. Note that these seasons are not of equal length everywhere. The thawing season varies from 7 months in Mongolia to 0 months near the North Pole. The freezing season thus varies between 5 and 12 months, depending on the location.

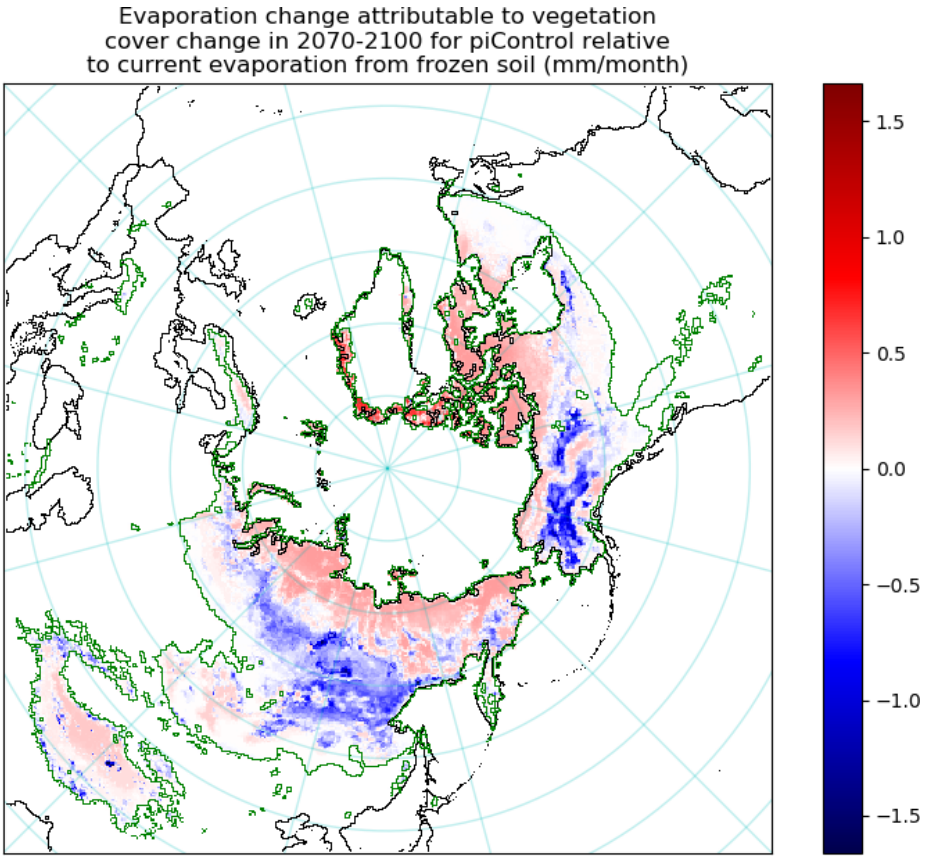

Figure 36: Change in evaporation from frozen soil due to change in vegetation for the piControl scenario, relative to the current situation (1982-2014)

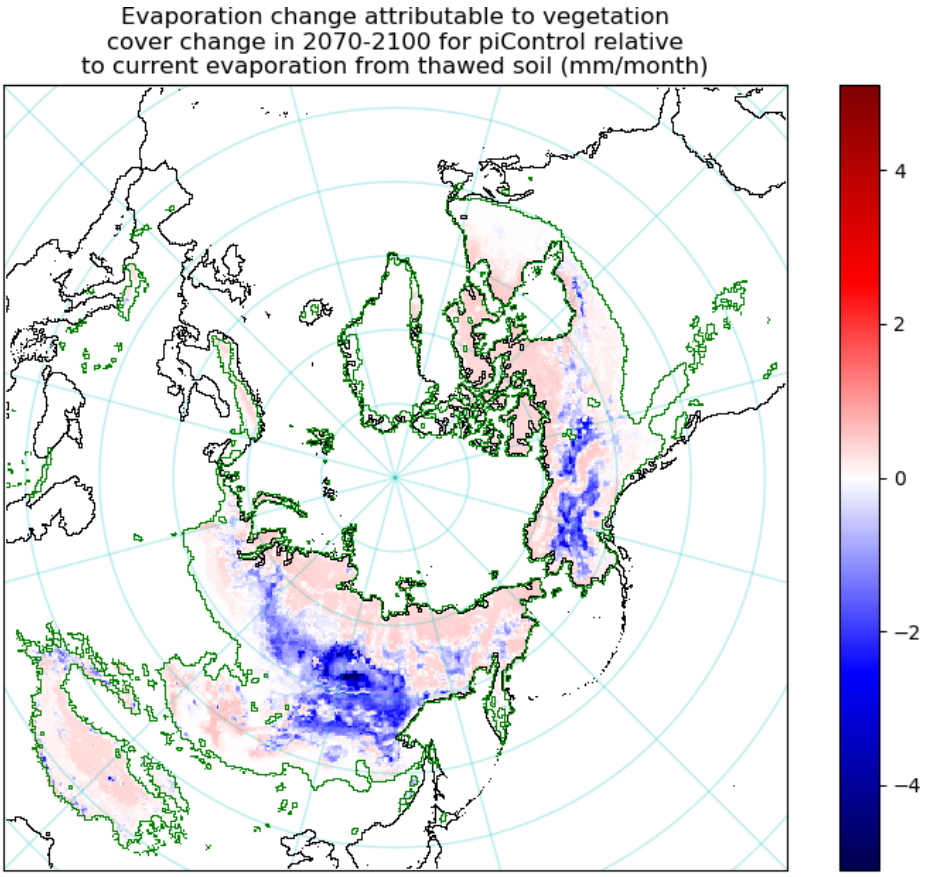

Figure 37: Change in evaporation from thawed soil due to change in vegetation for the piControl scenario, relative to the current situation (1982-2014)

Due to decreasing temperatures and taiga cover the evaporation is predicted to be lower in south Siberia, and the Yukon and Mackenzie river basins for the piControl scenario. Elsewhere there is a very small increase of evaporation of 2-5 mm per month. In the RCP8.5 scenario evaporation increases for most of the permafrost area by 6-7 mm per month. Exceptions are Tibet, the central Yakutian lowland and the Canadian Arctic archipelago (figures 38 and 39). The evaporation during the time of the year that the soil is frozen (figures 36 and 38) changes in a similar pattern as during the period that the soil is thawed (figures 37 and 39). The total evaporation is larger when the soil is not frozen, due to higher temperatures.

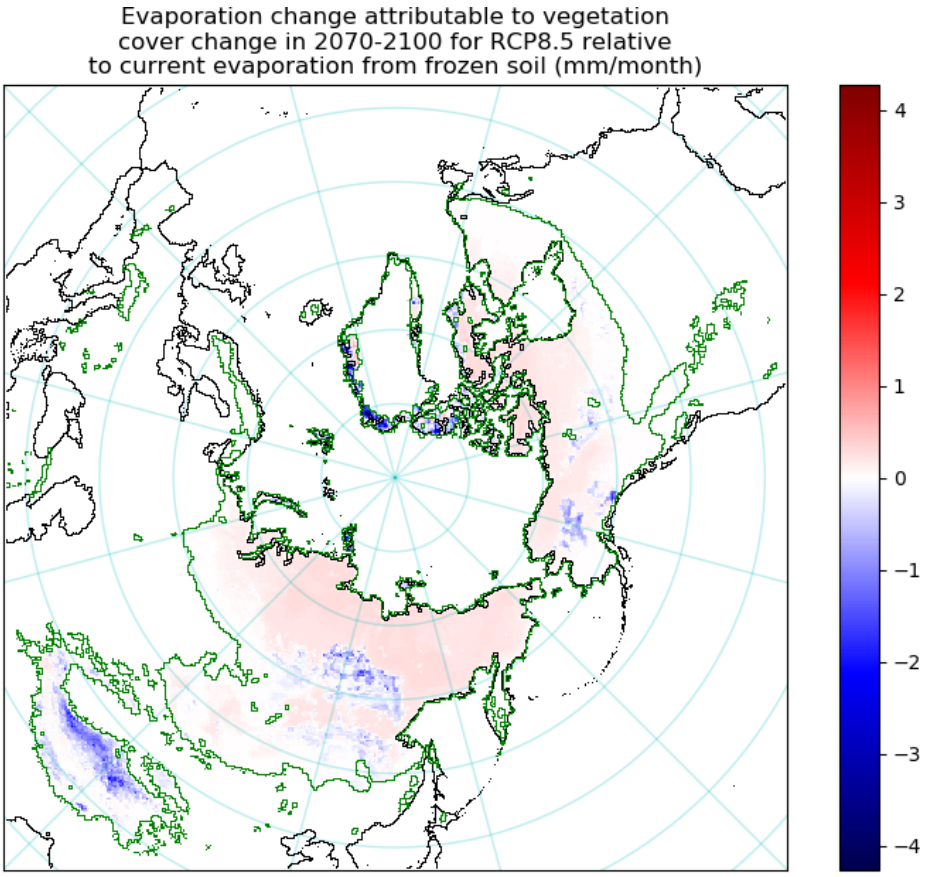

Figure 38: Change in evaporation from frozen soil due to change in vegetation for the RCP8.5 scenario, relative to the current situation (1982-2014)

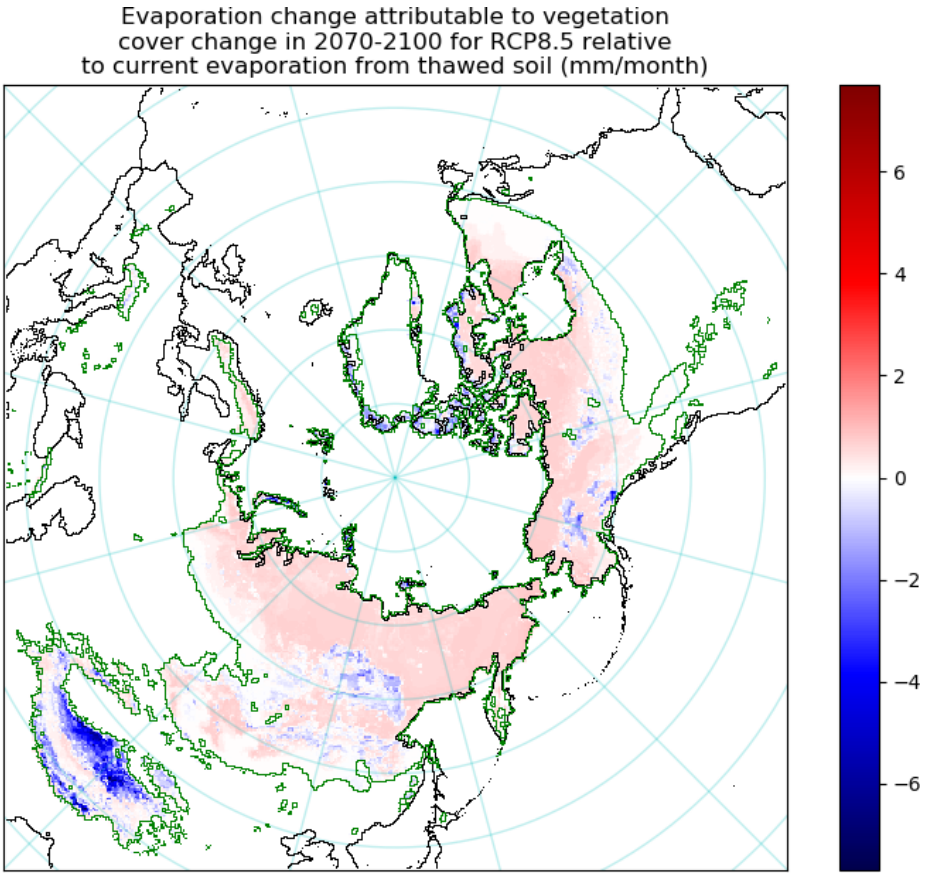

Figure 39: Change in evaporation from thawed soil due to change in vegetation for the RCP8.5 scenario, relative to the current situation (1982-2014)

4.3 Moisture recycling

4.3.1 Source regions

Utilizing U-track moisture tracking data (Tuinenburg et al. (2012), Tuinenburg and Staal (2020)) allows me to determine source and sink relations for precipitation over the area of interest. Since permafrost emits most methane when it is thawed (due to microbial activity), the most important regions to consider will be those that transport water to the permafrost while it is thawed. Therefore, the results are split in thawing ('summer') and freezing ('winter') seasons. The method is applied to each month separately. The sum for the whole thawing season is shown in figure 40.

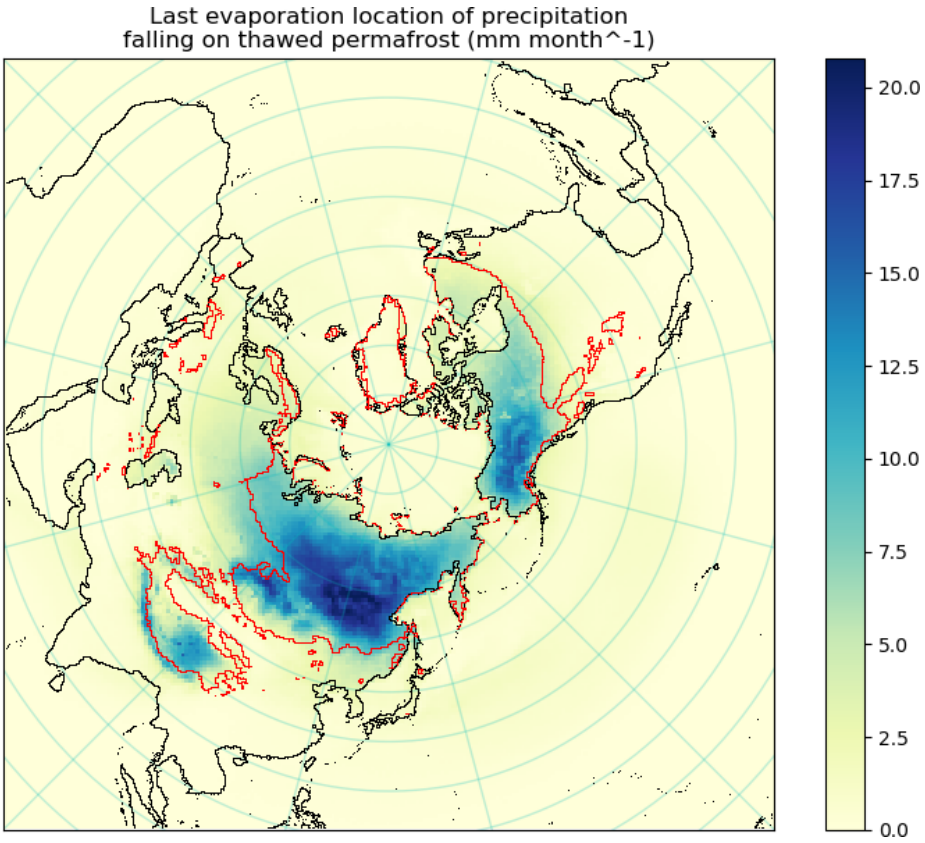

Figure 40: Last evaporation location for precipitation falling on thawed permafrost.

The generally eastward atmospheric flow in the mid-latitudes can be seen in figure 40. Eastern Europe and the Caspian sea are major sources for precipitation over the permafrost located further east. Large ocean areas also contribute to precipitation over thawed permafrost, such as the Persian Gulf, Arabian Sea and the northern Pacific Ocean. However, most precipitation originates from the permafrost itself. Especially in southern Siberia and interior Alaska/Yukon Territory. These inland regions have relatively high summer temperatures, causing a lot of evaporation, and are completely surrounded by mountains. This makes it harder for moisture to escape the region and precipitate on non-permafrost soils.

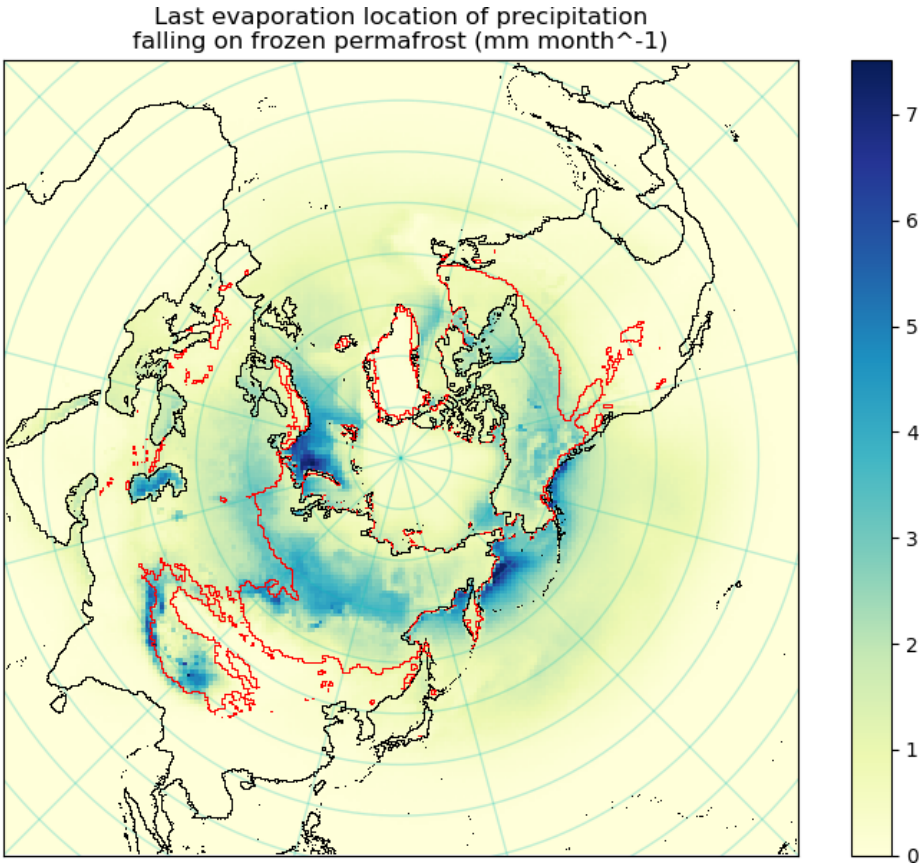

Figure 41: Last evaporation location for precipitation falling on frozen permafrost.

Snow falling on the permafrost originates primarily from the Barentsz, Bering and Caspian seas (figure 41). The North-Pacific and Atlantic Oceans, the Mediterranean and Red seas and the Persion Gulf also contribute significantly. Because the temperature is lower in winter than in summer, the total evaporation is much lower than in figure 40.

In figure 42, we see that the interior regions of Siberia, Alaska and Northwest-Territories contribute less to precipitation on thawing permafrost in the piControl scenario compared to the current situation. It shows a similar pattern as the evaporation change, in figures 36 and 37. The contribution of Tibet, Mongolia, and the Russian Far East change little, because a large fraction of the evaporation of these regions does not precipitate on permafrost soils. This is contrasted by the large increase in contribution from Northern Canada. Moisture evaporated here collides with the Arctic Cordillera or Greenland ice-sheet. Therefore, a large fraction precipitates on permafrost soils.

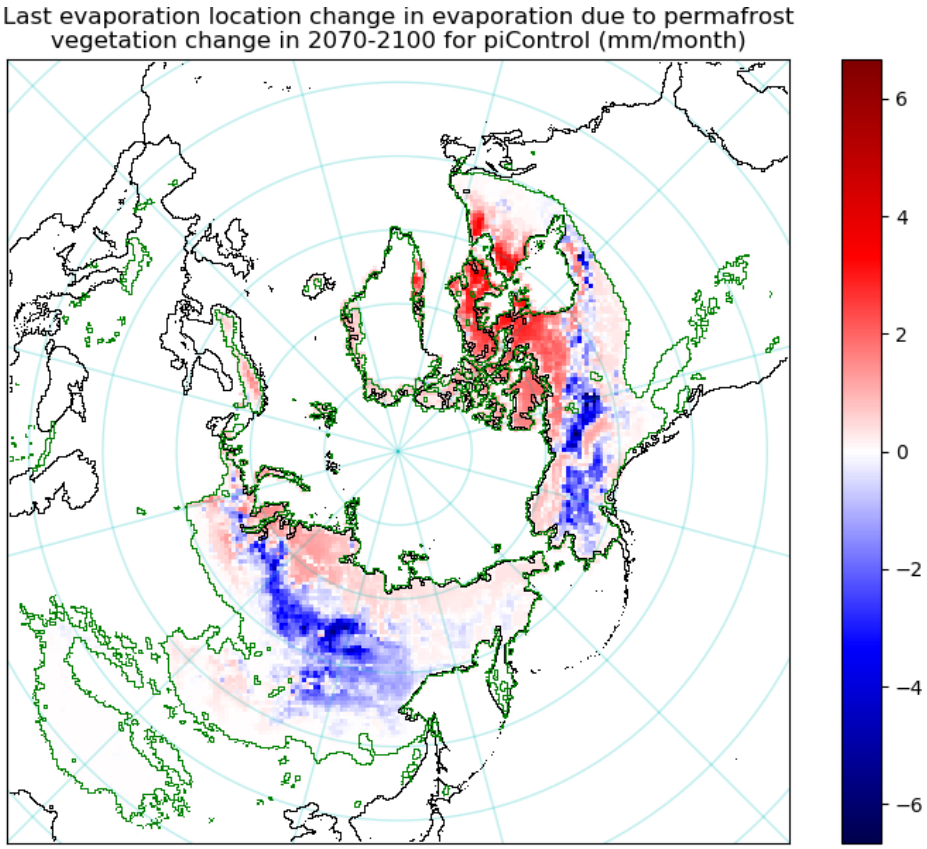

Figure 42: Change in evaporation of the last evaporation location for precipitation falling on thawed permafrost for the piControl scenario in 2070-2100, relative to the current situation (1982-2014).

In a strong warming scenario, RCP8.5, evaporation increases for most of the Arctic (see figures 38 and 39). Therefore, we also see an increase in evaporation which precipitates on thawing permafrost in figure 43. The largest change is again in Northern Canada.

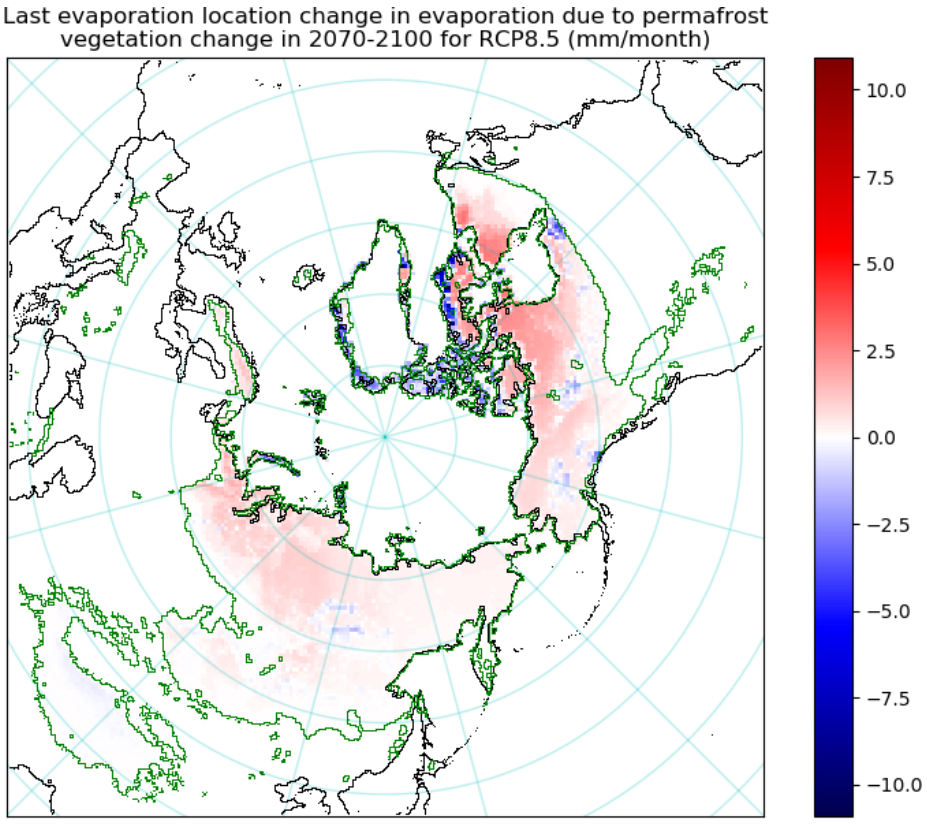

Figure 43: Change in evaporation of the last evaporation location for precipitation falling on thawed permafrost for the RCP8.5 scenario in 2070-2100, relative to the current situation (1982-2014)

4.3.2 Sink regions

The evaporation changes due to vegetation changes in the permafrost determined in section 4.2.2 will lead to changes in precipitation downwind. Using the U-track data with the evaporation data from figures 37 and 39 will result in this data. As above, I will focus on precipitation falling on thawed soils, as this will have the largest impact on vegetation.

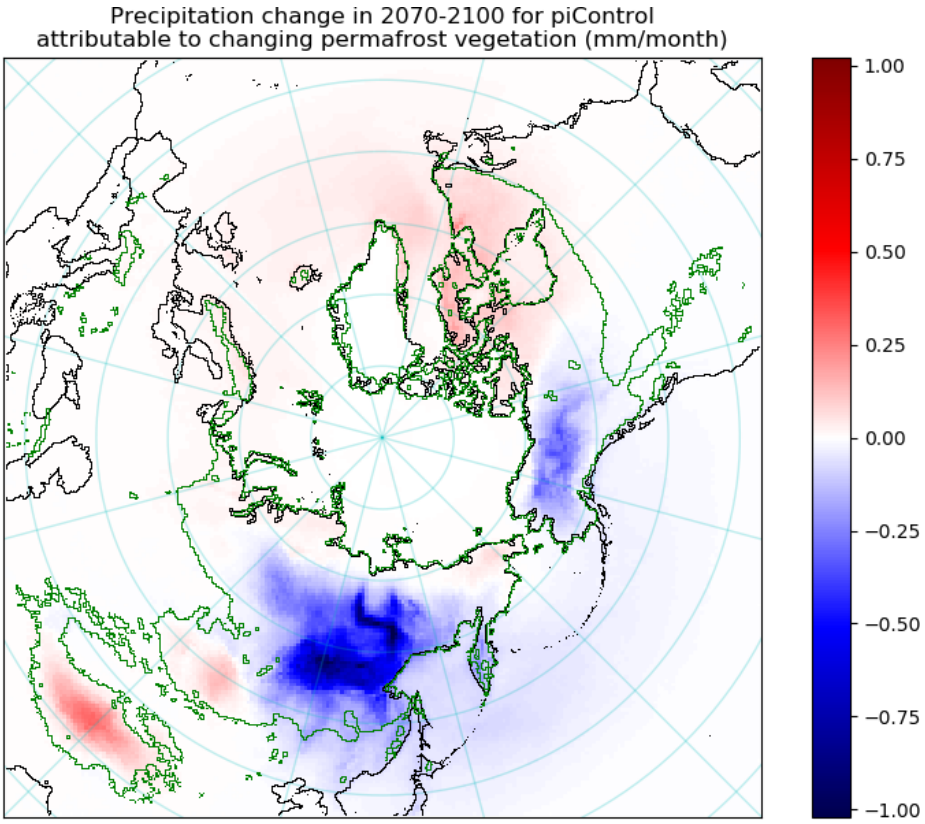

Figure 44: Change in precipitation which occurs solely because the vegetation on the permafrost changes for 2070-2100 in the piControl scenario, relative to the current situation (1982-2014)

One may be tempted to draw conclusions based on structures in figures 44 and 45, but nowhere in neither scenario does the expected change exceed 5% of the expected precipitation rate for each location in each scenario. This is much lower than any of the uncertainties derived for the variables involved. Therefore, the only conclusion that can be drawn is that the precipitation change attributable solely to vegetation change in the permafrost is too small to be detected through the method used in my thesis. For precipitation falling on frozen soil (i.e., in the form of snow or freezing rain), the same conclusion can be drawn.

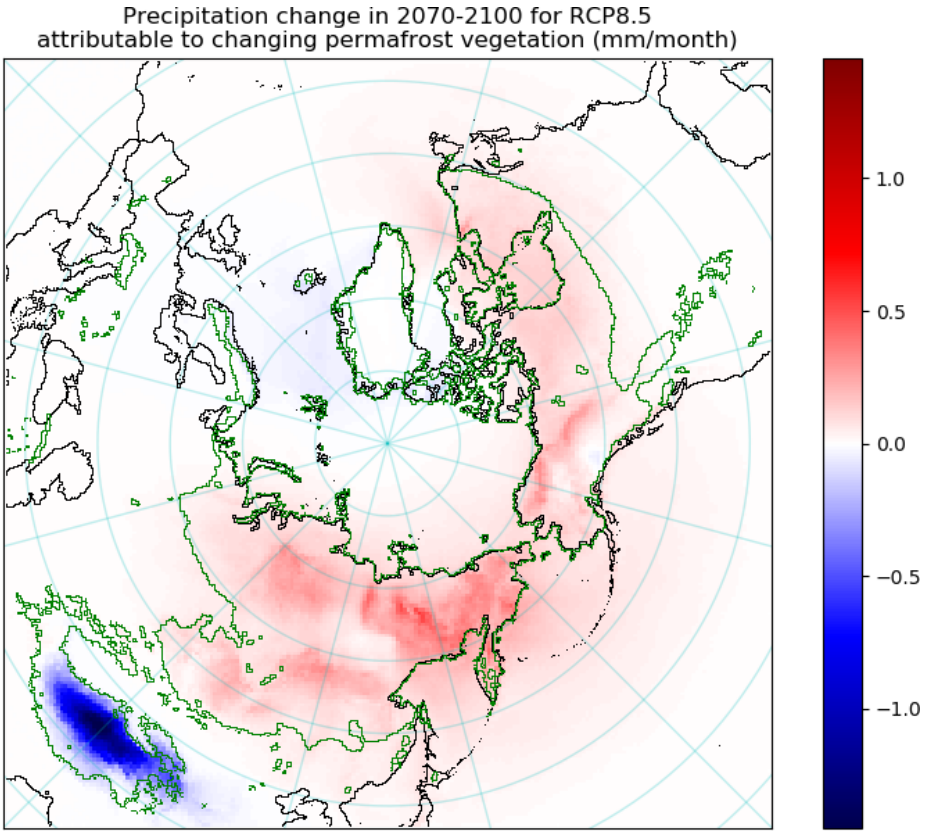

Figure 45: Change in precipitation which occurs solely because the vegetation on the permafrost changes for 2070-2100 in the RCP8.5 scenario, relative to the current situation (1982-2014)

4.3.3 Sensitivity of precipitation to tundra region evaporation

The goal of the Pleistocene Park is to restore the mammoth steppe ecosystem where there is tundra today. Part of the reasoning is that a higher transpiration rate from grasses, compared to tundra vegetation, would dry the soil and therefore reduce CH_4 emissions from thawing permafrost soil. The expected increase in transpiration could not be shown (see section 3.8.2), though it is not clear whether the region used to estimate the expected evaporation accurately describes the situation that would arise if tundra would be replaced with mammoth steppe. Therefore, the tundra vegetation cover from section 3.3 is multiplied with U-track data, to get an impression of the area affected by evaporation from tundra regions. These regions would see the largest change if tundra would be replaced by mammoth steppe, though the magnitude and direction are unknown. Therefore, the units are arbitrary and not shown.

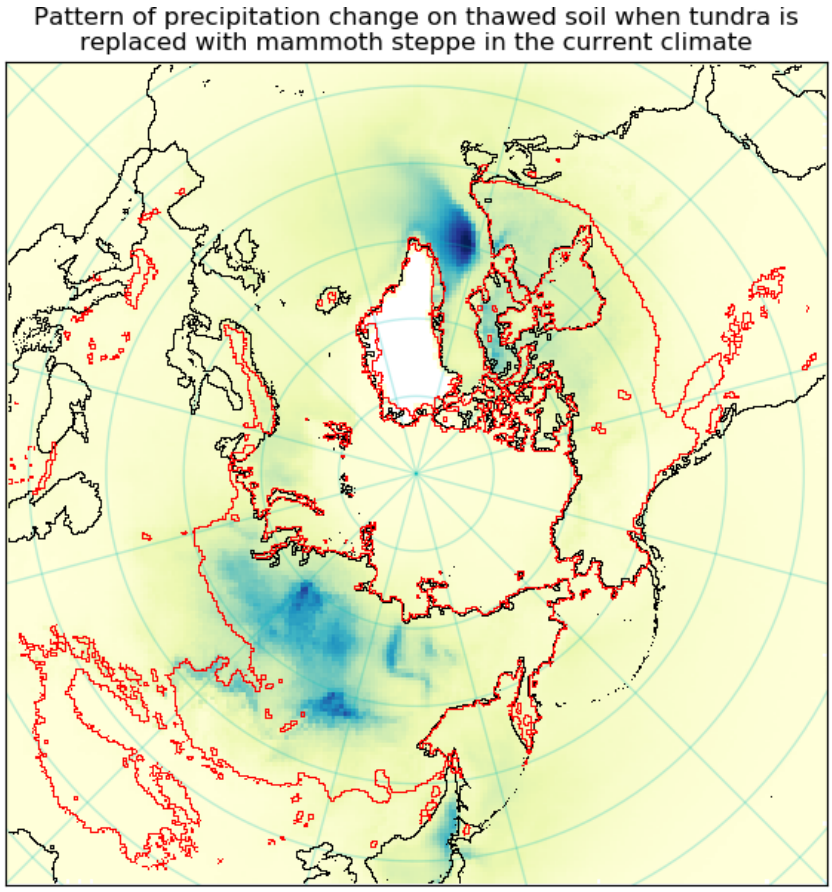

Figure 46: Regions most affected by precipitation on thawed soil last evaporated from tundra in the current climate.

Figure 46 shows that the Central Siberian Plateau, South Siberian Mountains and Eastern Canada are regions which would be affected most when tundra would be replaced by mammoth steppe in the current climate. These are not regions of which the CH_4 emission is highly sensitive to changes in the water table depth (see section 3.7.3). Therefore, I expect that the influence of this ecosystem change does not increase CH_4 emissions from thawing permafrost significantly. It is likely that the cooling of the permafrost, due to trampling of snow (see section 2.1), will decrease CH_4 emissions more than that increased precipitation would increase them.

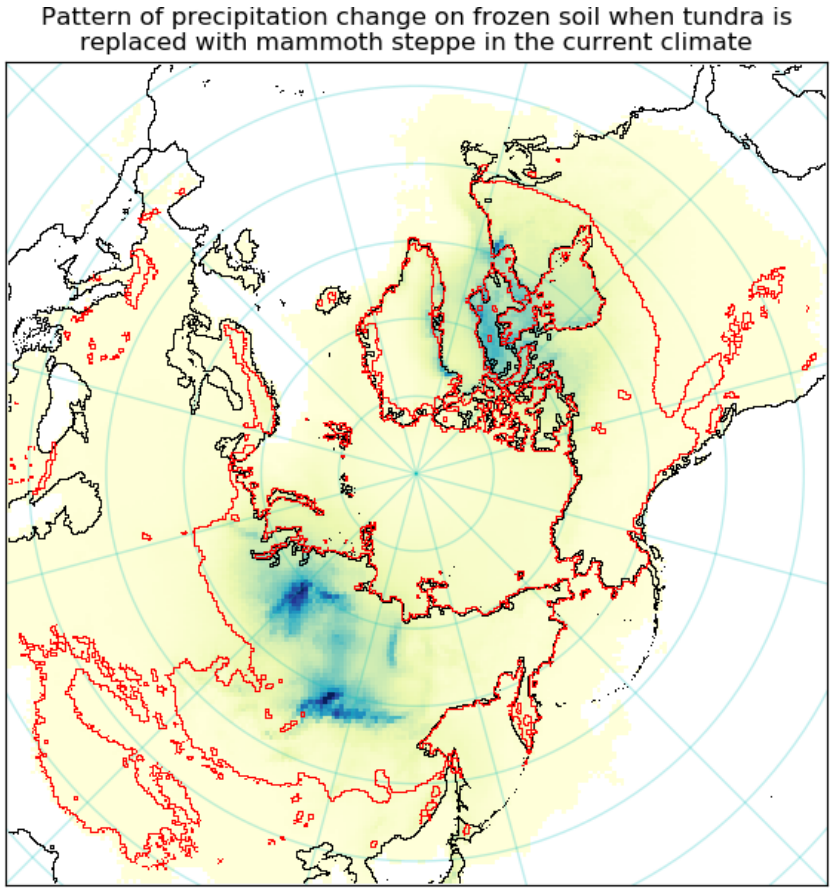

Figure 47: Regions most affected by precipitation on frozen soil last evaporated from tundra in the current climate.

From figure 47 it appears that the pattern of liquid precipitation (in figure 46) is similar to the pattern of solid precipitation. During the freezing season, the precipitation is concentrated a bit more in mountainous regions.

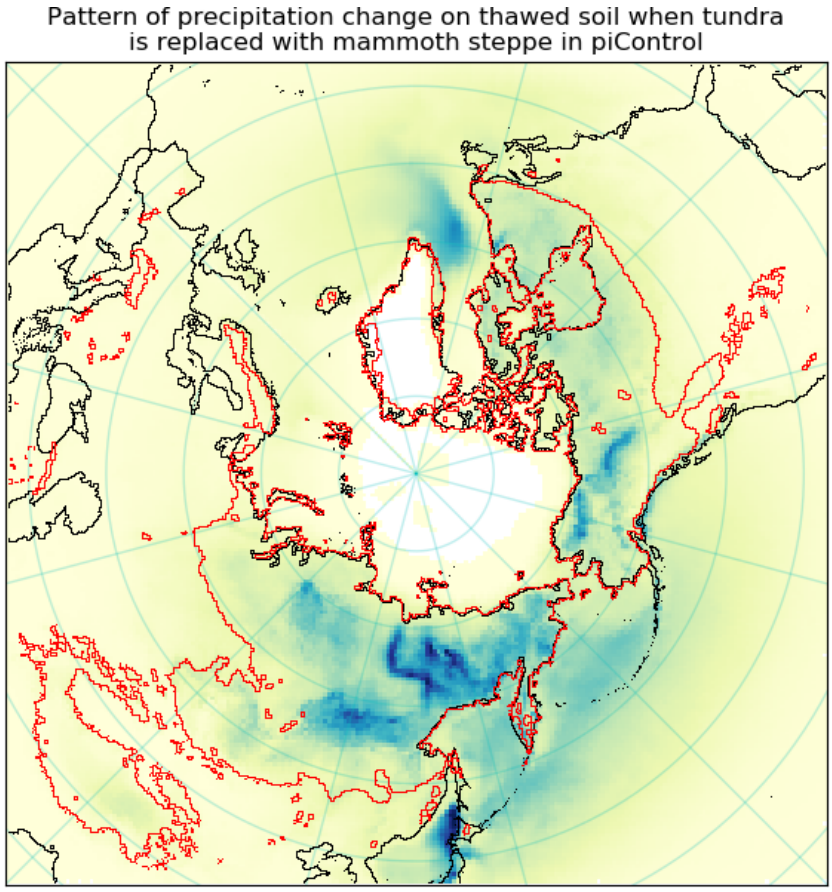

Figure 48: Regions most affected by precipitation on thawed soil last evaporated from tundra in the piControl scenario

For the pre-industrial control scenario, the affected areas also include the Kolyma region, Alaska and the Yukon Territory due to the larger area which is covered with tundra (see figure 48). However, evaporation will be lower than in the current climate, because of lower temperatures. It is unlikely that the Pleistocene Park would expand beyond its current borders in this scenario, because there is no global warming in this scenario.

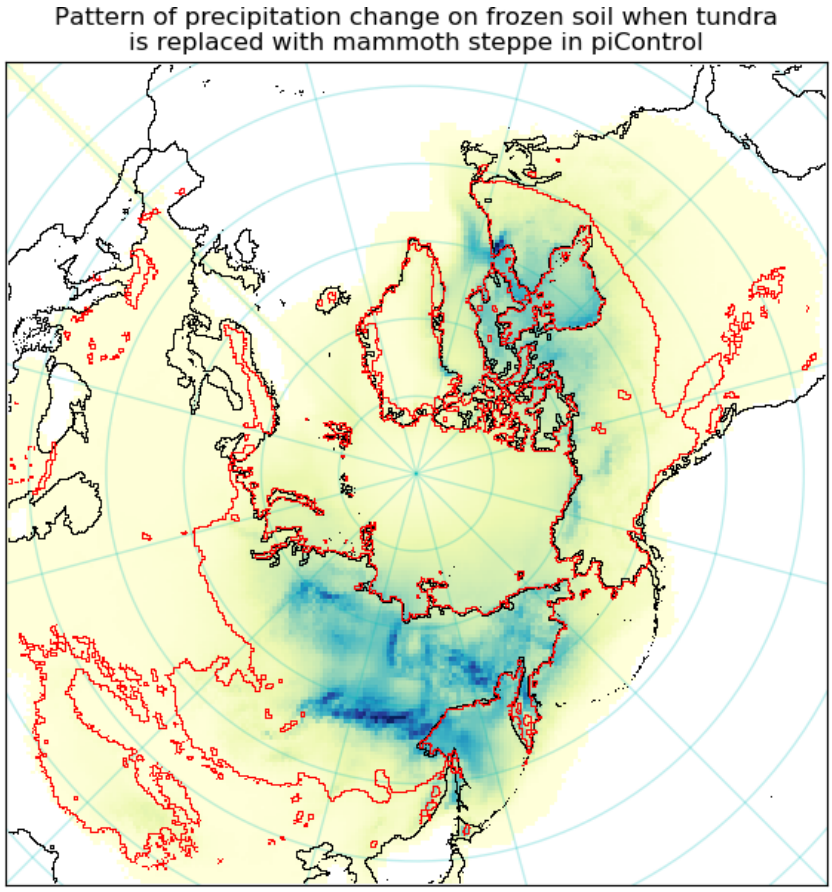

Figure 49: Regions most affected by precipitation on frozen soil last evaporated from tundra in the piControl scenario

During the time of the year that the soil is frozen in the piControl scenario (shown in figure 49, which is slightly longer than in the current climate), precipitation which most recently evaporated from the tundra is more concentrated towards the Southern Siberian Mountains, compared to the thawing season shown in figure 48.

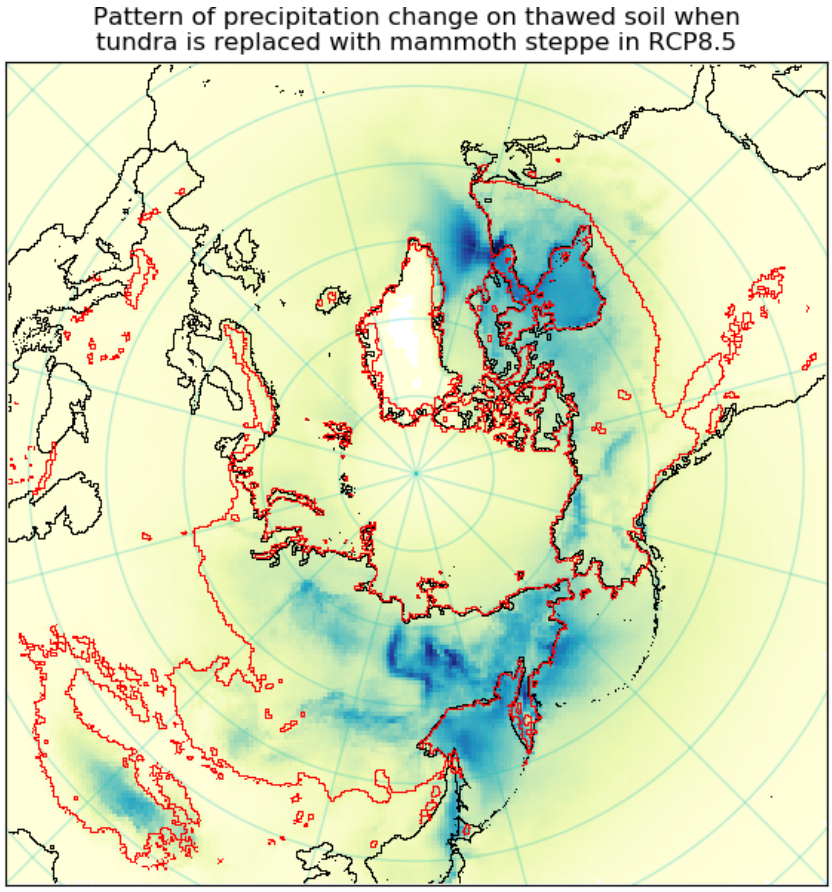

Figure 50: Regions most affected by precipitation on thawed soil last evaporated from tundra in the RCP8.5 scenario

If expansion of the Pleistocene Park is delayed until the situation is as in RCP8.5 during 2070-2100, then there will be little tundra left to replace with mammoth steppe. Only the Arctic Ocean coastline, the Canadian Arctic Archipelago and Tibet are projected to have tundra vegetation left. Water last evaporated from these regions excluding Tibet generally precipitates in the mountains of Eastern Siberia and Northeastern Canada (figure 50).

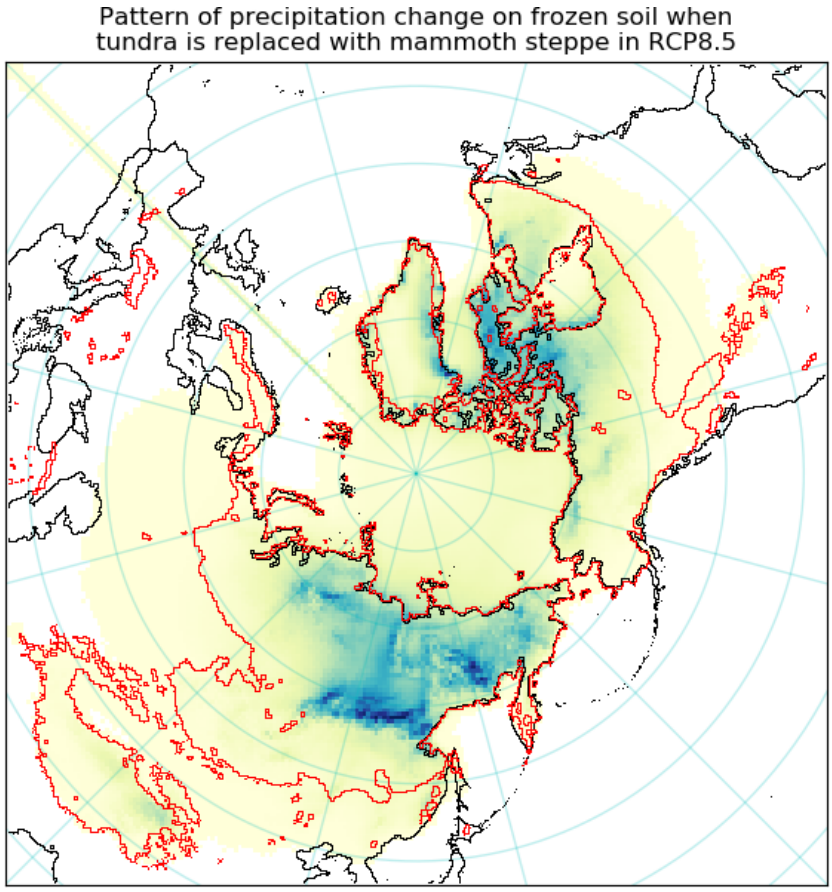

Figure 51: Regions most affected by precipitation on frozen soil last evaporated from tundra in the RCP8.5 scenario

In the RCP8.5 scenario, there is a significant fraction of snow falling in Central Siberia, which last evaporated from the tundra (figure 51). As above, the area of the tundra is smaller in the RCP8.5 scenario than in the other scenarios. Furthermore, I expect that the water from snowmelt will runoff quickly to rivers. Therefore, the impact of this snow on methane emissions in the region is expected to be small.

4.4 Methane flux change

Methane flux changes are assessed by comparing the fluxes from future scenarios with a historical run using CMIP6 and ISIMIP data. Surface temperature and precipitation projections are taken from the CMIP6 archive, while evaporation and runoff are taken from ISIMIP. It is assumed that all water left after evaporation and runoff are subtracted from the precipitation is added to the water

table level. Given the standard deviation of 24.1% associated with the equation from Olefeldt et al. (2013) (see section 3.7), any change smaller than 5-10 mg m^{-2} d^{-1} is considered insignificant.

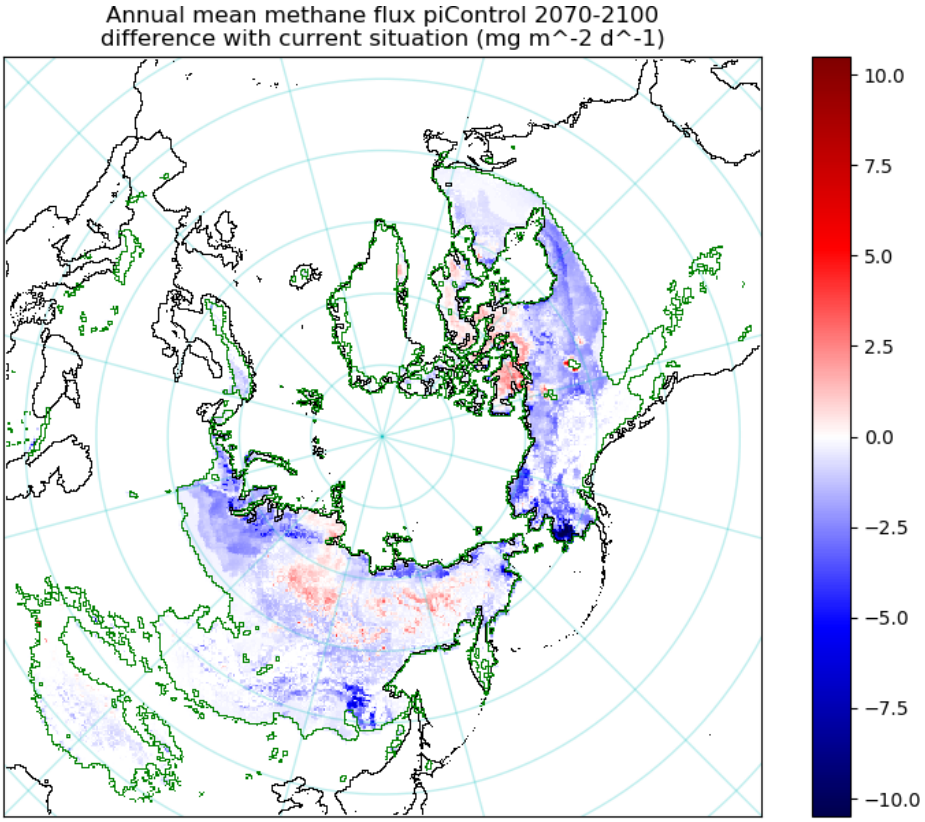

Figure 52: Change in the estimated annual mean methane flux in the piControl scenario for 2070-2100, relative to the current situation.

The difference in surface temperature between the piControl and historical runs is on average about 1K. Above the permafrost, this difference is mostly positive. The water table depth decreases slightly due to decreased precipitation. Therefore, the estimated methane flux change is, overall, slightly negative, and generally insignificant (figure 52). Water table levels decrease in the RCP8.5 scenario due to increased evaporation and runoff. The increase in temperature is generally sufficient to increase the estimated methane flux, except south of roughly the 60°north parallel. The northern coastal regions remain wet and are expected to show the largest increase in methane flux (figure 53).

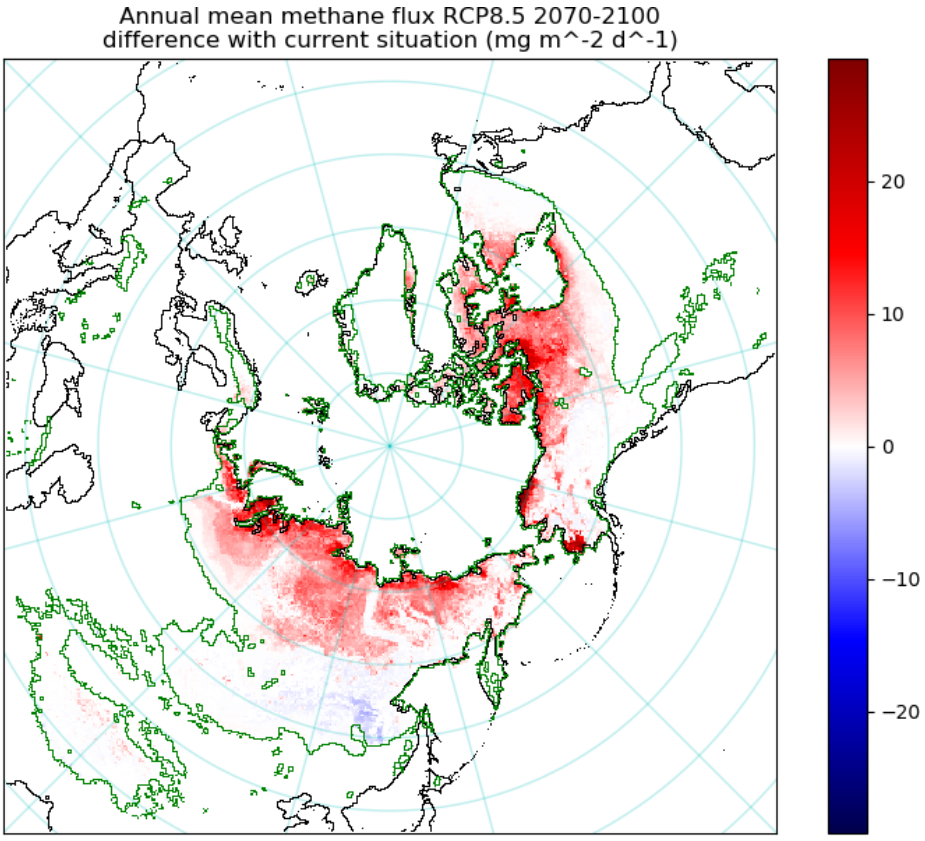

Figure 53: Change in the estimated annual mean methane flux in the RCP8.5 scenario for 2070-2100, relative to the current situation.

The estimated methane flux sensitivity to changes in the water table depth (figure 54) decreases strongly in the Yukon delta in the piControl scenario. This region was identified in section 3.7.3 as the region with the highest estimated methane flux. The change is large here because of the high methane flux present in the region now, and the high water table. Regions with low fluxes and relatively dry regions are less sensitive to the water table depth.

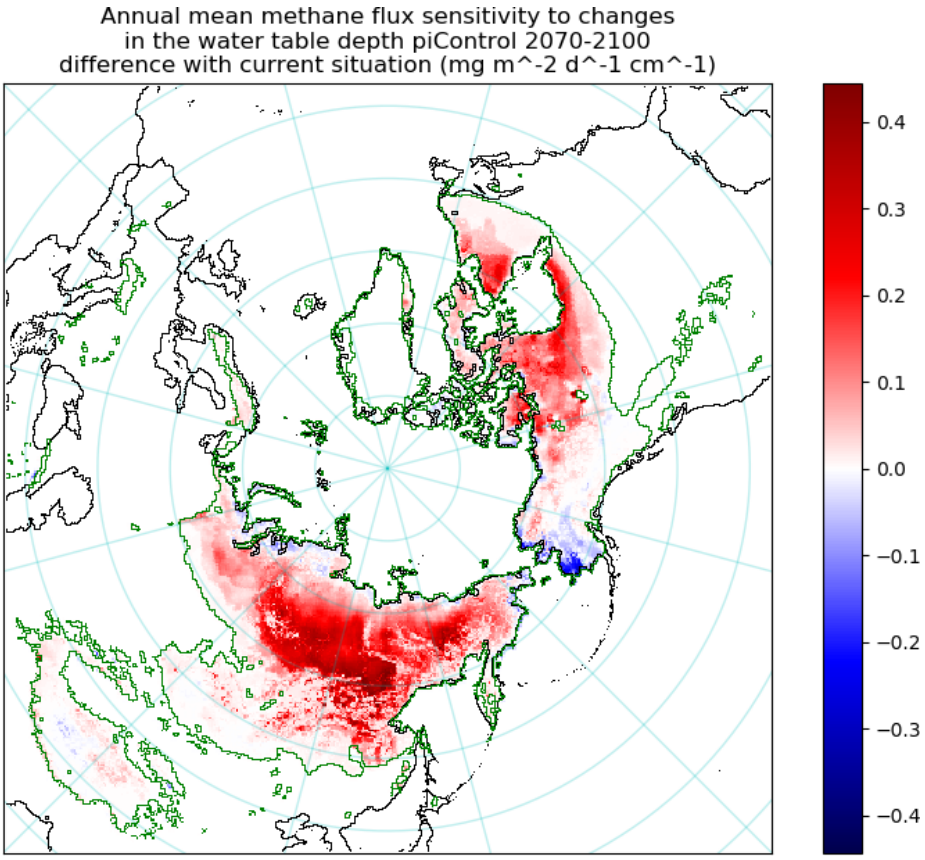

Figure 54: Change in the estimated annual mean methane flux sensitivity to changes in the water table depth, in the piControl scenario for 2070-2100, relative to the current situation.

The equation from Olefeldt et al. (2013) is valid for surface temperatures between 0°C and 15°C, and for water table depths between 40cm below and 10cm above the surface. Below the range of these values, the methane flux is assumed to be 0. For relatively warm areas, like central Siberia, summer monthly mean surface temperatures would often exceed 15°C. These areas are clipped at 15°C, but it is not clear how large the methane flux would be for higher surface temperatures.

In figure 55 we see that the sensitivity to the water table depth increases almost everywhere in the RCP8.5 scenario, despite the increasing drought. High temperatures in this scenario cause that methane fluxes are more sensitive to the water table depth. A small increase in the water table can cause a large increase in the estimated methane flux.

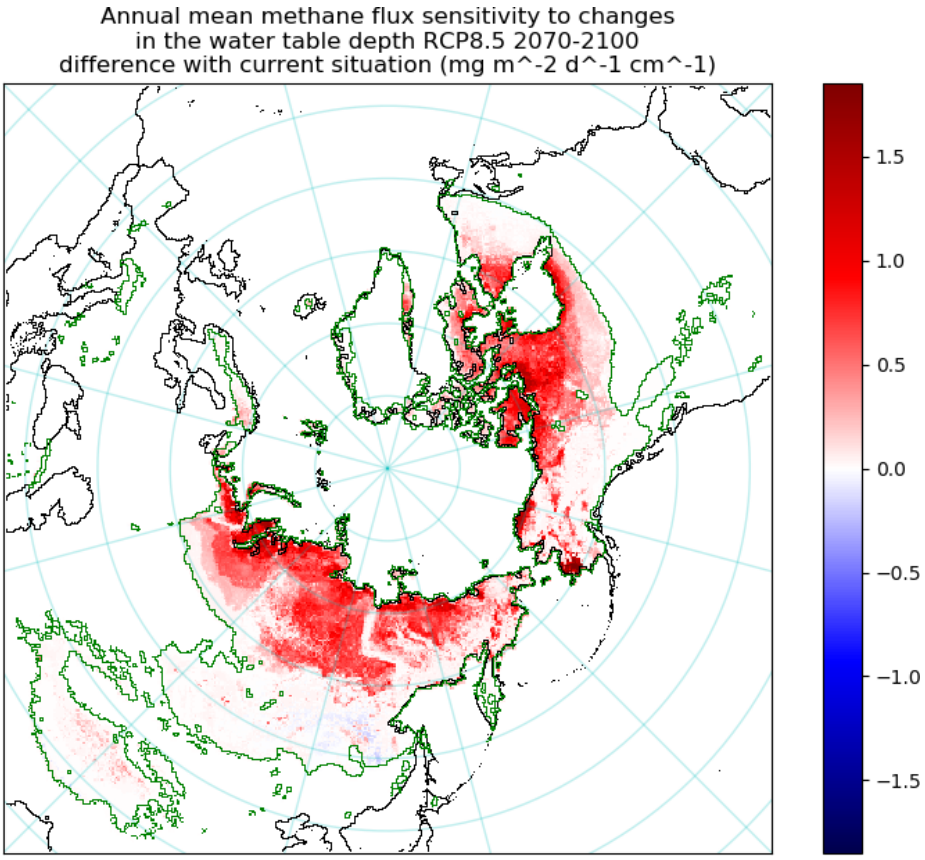

Figure 55: Change in the estimated annual mean methane flux sensitivity to changes in the water table depth, in the RCP8.5 scenario for 2070-2100, relative to the current situation.

5 Discussion

5.1 Accuracy of CMIP6 and ISIMIP future datasets

The accuracy of the datasets used for the future scenarios may be assessed by comparing runs with historical data with ERA5. This was done for all variables.

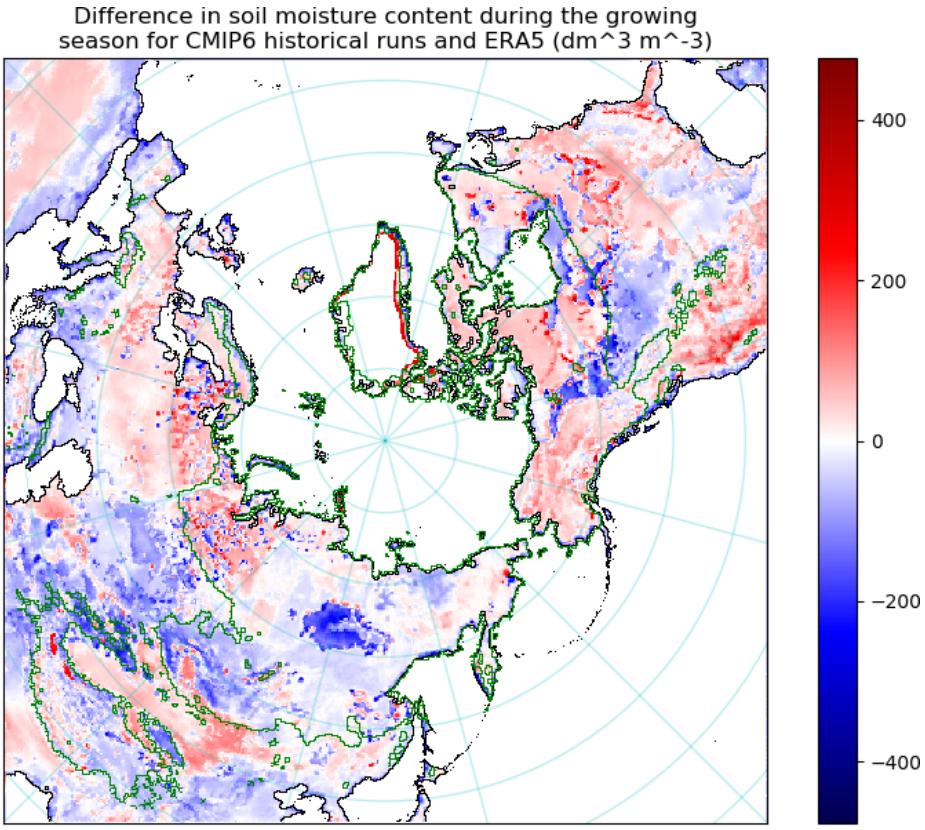

Figure 56: Growing season soil moisture content.

Figure 56 shows that the growing season soil moisture content differs between the historical runs of CMIP6 with ERA5 mostly in the central Yakutian lowland, the Mackenzie river basin and the Hudson bay lowland. The soil moisture content is used both to predict vegetation cover and the associated evaporation. Therefore, the influence of this variable on the final results is large. The results for these particular regions are therefore considered unreliable.

Inspection of the soil types used in ERA5 shows that the areas where the CMIP6 models show lower soil moisture content are characterised by organic soils.

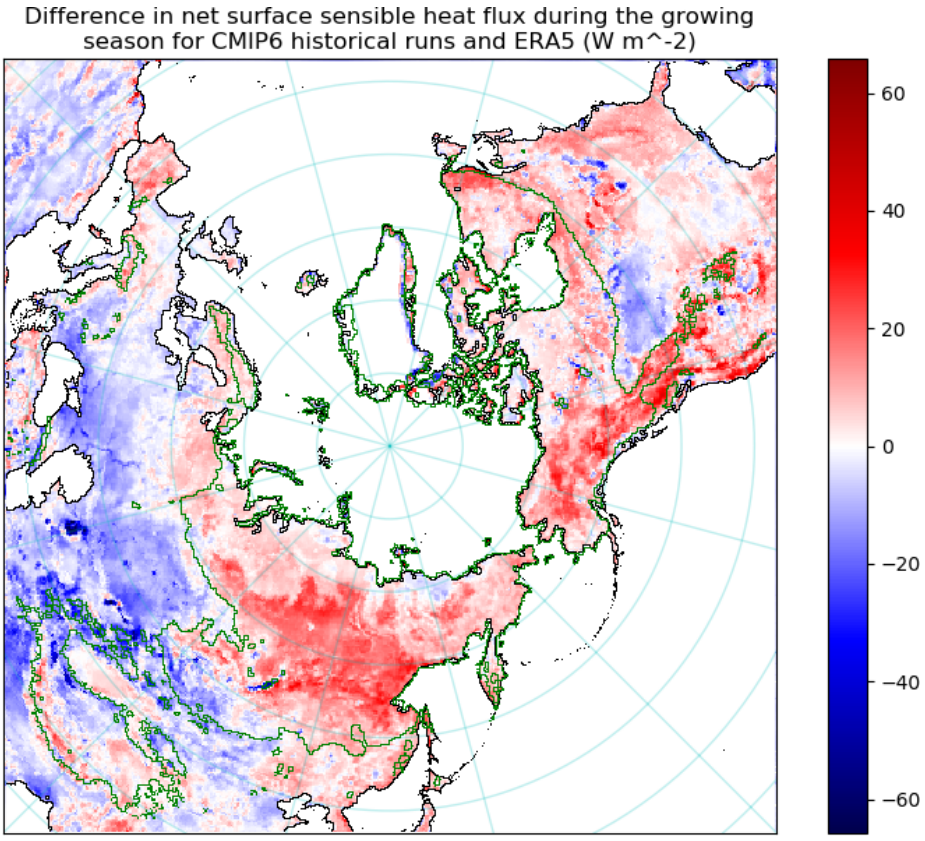

Figure 57: Growing season net surface sensible heat flux

The growing season net surface sensible heat flux, shown in figure 57, is larger in the CMIP6 historical runs than in ERA5 for most of the permafrost region. The growing season net surface sensible heat flux is used in combination with the net surface short-wave radiation flux to correct the vegetation cover. The influence on the final results is therefore considered to be small.

Furthermore, the surface net short-wave radiation flux differs 16.8 W m^{-2} (11.7%) on average over the permafrost area between ERA5 and CMIP6 historical runs during the growing season (2m air temperature higher than freezing). The 2m air temperature differs 1.2 K over the same region and time of year between ERA5 and CMIP6. These variables are therefore considered to agree well between those models.

5.2 Influence of thermokarst

The influence of thermokarst on the (relative) amount of run-off was studied, but no relation was found. A positive correlation between run-off and thermokarst

cover was expected from Olefeldt et al. (2016). A possible explanation could be that this process is still not well understood and is therefore not well represented in ERA5, from which the run-off data was taken.

5.3 Studying moisture recycling with isotopes

Besides numerical studies mentioned in the previous sections, moisture recycling can be studied in-situ by using isotope measurements. Due to fractionation processes, air parcels will obtain water containing different concentrations of isotopologues depending on the fractionation processes the water has experienced (e.g. Kurita et al. (2004), Peng et al. (2011)). In the atmosphere, these will be dominated by evaporation and condensation. However, Risi et al. (2013) and Sutanto et al. (2014) showed that the fraction of total evaporation attributed to plant transpiration by isotope-based studies is generally higher than other methods. Conversely, models tend to give lower fractions. When studying the effect of plant transpiration on evaporation, it is therefore important to consider the methods used and the associated uncertainties.

Isotope measurement can be used to verify model results, though many hundreds of measurements would be needed globally and at frequent time intervals to obtain similar results as is possible now with climate models. Any comparison which can be made between isotope related measurements and the results derived from models and satellite data would nevertheless be insightful, primarily for giving an indication of the uncertainty involved.

6 Conclusion

In the whole of this thesis, I make a distinction between precipitation falling on thawing permafrost (e.g. rain or sleet) and frozen permafrost (e.g. snow or freezing rain). Solid precipitation does not contribute to the release of methane and moisture from melting snow is assumed to runoff quickly, making a minimal contribution. Liquid precipitation is for a large part transported to the permafrost from taiga regions. Also continental regions to the west of the permafrost and the northern Pacific ocean contribute significantly. Tundra regions, which are the regions where the vegetation is projected to change the most, contribute much less to the precipitation of the permafrost. This is because these regions are colder and therefore evaporate less, but also because a larger portion of the evaporation precipitates over the ocean than is the case for regions covered in taiga.

It appears that the water balance will change such that the permafrost areas will have a smaller balance of precipitation minus evaporation and runoff. This occurs both in the piControl scenario and the RCP8.5 scenario. In the piControl scenario, the precipitation decreases more than the evaporation. In the RCP8.5 scenario, precipitation changes much less but the evaporation increases significantly. However, increased thaw may compensate for the loss of atmospheric moisture. As long as the soil is not completely devoid of ice, the soil will be

moistened from below in a warming scenario. How deep the thaw will be is as of yet unknown.

Taiga vegetation evaporates more water than tundra vegetation, although the difference is small. The expected increase in evaporation from mammoth steppe relative to tundra could not be shown using the method from this thesis. A better understanding of the characteristics of various vegetation types and the use of more advanced biological/climate models would definitely improve the analysis. Although the Altai-Sayan region, from which the evaporation characteristics of mammoth steppe were taken, represents most accurately the vegetation as encountered in the pollen records for the Pleistocene in the Arctic, it is not clear whether the evaporation expected in the Pleistocene Park will show the same trends as the vegetation in the Altai-Sayan mountains does at the current time.

Methane emissions were estimated from an equation from Olefeldt et al. (2013) taking into account the surface temperature, water table depth and the amount of sedge cover. This equation was derived from several hundred local flux measurements. Given the lack of large scale methane emission data, it is unclear whether this equation can be extrapolated to pan-Arctic scales. The deviation with the observations of 24% can thus be regarded as a lower limit for the uncertainty. Despite this high uncertainty, the limited temperature range for which the equation is derived (from 0°C to 15°C), and the fact that increased moisture from melting ice in the permafrost is not taken into account, it seems clear that methane emissions will increase in a warming climate scenario.

Given that the effect of changing the vegetation in the arctic on precipitation is small and that most of the precipitation which most recently evaporated from the tundra falls on areas which are not especially sensitive to increased moisture, there do not seem to be any adverse effects on the permafrost hydrology by expanding the Pleistocene Park. The greatest danger to the permafrost therefore seems to be the increasing temperatures. If the Pleistocene Park succeeds in preserving the permafrost, it is likely that methane emissions from the permafrost will decrease, rather than increase.

Acknowledgements

I would like to thank Obbe Tuinenburg and Thomas Röckmann for supervising my thesis.

Neither the European Commission nor ECMWF is responsible for any use that may be made of the Copernicus Information or Data it contains.

Regarding the CESM model data from CMIP6: Computing and data storage resources, including the Cheyenne supercomputer (doi:10.5065/D6RX99HX), were provided by the Computational and Information Systems Laboratory (CISL) at NCAR. I thank all the scientists, software engineers, and administrators who contributed to the development of CESM2.

References

Bader, D. C., Leung, R., Taylor, M., and McCoy, R. B. (2019). E3sm-project e3sm1.0 model output prepared for cmip6 cmip.

Best, M. J., Pryor, M., Clark, D. B., Rooney, G. G., Essery, R. L. H., Ménard, C. B., Edwards, J. M., Hendry, M. A., Porson, A., Gedney, N., Mercado, L. M., Sitch, S., Blyth, E., Boucher, O., Cox, P. M., Grimmond, C. S. B., and Harding, R. J. (2011). The joint uk land environment simulator (jules), model description – part 1: Energy and water fluxes. *Geoscientific Model Development*, 4(3):677–699.

Bond-Lamberty, B., Smith, A. P., and Bailey, V. (2016). Temperature and moisture effects on greenhouse gas emissions from deep active-layer boreal soils. *Biogeosciences*, 13(24):6669–6681.

Bondeau, A., Smith, P. C., Zaehle, S., Schaphoff, S., Lucht, W., Cramer, W., Gerten, D., Lotze-Campen, H., Müller, C., Reichstein, M., and Smith, B. (2007). Modelling the role of agriculture for the 20th century global terrestrial carbon balance. *Global Change Biology*, 13(3):679–706.

Bonfils, C. J. W., Phillips, T. J., Lawrence, D. M., Cameron-Smith, P., Riley, W. J., and Subin, Z. M. (2012). On the influence of shrub height and expansion on northern high latitude climate. *Environmental Research Letters*, 7(1):015503.

Brown, J., Ferrians, O., Heginbottom, J. A., and Melnikov, E. (2002). Circumarctic map of permafrost and ground-ice conditions, version 2.

Brubaker, K. L., Entekhabi, D., and Eagleson, P. S. (1993). Estimation of continental precipitation recycling. *Journal of Climate*, 6(6):1077–1089.

Buck, A. L. (1981). New equations for computing vapor pressure and enhancement factor. *Journal of Applied Meteorology*, 20(12):1527–1532.

Buck, A. L. (1996). *Model CR-1A Hygrometer with autofill*. Buck Research Instruments L.L.C., PO Box 19498, Boulder, CO 80308.

Caldwell, P. M., Mametjanov, A., Tang, Q., Van Roekel, L. P., Golaz, J., Lin, W., Bader, D. C., Keen, N. D., Feng, Y., Jacob, R., and et al. (2019). The doe e3sm coupled model version 1: Description and results at high resolution. *Journal of Advances in Modeling Earth Systems*, 11(12):4095–4146.

CAVM-Team (2003). Circumpolar arctic vegetation map. (1:7,500,000 scale). In *Conservation of Arctic Flora and Fauna (CAFF) Map No. 1.* U.S. Fish and Wildlife Service, Anchorage, Alaska.

Copernicus Climate Change Service (2017). ERA5: Fifth generation of ECMWF atmospheric reanalyses of the global climate. https://cds.climate.copernicus.eu/cdsapp!/home.

Dale Guthrie, R. (2001). Origin and causes of the mammoth steppe: a story of cloud cover, woolly mammal tooth pits, buckles, and inside-out beringia. *Quaternary Science Reviews*, 20(1):549 – 574. Beringian Paleoenvironments - Festschrift in Honour of D.M. Hopkins.

Danabasoglu, G. (2019). Ncar cesm2-waccm model output prepared for cmip6 cmip.

D'Arrigo, R. D., Kaufmann, R. K., Davi, N., Jacoby, G. C., Laskowski, C., Myneni, R. B., and Cherubini, P. (2004). Thresholds for warming-induced growth decline at elevational tree line in the yukon territory, canada. *Global Biogeochemical Cycles*, 18(3).

Diáková, K., Čapek, P., Kohoutová, I., Mpamah, P. A., Bárta, J., Biasi, C., Martikainen, P. J., and Šantrůčková, H. (2016). Heterogeneity of carbon loss and its temperature sensitivity in East-European subarctic tundra soils. *FEMS Microbiology Ecology*, 92(9). fiw140.

Dufour, A., Zolina, O., and Gulev, S. K. (2016). Atmospheric Moisture Transport to the Arctic: Assessment of Reanalyses and Analysis of Transport Components. *Journal of Climate*, 29(14):5061–5081.

Dufresne, J.-L., Foujols, M.-A., Denvil, S., Caubel, A., Marti, O., Aumont, O., Balkanski, Y., Bekki, S., Bellenger, H., Benshila, R., and et al. (2013). Climate change projections using the ipsl-cm5 earth system model: from cmip3 to cmip5. *Climate Dynamics*, 40(9–10):2123–2165.

Dunne, J. P., John, J. G., Adcroft, A. J., Griffies, S. M., Hallberg, R. W., Shevliakova, E., Stouffer, R. J., Cooke, W., Dunne, K. A., Harrison, M. J., Krasting, J. P., Malyshev, S. L., Milly, P. C. D., Phillipps, P. J., Sentman, L. T., Samuels, B. L., Spelman, M. J., Winton, M., Wittenberg, A. T., and Zadeh, N. (2012). Gfdl's esm2 global coupled climate–carbon earth system models. part i: Physical formulation and baseline simulation characteristics. *Journal of Climate*, 25(19):6646–6665.

Dunne, J. P., John, J. G., Shevliakova, E., Stouffer, R. J., Krasting, J. P., Malyshev, S. L., Milly, P. C. D., Sentman, L. T., Adcroft, A. J., Cooke, W., Dunne, K. A., Griffies, S. M., Hallberg, R. W., Harrison, M. J., Levy, H., Wittenberg, A. T., Phillips, P. J., and Zadeh, N. (2013). Gfdl's esm2 global coupled climate–carbon earth system models. part ii: Carbon system formulation and baseline simulation characteristics. *Journal of Climate*, 26(7):2247–2267.

Dury, M., Hambuckers, A., Warnant, P., Henrot, A., Favre, E., Ouberdous, M., and Francois, L. (2011). Responses of European forest ecosystems to 21st century climate: assessing changes in interannual variability and fire intensity. *iForest - Biogeosciences and Forestry*, (2):82–99.

EC-Earth (2019). Ec-earth-consortium ec-earth3-veg model output prepared for cmip6 scenariomip.

Estop-Aragonés, C., Cooper, M. D., Fisher, J. P., Thierry, A., Garnett, M. H., Charman, D. J., Murton, J. B., Phoenix, G. K., Treharne, R., Sanderson, N. K., Burn, C. R., Kokelj, S. V., Wolfe, S. A., Lewkowicz, A. G., Williams, M., and Hartley, I. P. (2018). Limited release of previously-frozen c and increased new peat formation after thaw in permafrost peatlands. *Soil Biology and Biochemistry*, 118:115 – 129.

Golaz, J., Caldwell, P. M., Van Roekel, L. P., Petersen, M. R., Tang, Q., Wolfe, J. D., Abeshu, G., Anantharaj, V., Asay-Davis, X. S., Bader, D. C., and et al. (2019). The doe e3sm coupled model version 1: Overview and evaluation at standard resolution. *Journal of Advances in Modeling Earth Systems*, 11(7):2089–2129.

Grace, J., Berninger, F., and Nagy, L. (2002). Impacts of Climate Change on the Tree Line. *Annals of Botany*, 90(4):537–544.

Grogan, P. (2012). Cold season respiration across a low arctic landscape: the influence of vegetation type, snow depth, and interannual climatic variation. *Arctic, Antarctic, and Alpine Research*, 44(4):446–456.

Guimberteau, M., Zhu, D., Maignan, F., Huang, Y., Yue, C., Dantec-Nédélec, S., Ottlé, C., Jornet-Puig, A., Bastos, A., Laurent, P., and et al. (2017). Orchidee-mict (revision 4126), a land surface model for the high-latitudes: model description and validation.

Guo, H., John, J. G., Blanton, C., McHugh, C., Nikonov, S., Radhakrishnan, A., Rand, K., Zadeh, N. T., Balaji, V., Durachta, J., Dupuis, C., Menzel, R., Robinson, T., Underwood, S., Vahlenkamp, H., Bushuk, M., Dunne, K. A., Dussin, R., Gauthier, P. P., Ginoux, P., Griffies, S. M., Hallberg, R., Harrison, M., Hurlin, W., Malyshev, S., Naik, V., Paulot, F., Paynter, D. J., Ploshay, J., Reichl, B. G., Schwarzkopf, D. M., Seman, C. J., Shao, A., Silvers, L., Wyman, B., Yan, X., Zeng, Y., Adcroft, A., Dunne, J. P., Held, I. M., Krasting, J. P., Horowitz, L. W., Milly, P., Shevliakova, E., Winton, M., Zhao, M., and Zhang, R. (2018). Noaa-gfdl gfdl-cm4 model output.

Haar, L., Gallagher, J. S., and Kell, G. S. (1984). *NBS/NRC steam tables : thermodynamic and transport properties and computer programs for vapor and liquid states of water in SI units*, volume 7 of *320*. Hemisphere Publishing Corp., Washington DC.

Hanasaki, N., Yoshikawa, S., Pokhrel, Y., and Kanae, S. (2018). A global hydrological simulation to specify the sources of water used by humans. *Hydrology and Earth System Sciences*, 22(1):789–817.

Holtmeier, F.-K. and Broll, G. (2007). Treeline advance – driving processes and adverse forces. *Landscape Online*, 1.

Horowitz, L. W., Naik, V., Sentman, L., Paulot, F., Blanton, C., McHugh, C., Radhakrishnan, A., Rand, K., Vahlenkamp, H., Zadeh, N. T., Wilson, C.,

Ginoux, P., He, J., John, J. G., Lin, M., Paynter, D. J., Ploshay, J., Zhang, A., and Zeng, Y. (2018). Noaa-gfdl gfdl-esm4 model output prepared for cmip6 aerchemmip.

IPCC (2014). *Climate Change 2014: Synthesis Report. Contribution of Working Groups I, II and III to the Fifth Assessment Report of the Intergovernmental Panel on Climate Change*. IPCC, Geneva, Switzerland.

Ito, A. and Inatomi, M. (2012). Water-use efficiency of the terrestrial biosphere: A model analysis focusing on interactions between the global carbon and water cycles. *Journal of Hydrometeorology*, 13(2):681–694.

Ito, A. and Oikawa, T. (2002). A simulation model of the carbon cycle in land ecosystems (sim-cycle): a description based on dry-matter production theory and plot-scale validation. *Ecological Modelling*, 151(2):143 – 176.

Jafarov, E. E., Coon, E. T., Harp, D. R., Wilson, C. J., Painter, S. L., Atchley, A. L., and Romanovsky, V. E. (2018). Modeling the role of preferential snow accumulation in through talik development and hillslope groundwater flow in a transitional permafrost landscape. *Environmental Research Letters*, 13(10):105006.

Jones, C. D., Hughes, J. K., Bellouin, N., Hardiman, S. C., Jones, G. S., Knight, J., Liddicoat, S., O'Connor, F. M., Andres, R. J., Bell, C., Boo, K.-O., Bozzo, A., Butchart, N., Cadule, P., Corbin, K. D., Doutriaux-Boucher, M., Friedlingstein, P., Gornall, J., Gray, L., Halloran, P. R., Hurtt, G., Ingram, W. J., Lamarque, J.-F., Law, R. M., Meinshausen, M., Osprey, S., Palin, E. J., Parsons Chini, L., Raddatz, T., Sanderson, M. G., Sellar, A. A., Schurer, A., Valdes, P., Wood, N., Woodward, S., Yoshioka, M., and Zerroukat, M. (2011). The hadgem2-es implementation of cmip5 centennial simulations. *Geoscientific Model Development*, 4(3):543–570.

Ju, J. and Masek, J. G. (2016). The vegetation greenness trend in canada and us alaska from 1984–2012 landsat data. *Remote Sensing of Environment*, 176:1 – 16.

Kurita, N., Yoshida, N., Inoue, G., and Chayanova, E. A. (2004). Modern isotope climatology of Russia: A first assessment. *Journal of Geophysical Research (Atmospheres)*, 109(D3):D03102.

Köppen, W. (1884). Die wärmezonen der erde, nach der dauer der heissen, gemässigten und kalten zeit und nach der wirkung der wärme auf die organische welt betrachtet. *Meteorologische Zeitschrift*, 1:215–226.

Körner, C. (1998). A re-assessment of high elevation treeline positions and their explanation. *Oecologia*, 115:445–459.

Lai, D. Y. F. (2009). Methane dynamics in northern peatlands: A review. *Pedosphere*, 19(4):409–421.

Lawrence, D. M., Koven, C. D., Swenson, S. C., Riley, W. J., and Slater, A. G. (2015). Permafrost thaw and resulting soil moisture changes regulate projected high-latitude CO2and CH4emissions. *Environmental Research Letters*, 10(9):094011.

Lee, W.-L., Wang, Y.-C., Shiu, C.-J., Tsai, I.-C., Tu, C.-Y., Lan, Y.-Y., Chen, J.-P., Pan, H.-L., and Hsu, H.-H. (2020). Taiwan earth system model version 1: Description and evaluation of mean state.

Liang, M., Sugimoto, A., Tei, S., Bragin, I. V., Takano, S., Morozumi, T., Shingubara, R., Maximov, T. C., Kiyashko, S. I., Velivetskaya, T. A., and Ignatiev, A. V. (2014). Importance of soil moisture and n availability to larch growth and distribution in the arctic taiga-tundra boundary ecosystem, northeastern siberia. 8:327–341.

Loranty, M. M., Abbott, B. W., Blok, D., Douglas, T. A., Epstein, H. E., Forbes, B. C., Jones, B. M., Kholodov, A. L., Kropp, H., Malhotra, A., Mamet, S. D., Myers-Smith, I. H., Natali, S. M., O'Donnell, J. A., Phoenix, G. K., Rocha, A. V., Sonnentag, O., Tape, K. D., and Walker, D. A. (2018). Reviews and syntheses: Changing ecosystem influences on soil thermal regimes in northern high-latitude permafrost regions. *Biogeosciences*, 15(17):5287–5313.

MacDonald, G., Kremenetski, K., and Beilman, D. (2008). Climate change and the northern russian treeline zone. *Philosophical Transactions of the Royal Society B: Biological Sciences*, 363(1501):2283–2299.

Martens, B., Miralles, D. G., Lievens, H., van der Schalie, R., de Jeu, R. A. M., Fernández-Prieto, D., Beck, H. E., Dorigo, W. A., and Verhoest, N. E. C. (2017). Gleam v3: satellite-based land evaporation and root-zone soil moisture. *Geoscientific Model Development*, 10(5):1903–1925.

McGuire, A. D., Lawrence, D. M., Koven, C., Clein, J. S., Burke, E., Chen, G., Jafarov, E., MacDougall, A. H., Marchenko, S., Nicolsky, D., Peng, S., Rinke, A., Ciais, P., Gouttevin, I., Hayes, D. J., Ji, D., Krinner, G., Moore, J. C., Romanovsky, V., Schädel, C., Schaefer, K., Schuur, E. A. G., and Zhuang, Q. (2018). Dependence of the evolution of carbon dynamics in the northern permafrost region on the trajectory of climate change. *Proceedings of the National Academy of Sciences of the United States of America*, 115:3882–3887.

Merbold, L., Kutsch, W. L., Corradi, C., Kolle, O., Rebmann, C., Stoy, P. C., Zimov, S. A., and Schulze, E.-D. (2009). Artificial drainage and associated carbon fluxes (co2/ch4) in a tundra ecosystem. *Global Change Biology*, 15(11):2599–2614.

Michaelson, G. J. and Ping, C. L. (2003). Soil organic carbon and co2 respiration at subzero temperature in soils of arctic alaska. *Journal of Geophysical Research: Atmospheres*, 108(D2):ALT 5–1–ALT 5–10.

Miralles, D. G., Holmes, T. R. H., De Jeu, R. A. M., Gash, J. H., Meesters, A. G. C. A., and Dolman, A. J. (2011). Global land-surface evaporation estimated from satellite-based observations. *Hydrology and Earth System Sciences*, 15(2):453–469.

Müller Schmied, H., Adam, L., Eisner, S., Fink, G., Flörke, M., Kim, H., Oki, T., Portmann, F. T., Reinecke, R., Riedel, C., Song, Q., Zhang, J., and Döll, P. (2016). Variations of global and continental water balance components as impacted by climate forcing uncertainty and human water use. *Hydrology and Earth System Sciences*, 20(7):2877–2898.

Natali, S. M., Schuur, E. A. G., Mauritz, M., Schade, J. D., Celis, G., Crummer, K. G., Johnston, C., Krapek, J., Pegoraro, E., Salmon, V. G., and Webb, E. E. (2015). Permafrost thaw and soil moisture driving co2 and ch4 release from upland tundra. *Journal of Geophysical Research: Biogeosciences*, 120(3):525–537.

NOAA (2020). National weather service forecast office. *NOAA*. Accessed: 19-05-2020.

Olefeldt, D., Goswami, S., Grosse, G., Hayes, D., Hugelius, G., Kuhry, P., McGuire, A. D., Romanovsky, V. E., Sannel, A. B. K., Schuur, E. A. G., and Turetsky, M. R. (2016). Circumpolar distribution and carbon storage of thermokarst landscapes. *Nature Communications*, 7(13043).

Olefeldt, D., Turetsky, M. R., Crill, P. M., and McGuire, A. D. (2013). Environmental and physical controls on northern terrestrial methane emissions across permafrost zones. *Global Change Biology*, 19(2):589–603.

Olson, D. M., Dinerstein, E., Wikramanayake, E. D., Burgess, N. D., Powell, G. V. N., Underwood, E. C., D'amico, J. A., Itoua, I., Strand, H. E., Morrison, J. C., Loucks, C. J., Allnutt, T. F., Ricketts, T. H., Kura, Y., Lamoreux, J. F., Wettengel, W. W., Hedao, P., and Kassem, K. R. (2001). Terrestrial Ecoregions of the World: A New Map of Life on Earth: A new global map of terrestrial ecoregions provides an innovative tool for conserving biodiversity. *BioScience*, 51(11):933–938.

Park, S., Shin, J., Kim, S., Oh, E., and Kim, Y. (2019). Global climate simulated by the seoul national university atmosphere model version 0 with a unified convection scheme (sam0-unicon). *Journal of Climate*, 32(10):2917–2949.

Pavelková Řičánková, V., Robovský, J., and Riegert, J. (2014). Ecological structure of recent and last glacial mammalian faunas in northern eurasia: The case of altai-sayan refugium. *PLoS ONE*, 9(1).

Peng, T.-R., Liu, K.-K., Wang, C.-H., and Chuang, K.-H. (2011). A water isotope approach to assessing moisture recycling in the island-based precipitation of taiwan: A case study in the western pacific. *Water Resources Research*, 47(8).

Pogoda (2020). Pogoda i klimat. *Pogoda*. Accessed: 19-05-2020.

Rackow, T., Goessling, H. F., Jung, T., Sidorenko, D., Semmler, T., Barbi, D., and Handorf, D. (2016). Towards multi-resolution global climate modeling with echam6-fesom. part ii: climate variability. *Climate Dynamics*, 50(7–8):2369–2394.

Rawlins, M. A., Steele, M., Holland, M. M., Adam, J. C., Cherry, J. E., Francis, J. A., Groisman, P. Y., Hinzman, L. D., Huntington, T. G., Kane, D. L., Kimball, J. S., Kwok, R., Lammers, R. B., Lee, C. M., Lettenmaier, D. P., McDonald, K. C., Podest, E., Pundsack, J. W., Rudels, B., Serreze, M. C., Shiklomanov, A., Skagseth, , Troy, T. J., Vörösmarty, C. J., Wensnahan, M., Wood, E. F., Woodgate, R., Yang, D., Zhang, K., and Zhang, T. (2010). Analysis of the arctic system for freshwater cycle intensification: Observations and expectations. *Journal of Climate*, 23(21):5715–5737.

Reinecke, R., Foglia, L., Mehl, S., Trautmann, T., Cáceres, D., and Döll, P. (2019). Challenges in developing a global gradient-based groundwater model (g^3m v1.0) for the integration into a global hydrological model. *Geoscientific Model Development*, 12(6):2401–2418.

Risi, C., Noone, D., Frankenberg, C., and Worden, J. (2013). Role of continental recycling in intraseasonal variations of continental moisture as deduced from model simulations and water vapor isotopic measurements. *Water Resources Research*, 49(7):4136–4156.

Roberts, M. (2017). Mohc hadgem3-gc31-mm model output prepared for cmip6 highresmip.

Seibert, P. and Frank, A. (2004). Source-receptor matrix calculation with a lagrangian particle dispersion model in backward mode. *Atmospheric Chemistry and Physics*, 4(1):51–63.

Seland, , Bentsen, M., Graff, L., Olivié, D., Toniazzo, T., Gjermundsen, A., Debernard, J., Gupta, A., He, Y., Kirkevåg, A., Schwinger, J., Tjiputra, J., Aas, K., Bethke, I., Fan, Y., Griesfeller, J., Grini, A., Guo, C., Ilicak, M., and Michael, S. (2020). The norwegian earth system model, noresm2 – evaluation of the cmip6 deck and historical simulations.

Serreze, M. C., Bromwich, D. H., Clark, M. P., Etringer, A. J., Zhang, T., and Lammers, R. (2002). Large-scale hydro-climatology of the terrestrial Arctic drainage system. *Journal of Geophysical Research (Atmospheres)*, 108(D2):8160.

Shingubara, R., Sugimoto, A., Murase, J., Iwahana, G., Tei, S., Liang, M., Takano, S., Morozumi, T., and Maximov, T. C. (2019). Multi-year effect of wetting on ch_4 flux at taiga-tundra boundary in northeastern siberia deduced from stable isotope ratios of ch_4. *Biogeosciences*, 16(3):755–768.

Sidorenko, D., Rackow, T., Jung, T., Semmler, T., Barbi, D., Danilov, S., Dethloff, K., Dorn, W., Fieg, K., Goessling, H. F., and et al. (2014). Towards multi-resolution global climate modeling with echam6–fesom. part i: model formulation and mean climate. *Climate Dynamics*, 44(3–4):757–780.

Smith, B., Wårlind, D., Arneth, A., Hickler, T., Leadley, P., Siltberg, J., and Zaehle, S. (2014). Implications of incorporating n cycling and n limitations on primary production in an individual-based dynamic vegetation model. *Biogeosciences*, 11(7):2027–2054.

Song, X., Wang, G., Ran, F., Huang, K., Sun, J., and Song, C. (2020). Soil moisture as a key factor in carbon release from thawing permafrost in a boreal forest. *Geoderma*, 357:113975.

Song, X.-P., Hansen, M., Stehman, S., Potapov, P., Tyukavina, A., Vermote, E., and Townshend, J. (2018). Global land change from 1982 to 2016. *Nature*, 560.

Song, Z. (2020). Fio-esm: The earth system model coupled with ocean surface gravity waves. *Climate Change Research Letters*, 9(1):26–39.

Staal, A., Tuinenburg, O. A., Bosmans, J. H. C., Holmgren, M., Van Nes, E. H., Scheffer, M., Zemp, D. C., and Dekker, S. C. (2018). Forest-rainfall cascades buffer against drought across the amazon. *Nature*, 8:539–543.

Stacke, T. and Hagemann, S. (2012). Development and evaluation of a global dynamical wetlands extent scheme. *Hydrology and Earth System Sciences*, 16(8):2915–2933.

Sutanto, S. J., van den Hurk, B., Dirmeyer, P. A., Seneviratne, S. I., Röckmann, T., Trenberth, K. E., Blyth, E. M., Wenninger, J., and Hoffmann, G. (2014). Hess opinions "a perspective on isotope versus non-isotope approaches to determine the contribution of transpiration to total evaporation". *Hydrology and Earth System Sciences*, 18:2815–2827.

SWIPA (2017). *Snow, Water, Ice and Permafrost in the Arctic (SWIPA)*. Arctic Monitoring and Assessment Programme (AMAP), Oslo, Norway, Gaustadalléen 21, N-0349 Oslo, Norway.

Takata, K., Emori, S., and Watanabe, T. (2003). Development of the minimal advanced treatments of surface interaction and runoff. *Global and Planetary Change*, 38(1):209 – 222. Project for Intercomparison of Land-surface Parameterization Schemes, Phase 2(e).

Tang, G., Zheng, J., Xu, X., Yang, Z., Graham, D. E., Gu, B., Painter, S. L., and Thornton, P. E. (2016). Biogeochemical modeling of co_2 and ch_4 production in anoxic arctic soil microcosms. *Biogeosciences*, 13(17):5021–5041.

Thiery, W., Davin, E. L., Lawrence, D. M., Hirsch, A. L., Hauser, M., and Seneviratne, S. I. (2017). Present-day irrigation mitigates heat extremes. *Journal of Geophysical Research: Atmospheres*, 122(3):1403–1422.

Trenberth, K. E. (1999). Atmospheric moisture recycling: Role of advection and local evaporation. *Journal of Climate*, 12(5):1368–1381.

Tuinenburg, O., Hutjes, R., and Kabat, P. (2012). The fate of evaporated water from the ganges basin. *J. Geophys. Res.*, 117.

Tuinenburg, O. A. and Staal, A. (2020). Tracking the global flows of atmospheric moisture and associated uncertainties. *Hydrology and Earth System Sciences*, 24(5):2419–2435.

Tuovinen, J.-P., Aurela, M., Hatakka, J., Räsänen, A., Virtanen, T., Mikola, J., Ivakhov, V., Kondratyev, V., and Laurila, T. (2019). Interpreting eddy covariance data from heterogeneous siberian tundra: land-cover-specific methane fluxes and spatial representativeness. *Biogeosciences*, 16(2):255–274.

Van der Molen, M., Van Huissteden, K., Parmentier, F.-J., Petrescu, A. M. R., Dolman, H. A., Maximov, T., Kononov, A., Karsanaev, S., and Suzdalov, D. (2007). The growing season greenhouse gas balance of a continental tundra site in the indigirka lowlands, ne siberia. *Biogeosciences*, 4:985–1003.

Vazquez, M., Nieto, R., Drumond, A., and Gimeno, L. (2016). Moisture transport into the arctic: Source-receptor relationships and the roles of atmospheric circulation and evaporation: Moisture transport into the arctic. *Journal of Geophysical Research: Atmospheres*, 121.

Voldoire, A. (2019). Cnrm-cerfacs cnrm-cm6-1-hr model output prepared for cmip6 highresmip.

Volodin, E., Mortikov, E., Gritsun, A., Lykossov, V., Galin, V., Diansky, N., Gusev, A., Kostrykin, S., Iakovlev, N., Shestakova, A., and Emelina, S. (2019). Inm inm-cm4-8 model output prepared for cmip6 pmip.

Volodin, E., Mortikov, E., Kostrykin, S., Galin, V., Lykossov, V., Gritsun, A., Diansky, N., Gusev, A., and Iakovlev, N. (2017). Simulation of the present-day climate with the climate model inmcm5. *Climate Dynamics*.

von Storch, J.-S., Putrasahan, D., Lohmann, K., Gutjahr, O., Jungclaus, J., Bittner, M., Haak, H., Wieners, K.-H., Giorgetta, M., Reick, C., Esch, M., Gayler, V., de Vrese, P., Raddatz, T., Mauritsen, T., Behrens, J., Brovkin, V., Claussen, M., Crueger, T., Fast, I., Fiedler, S., Hagemann, S., Hohenegger, C., Jahns, T., Kloster, S., Kinne, S., Lasslop, G., Kornblueh, L., Marotzke, J., Matei, D., Meraner, K., Mikolajewicz, U., Modali, K., Müller, W., Nabel, J., Notz, D., Peters, K., Pincus, R., Pohlmann, H., Pongratz, J., Rast, S., Schmidt, H., Schnur, R., Schulzweida, U., Six, K., Stevens, B., Voigt, A., and Roeckner, E. (2017). Mpi-m mpiesm1.2-hr model output prepared for cmip6 highresmip.

Wada, Y., Wisser, D., and Bierkens, M. F. P. (2014). Global modeling of withdrawal, allocation and consumptive use of surface water and groundwater resources. *Earth System Dynamics*, 5(1):15–40.

Walz, J., Knoblauch, C., Tigges, R., Opel, T., Schirrmeister, L., and Pfeiffer, E.-M. (2018). Greenhouse gas production in degrading ice-rich permafrost deposits in northeastern siberia. *Biogeosciences*, 15(17):5423–5436.

Wang, T., Ciais, P., Piao, S. L., Ottlé, C., Brender, P., Maignan, F., Arain, A., Cescatti, A., Gianelle, D., Gough, C., Gu, L., Lafleur, P., Laurila, T., Marcolla, B., Margolis, H., Montagnani, L., Moors, E., Saigusa, N., Vesala, T., Wohlfahrt, G., Koven, C., Black, A., Dellwik, E., Don, A., Hollinger, D., Knohl, A., Monson, R., Munger, J., Suyker, A., Varlagin, A., and Verma, S. (2011). Controls on winter ecosystem respiration in temperate and boreal ecosystems. *Biogeosciences*, 8(7):2009–2025.

Watanabe, M., Suzuki, T., O'ishi, R., Komuro, Y., Watanabe, S., Emori, S., Takemura, T., Chikira, M., Ogura, T., Sekiguchi, M., and et al. (2010). Improved climate simulation by miroc5: Mean states, variability, and climate sensitivity. *Journal of Climate*, 23(23):6312–6335.

Wu, T. (2012). A mass-flux cumulus parameterization scheme for large-scale models: description and test with observations. *Climate Dynamics*, 38(3):725–744.

Wu, T., Lu, Y., Fang, Y., , X., Li, L., Li, W., Jie, W., Zhang, J., Liu, Y., Zhang, L., Zhang, F., Zhang, Y., Wu, F., Li, J., Chu, M., Wang, Z., Shi, X., Liu, X., Wei, M., and Liu, X. (2019). The beijing climate center climate system model (bcc-csm): the main progress from cmip5 to cmip6. *Geoscientific Model Development*, 12:1573–1600.

Yu, Y. (2018). Cas fgoals-f3-l model output prepared for cmip6 cmip.

Yukimoto, S., Koshiro, T., Kawai, H., Oshima, N., Yoshida, K., Urakawa, S., Tsujino, H., Deushi, M., Tanaka, T., Hosaka, M., Yoshimura, H., Shindo, E., Mizuta, R., Ishii, M., Obata, A., and Adachi, Y. (2019). Mri mri-esm2.0 model output prepared for cmip6 cmip.

Zeng, N., Mariotti, A., and Wetzel, P. (2005). Terrestrial mechanisms of interannual co2 variability. *Global Biogeochemical Cycles*, 19(1).

Zhou Guangqing, Zhang Yunquan, J. J. Z. H. W. B. C. H. W. T. H. H. Z. J. Y. L. Z. M. (2020). Earth system model: Cas-esm. *Frontiers of Data and Computing*, 2(1):38.

Zimov, S. (2005). Pleistocene park: Return of the mammoth's ecosystem. *Science*, 308:796–798.

Zimov, S., Schuur, E., and Chapin III, F. S. (2006). Permafrost and the global carbon budget. *Science*, 312.

Zimov, S., Zimov, N., Tikhonov, A., and Chapin, F. (2012). Mammoth steppe: a high-productivity phenomenon. *Quaternary Science Reviews*, 57:26 – 45.

Zona, D., Gioli, B., Commane, R., Lindaas, J., Wofsy, S. C., Miller, C. E., Dinardo, S. J., Dengel, S., Sweeney, C., Karion, A., Chang, R. Y.-W., Henderson, J. M., Murphy, P. C., Goodrich, J. P., Moreaux, V., Liljedahl, A., Watts, J. D., Kimball, J. S., Lipson, D. A., and Oechel, W. C. (2016). Cold season emissions dominate the arctic tundra methane budget. *Proceedings of the National Academy of Sciences*, 113(1):40–45.

Appendix

A List of CMIP6 models

AWI-CM-1-1-MR (Sidorenko et al. (2014), Rackow et al. (2016))

variable	scenario
Air temperature	RCP8.5
Air temperature	historical
Downward short-wave radiation flux	RCP8.5
Evaporation	RCP8.5
Precipitation	RCP8.5
Relative humidity	RCP8.5
Sensible heat flux	RCP8.5
Surface temperature	RCP8.5
Upward short-wave radiation flux	RCP8.5

BCC-CSM2-MR (Wu (2012), Wu et al. (2019))

variable	scenario
Air temperature	historical
Downward short-wave radiation flux	all
Evaporation	historical
Precipitation	all
Sensible heat flux	all
Soil liquid water content	all
Soil moisture content	all
Surface temperature	all
Upper portion soil moisture content	all
Upward short-wave radiation flux	all

CAS-ESM2-0 (Zhou Guangqing, 2020)

variable	scenario
Air temperature	historical
Downward short-wave radiation flux	historical
Evaporation	historical
Precipitation	historical
Relative humidity	historical
Sensible heat flux	historical
Surface temperature	historical
Upper portion soil moisture content	historical
Upward short-wave radiation flux	historical

CESM2

variable	scenario
Air temperature	historical
Downward short-wave radiation flux	RCP8.5
Downward short-wave radiation flux	historical
Evaporation	RCP8.5
Evaporation	historical
Precipitation	RCP8.5
Precipitation	historical
Relative humidity	RCP8.5
Relative humidity	historical
Sensible heat flux	RCP8.5
Sensible heat flux	historical
Soil liquid water content	RCP8.5
Soil liquid water content	historical
Soil moisture content	RCP8.5
Soil moisture content	historical
Surface temperature	RCP8.5
Surface temperature	historical
Upper portion soil moisture content	RCP8.5
Upper portion soil moisture content	historical
Upward short-wave radiation flux	RCP8.5
Upward short-wave radiation flux	historical

CESM2-WACCM (Danabasoglu, 2019)

variable	scenario
Air temperature	historical
Downward short-wave radiation flux	RCP8.5
Downward short-wave radiation flux	historical
Evaporation	RCP8.5
Evaporation	historical
Precipitation	RCP8.5
Precipitation	historical
Relative humidity	RCP8.5
Relative humidity	historical
Sensible heat flux	RCP8.5
Sensible heat flux	historical
Soil liquid water content	RCP8.5
Soil liquid water content	historical
Soil moisture content	RCP8.5
Soil moisture content	historical
Surface temperature	RCP8.5
Surface temperature	historical
Upper portion soil moisture content	RCP8.5
Upper portion soil moisture content	historical

Upward short-wave radiation flux	RCP8.5
Upward short-wave radiation flux	historical

CESM2-WACCM-FV2 (Danabasoglu, 2019)

variable	scenario
Air temperature	historical
Downward short-wave radiation flux	historical
Evaporation	historical
Precipitation	historical
Relative humidity	historical
Sensible heat flux	historical
Soil moisture content	historical
Surface temperature	historical
Upward short-wave radiation flux	historical

CNRM-CM6-1-HR (Voldoire, 2019)

variable	scenario
Air temperature	RCP8.5
Air temperature	piControl
Sensible heat flux	RCP8.5
Sensible heat flux	piControl

E3SM-1-0 (Bader et al., 2019)

variable	scenario
Air temperature	historical
Downward short-wave radiation flux	historical
Evaporation	historical
Precipitation	historical
Sensible heat flux	historical
Soil moisture content	historical
Surface temperature	historical
Upper portion soil moisture content	historical
Upward short-wave radiation flux	historical

E3SM-1-1 (Caldwell et al. (2019), Golaz et al. (2019))

variable	scenario
Air temperature	historical
Downward short-wave radiation flux	historical
Evaporation	historical
Precipitation	historical
Sensible heat flux	historical
Surface temperature	historical
Upward short-wave radiation flux	historical

E3SM-1-1-ECA (Caldwell et al. (2019), Golaz et al. (2019))

variable	scenario
Air temperature	historical
Downward short-wave radiation flux	historical
Evaporation	historical
Precipitation	historical
Sensible heat flux	historical
Soil moisture content	historical
Surface temperature	historical
Upper portion soil moisture content	historical
Upward short-wave radiation flux	historical

EC-Earth3 (EC-Earth, 2019)

variable	scenario
Air temperature	RCP8.5
Air temperature	historical
Downward short-wave radiation flux	RCP8.5
Downward short-wave radiation flux	historical
Evaporation	RCP8.5
Evaporation	historical
Precipitation	RCP8.5
Precipitation	historical
Relative humidity	RCP8.5
Relative humidity	historical
Sensible heat flux	RCP8.5
Sensible heat flux	historical
Soil moisture content	RCP8.5
Soil moisture content	historical
Surface temperature	RCP8.5
Surface temperature	historical
Upper portion soil moisture content	RCP8.5
Upper portion soil moisture content	historical
Upward short-wave radiation flux	RCP8.5
Upward short-wave radiation flux	historical

EC-Earth3-Veg (EC-Earth, 2019)

variable	scenario
Air temperature	all
Downward short-wave radiation flux	all
Evaporation	all
Precipitation	all
Relative humidity	all
Sensible heat flux	all
Soil moisture content	all
Surface temperature	RCP8.5

Surface temperature	historical
Upper portion soil moisture content	all
Upward short-wave radiation flux	all

FGOALS-f3-L (Yu, 2018)

variable	scenario
Air temperature	historical
Downward short-wave radiation flux	RCP8.5
Downward short-wave radiation flux	historical
Evaporation	RCP8.5
Evaporation	historical
Precipitation	RCP8.5
Precipitation	historical
Relative humidity	RCP8.5
Relative humidity	historical
Sensible heat flux	RCP8.5
Sensible heat flux	historical
Surface temperature	RCP8.5
Surface temperature	historical
Upward short-wave radiation flux	RCP8.5
Upward short-wave radiation flux	historical

FIO-ESM-2-0 (Song, 2020)

variable	scenario
Air temperature	RCP8.5
Precipitation	RCP8.5
Precipitation	historical
Sensible heat flux	RCP8.5
Upper portion soil moisture content	RCP8.5
Upper portion soil moisture content	historical

GFDL-CM4 (Guo et al., 2018)

variable	scenario
Soil moisture content	RCP8.5
Soil moisture content	historical
Upper portion soil moisture content	RCP8.5
Upper portion soil moisture content	historical

GFDL-ESM4 (Horowitz et al., 2018)

variable	scenario
Air temperature	RCP8.5
Air temperature	historical
Downward short-wave radiation flux	RCP8.5
Downward short-wave radiation flux	historical

Evaporation	RCP8.5
Evaporation	historical
Precipitation	RCP8.5
Precipitation	historical
Relative humidity	RCP8.5
Sensible heat flux	RCP8.5
Sensible heat flux	historical
Soil liquid water content	RCP8.5
Soil liquid water content	historical
Soil moisture content	RCP8.5
Surface temperature	RCP8.5
Surface temperature	historical
Upper portion soil moisture content	RCP8.5
Upward short-wave radiation flux	RCP8.5
Upward short-wave radiation flux	historical

HadGEM3-GC31-MM (Roberts, 2017)

variable	scenario
Air temperature	piControl
Evaporation	piControl
Precipitation	piControl
Relative humidity	piControl
Sensible heat flux	piControl
Soil moisture content	piControl
Surface temperature	piControl

INM-CM4-8 (Volodin et al., 2019)

variable	scenario
Air temperature	all
Downward short-wave radiation flux	all
Evaporation	all
Precipitation	all
Relative humidity	all
Sensible heat flux	all
Soil moisture content	all
Surface temperature	all
Upward short-wave radiation flux	all

INM-CM5-0 (Volodin et al., 2017)

variable	scenario
Air temperature	all
Downward short-wave radiation flux	all
Evaporation	all
Precipitation	all
Relative humidity	RCP8.5

Relative humidity	historical
Sensible heat flux	all
Soil moisture content	all
Surface temperature	all
Upward short-wave radiation flux	all

MPI-ESM1-2-HR (von Storch et al., 2017)

variable	scenario
Air temperature	all
Downward short-wave radiation flux	all
Evaporation	all
Precipitation	all
Relative humidity	all
Sensible heat flux	all
Soil moisture content	all
Surface temperature	all
Upper portion soil moisture content	all
Upward short-wave radiation flux	all

MPI-ESM2-0 (Yukimoto et al., 2019)

variable	scenario
Air temperature	historical
Downward short-wave radiation flux	all
Evaporation	all
Precipitation	all
Relative humidity	all
Sensible heat flux	RCP8.5
Sensible heat flux	piControl
Soil moisture content	all
Surface temperature	all
Upper portion soil moisture content	all
Upward short-wave radiation flux	all

NorESM2-MM (Seland et al., 2020)

variable	scenario
Air temperature	RCP8.5
Air temperature	historical
Downward short-wave radiation flux	RCP8.5
Downward short-wave radiation flux	historical
Evaporation	RCP8.5
Evaporation	historical
Precipitation	RCP8.5
Precipitation	historical
Relative humidity	RCP8.5
Relative humidity	historical

Sensible heat flux	RCP8.5
Sensible heat flux	historical
Soil liquid water content	RCP8.5
Soil liquid water content	historical
Soil moisture content	RCP8.5
Soil moisture content	historical
Surface temperature	RCP8.5
Surface temperature	historical
Upper portion soil moisture content	RCP8.5
Upper portion soil moisture content	historical
Upward short-wave radiation flux	RCP8.5
Upward short-wave radiation flux	historical

SAM0-UNICON (Park et al., 2019)

variable	scenario
Air temperature	historical
Downward short-wave radiation flux	historical
Evaporation	historical
Precipitation	historical
Relative humidity	historical
Sensible heat flux	historical
Soil moisture content	historical
Surface temperature	historical
Upper portion soil moisture content	historical
Upward short-wave radiation flux	historical

TaiESM1 (Lee et al., 2020)

variable	scenario
Evaporation	historical
Precipitation	historical
Soil moisture content	historical
Surface temperature	historical
Upper portion soil moisture content	historical

Table 2: Table of variables used for each CMIP6 model run

B List of ISIMIP models

Besides the computer model, also the climate forcing may be different for various ISIMIP runs. Therefore, this table also shows the climate forcing of the runs used in my thesis. 'all' indicates that output data with HadGEM2-ES (Jones et al., 2011), IPSL-CM5A-LR (Dufresne et al., 2013) and MIROC5 (Watanabe et al., 2010) climate forcing were used. If not all climate forcings were used for a particular model, it means the missing climate forcings were not available at the time of retrieval. GFDL-ESM (Dunne et al. (2012), Dunne et al. (2013)) forcing was also available, though these evaporation data deviate from the other forcings for the selected scenarios and are therefore not used. 'all' for runoff datasets does include GFDL-ESM.

Model references are:

- CARAIB (Dury et al., 2011)
- CLM4.5 (Thiery et al., 2017)
- H08 (Hanasaki et al., 2018)
- JULES-W1 (Best et al., 2011)
- LPJ-GUESS (Smith et al., 2014)
- LPJmL (Bondeau et al., 2007)
- MATSIRO (Takata et al., 2003)
- MPI-HM (Stacke and Hagemann, 2012)
- ORCHIDEE(-DGVM) (Guimberteau et al., 2017)
- PCR-GLOBWB (Wada et al., 2014)
- VEGAS (Zeng et al., 2005)
- VISIT (Ito and Oikawa (2002), Ito and Inatomi (2012))
- WaterGAP2 (Müller Schmied et al., 2016)

Evaporation

Model	Scenario	Forcing
CARAIB	historical	all
CARAIB	piControl	all
CLM4.5	piControl	all
CLM4.5	RCP8.5	all
H08	all	all
JULES-W1	RCP8.5	all
LPJ-GUESS	historical	all

LPJ-GUESS	piControl	all
LPJmL	all	all
MATSIRO	all	all
MPI-HM	historical	IPSL-CM5A-LR
MPI-HM	historical	MIROC5
MPI-HM	piControl	IPSL-CM5A-LR
MPI-HM	piControl	MIROC5
ORCHIDEE-DGVM	historical	IPSL-CM5A-LR
ORCHIDEE-DGVM	piControl	IPSL-CM5A-LR
ORCHIDEE	all	all
PCR-GLOBWB	historical	all
PCR-GLOBWB	piControl	all
VEGAS	historical	IPSL-CM5A-LR
VEGAS	piControl	IPSL-CM5A-LR
VISIT	historical	all
VISIT	piControl	all
WaterGAP2	all	all

Runoff

Model	Scenario	Forcing
CARAIB	historical	all
CARAIB	piControl	all
CLM4.5	piControl	all
CLM4.5	RCP8.5	all
MATSIRO	all	all
VEGAS	historical	IPSL-CM5A-LR
VEGAS	piControl	IPSL-CM5A-LR
VISIT	historical	all
VISIT	piControl	all

Table 3: Table of models and scenarios used for ISIMIP